A MULTI-SENSOR APPROACH TO DETERMINING VOLCANIC PLUME HEIGHTS IN THE NORTH PACIFIC

By

Angela L. Ekstrand

RECOMMENDED:

Peter Webley

Ken Dean

Anupma Prakash

Advisory Committee Chair

Anupma Prakash

Chair, Department of Geology and Geophysics

APPROVED:

Dean, College of Natural Science and Mathematics

Dean of the Graduate School

April 10, 2012

Date

A MULTI-SENSOR APPROACH TO DETERMINING VOLCANIC PLUME HEIGHTS IN THE NORTH PACIFIC

A

THESIS

Presented to the Faculty

of the University of Alaska Fairbanks

in Partial Fulfillment of the Requirements

for the Degree of

MASTER OF SCIENCE

By

Angela L. Ekstrand, B.S.

Fairbanks, Alaska

May 2012

Abstract

During a volcanic eruption, accurate height information is necessary to forecast a volcanic plume's trajectory with volcanic ash transport and dispersion (VATD) models. Recent events in the North Pacific (NOPAC) displayed significant discrepancies between different methods of plume height determination. This thesis describes two studies that attempted to resolve this discrepancy, and identify the most accurate method for plume height determination. The first study considered the 2009 eruption of Redoubt Volcano. This study found that the basic satellite temperature method, in which satellite thermal infrared temperatures are compared to temperature-altitude profiles, vastly underestimates volcanic plume height due to decreased optical depth of plumes soon after eruption. This study also found that the Multi-angle Imaging SpectroRadiometer (MISR) produced very accurate plume heights, even for optically thin plumes. The second study investigated the application of MISR data to multiple eruptions in the NOPAC: Augustine Volcano in 2006, Okmok, Cleveland, and Kasatochi volcanoes in 2008, and Redoubt and Sarychev Peak volcanoes in 2009. This study found that MISR data analysis retrieves accurate plume heights regardless of grain size, altitude, or water content. Exceptions include plumes of low optical depth over bright backgrounds. MISR is also capable of identifying ash clouds by aerosol type.

Table of Contents

Page

List of Figures

Page

List of Tables

Page

Acknowledgements

Many individuals contributed significantly to this work; many thanks to those mentioned here. This manuscript could not have been completed without the guidance of my advisor, Jonathan Dehn (UAF-GI/AVO). Peter Webley (UAF-GI/AVO) provided tireless assistance and feedback throughout every step of the thesis process. Anupma Prakash (UAF-GI/UAF Department of Geology and Geophysics) was significant to ensuring the success of the ArcGIS component of this work. Kenneson Dean (UAF-GI/AVO) provided a depth of experience and insight unparalleled at the Alaska Volcano Observatory, and as such, his advice was significant in the creation of this work. Michael Garay and David Nelson (JPL-CIT/Raytheon) provided unique insight into the MISR sensor, and tireless editing of and feedback on this work. David Nelson (Raytheon) also processed MISR data for this study with the unreleased 2.0 development version of MINX at JPL, California Institute of Technology. Other individuals helped significantly in the creation of the work as well. Thank you to: Torge Steensen (UAF-GI/AVO) for providing VAR code results; David McAlpin (UAF-GI) for processing Redoubt DEM data; Jeremy Harbeck (UAF-GI) for assistance in IDL processing; Ralph Kahn (NASA GSFC) for insight into and feedback on the satellite temperature method; Ralph Kahn (NASA GSFC) and Simona Scollo (INGV) for insight into the aerosol method detailed in Chapter 3; Lovro Valcic (UAF-GI) and Scott McFarlane (UAF-GI) for assistance in the processing of satellite data; Mike Pavolonis (NOAA) for feedback on the satellite temperature method; Peter Kelly (USGS) for providing gas flight data; Dave Schneider (USGS) for providing radar and photographic data; Mike Fromm (NRL) for providing Kasatochi and Redoubt lidar data; Also thank you to the Alaska Space Grant Program for funding to assist with presenting and publishing these results.

Chapter 1 Introduction

1.1 Background

During an active eruption, accurate plume height information must be acquired quickly for use in volcanic ash transport and dispersion models (VATD) models (Searcy et al., 1998), which are necessary for forecasting ash cloud motion. Total erupted mass (i.e., the product of mass eruption rate and duration) also relies on accurate estimates of plume height – plume height is often an input parameter in estimates that use inverse modeling (modeling that converts observed measurements to model parameters rather than the opposite; e.g., Folch et al., 2008) or empirical relationships (e.g., Sparks et al., 1997; Mastin, 2009). The understanding of plume height and composition is particularly important in the North Pacific (NOPAC) due to the high concentration of flight paths in this region (Miller and Casadevall, 2000). Example flight routes are given in Figure 1.1 (from Dean et al., in press), and these routes are concentrated directly over the active volcanoes in the NOPAC region.

During the eruption of Kasatochi Volcano in the Aleutian Islands, Alaska (Figure 1.2) in 2008, it was observed that the methods by which Alaska Volcano Observatory determines plume height did not agree: satellite-based lidar heights were much higher (on the order of 20 km above sea level, or ASL; Fromm et al., 2008) than satellite infrared temperature-derived heights (on the order of ~8 to 12 km ASL, unpublished data, Peter Webley; satellite infrared temperature method explained in Chapter 2). Kasatochi was an unsuitable study for determining the cause of this discrepancy, due to the eruption's short duration and limited dataset, and the volcano's remote location. However, when Redoubt Volcano (Figure 1.2) erupted in 2009, a similar discrepancy between radar and satellite temperature heights was observed – radar heights were much higher

than temperature heights, sometimes on the order of several kilometers (Ekstrand et al., 2009; 2010; also data presented here in Chapter 2 from Ekstrand et al., in press). Due to its location in the Cook Inlet region, there was a great volume of data available for the Redoubt eruption, including satellite, radar, and gas flight data, and thus, this eruption was well suited to a study that investigated this height discrepancy.

This study of Redoubt plume heights is presented in Chapter 2. The evidence presented in this chapter will show that the basic satellite temperature method (Kienle and Shaw, 1979; Sparks et al., 1997) underestimates plume heights due to the increasing transparency and thus reduced optical depth of an ash cloud as it disperses. This study also found that stereo height retrievals from the Multi-angle Imaging SpectroRadiometer (MISR) satellite sensor provide much more accurate plume heights.

Chapter 3 details a study of MISR height data for several eruptions in the NOPAC, most in the Alaskan-Aleutian Islands or in Alaska's Cook Inlet region, including Augustine in 2006, Okmok, Cleveland and Kasatochi in 2008, and Redoubt and Sarychev Peak (Russia) in 2009 (Figure 1.2). This study demonstrates the effectiveness, and the few limitations, of MISR stereo height data and argues for its more frequent use for volcanic plume height determination. Additionally, this study argues that MISR is an effective sensor for providing aerosol optical depth, size, and shape properties that can classify plumes as containing ash by the method of Scollo et al. (2012). Though the sensor has been used in recent years for the study of volcanic plumes (e.g., Scollo et al., 2010; 2012), this is the first survey-type study which examines a number of eruptions rather than a single eruption.

1.2 Height retrieval methods

Many height retrieval methods are available for the volcanoes in the NOPAC, and only certain ones were selected for analysis in this study. Table 1.1 shows a selection of the methods available for analysis, gives an estimate of their spatial and temporal effectiveness, and describes how these methods apply to NOPAC volcanoes. These methods include satellite temperature (Kienle and Shaw, 1979; Sparks et al., 1997), satellite-based lidar (Winker et al., 2009), satellite-based stereo, displacement (Holasek et al., 1996), shadow (Holasek and Self, 1995; Holasek et al., 1996; Sparks et al., 1997), ground-based radar (Rose et al., 1995; Wood et al., 2007; Hoblitt and Schneider, 2009; Schneider and Hoblitt, in press), flight measurements (Werner et al., in press), flight observations, ground observations (Tupper and Wunderman, 2009), and photos (see Chapters 2 and 3).

The original research question asked why temperature heights were lower than other methods for recent eruptions in the NOPAC, so it was necessary to include satellite temperature data in subsequent analysis. However, the Geostationary Operational Environmental Satellite (GOES) and the Multifunctional Transport Satellite (MTSAT) both have poorer spatial resolution (4 km at nadir for both satellites, in thermal infrared bands, and closer to 2-8 km at 60 deg N for GOES; Webley et al., 2009) and were thus eliminated from analysis. Though these sensors provide frequent data, the temperatures would be based on distorted pixels that were too large to observe all plumes of interest; for those plumes for which GOES and MTSAT provided good coverage, the data volume would have been overwhelming. The Advanced Very High Resolution Radiometer (AVHRR) and the Moderate Resolution Imaging SpectroRadiometer (MODIS) provided frequent, but not overwhelming data volume, and allowed for visualization of smaller plume features (such as the April 1 and 5, 2009 Redoubt Volcano plumes discussed in Chapter 2).

Since GOES data were not used, the displacement method was also not used (the displacement method takes into consideration zenith angles and apparent plume offset from the vent to geometrically calculate true plume height; Holasek et al., 1996). Though AVHRR and MODIS data were used, no shadows were contained in any of the images, eliminating the shadow method from consideration.

Cloud-Aerosol Lidar with Orthogonal Polarization (CALIOP; Winker et al., 2009) provided the original comparison to temperature data for the Kasatochi 2008 eruption, but the eruption was so short-lived that few observations were available in total for it, regardless of method. CALIOP observations were available for Redoubt Volcano too, but none were time coincident with other datasets – they were all observed a great distance from the vent (personal communication, Mike Fromm). Since these studies were concerned with determining which methods provide quick, accurate methods of height assessment, CALIOP data were eliminated from analysis, and are only mentioned in passing in Chapter 2.

Two ground-based radar stations were available in the Cook Inlet region for the Redoubt 2009 eruption (Hoblitt and Schneider, 2009; Schneider and Hoblitt, in press), and this led to the choice of radar for comparative analysis with satellite temperature data, and to the choice of Redoubt as an excellent candidate for this study. Radar observations were collected frequently; an eruption could be detected by USGS radar within 1 minute of its onset (Hoblitt and Schneider, 2009).

The use of MISR provided a technique that was independent of the thermal cloud properties upon which satellite temperature relies. MISR retrievals rely on a purely geometrical approach to height determination. As such, these height retrievals are not sensitive to radiometric calibration

uncertainties (Marchand et al., 2010) or the emissivity of the plume material (Scollo et al., 2010). However, as transparency increases (this is the same as optical depth, but in this case optical depth affects visible texture rather than emissivity) and the ash cloud disperses, the volcanic plume layer becomes transparent, and the pass becomes optically inhomogeneous, allowing for the sensor to detect clouds or ground features below (Scollo et al., 2012). Because this is a texture and transparency issue, and not an emissivity issue, Chapter 3 will demonstrate that MISR is capable of retrieving heights for much thinner clouds than satellite temperature.

Though the MISR sensor has relatively poor temporal resolution, its height determination method was unique enough to warrant investigation. Furthermore, since MISR is aboard the Terra sensor, MISR imagery should have time-coincident MODIS imagery (Diner et al., 1998), making a comparison of temperature and stereo height data always possible when MISR imaged a plume. Observation flight measured heights, flight observer heights, and photographic evidence were all incorporated based on availability, and the Redoubt and Augustine eruptions provided two cases in which satellite temperature, MISR, and these additional methods could be compared.

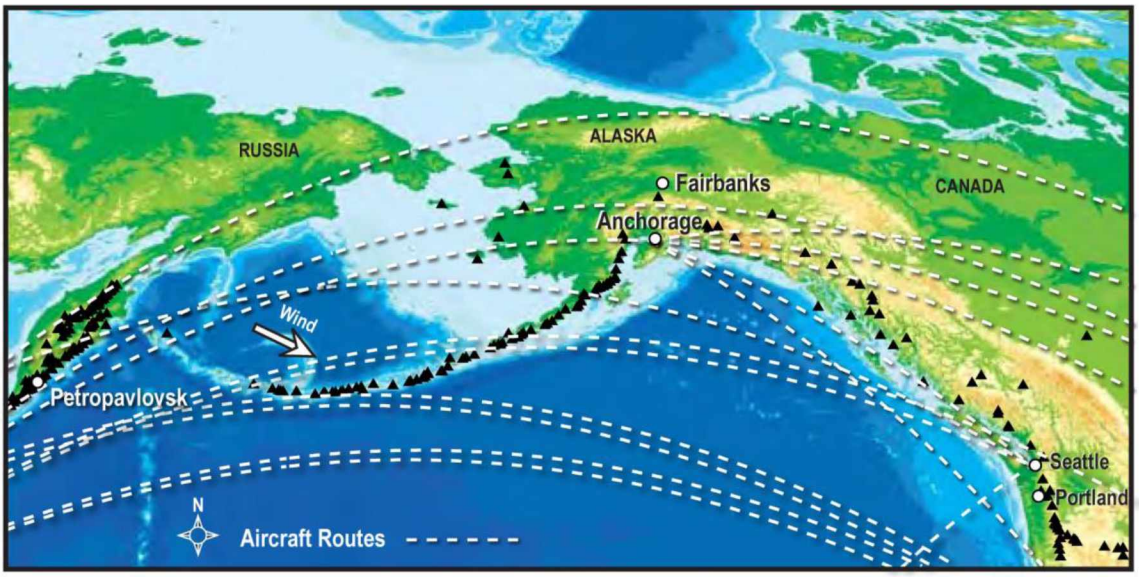

Figure 1.1: Examples of air traffic routes in the North Pacific. Not all routes are shown. The triangles represent active volcanoes. There are over 100 active volcanoes in this region, and the air traffic routes are some of the busiest in the world (Dean et al., 2002; Miller and Casadevall, 2000). Figure from Dean et al. (in press).

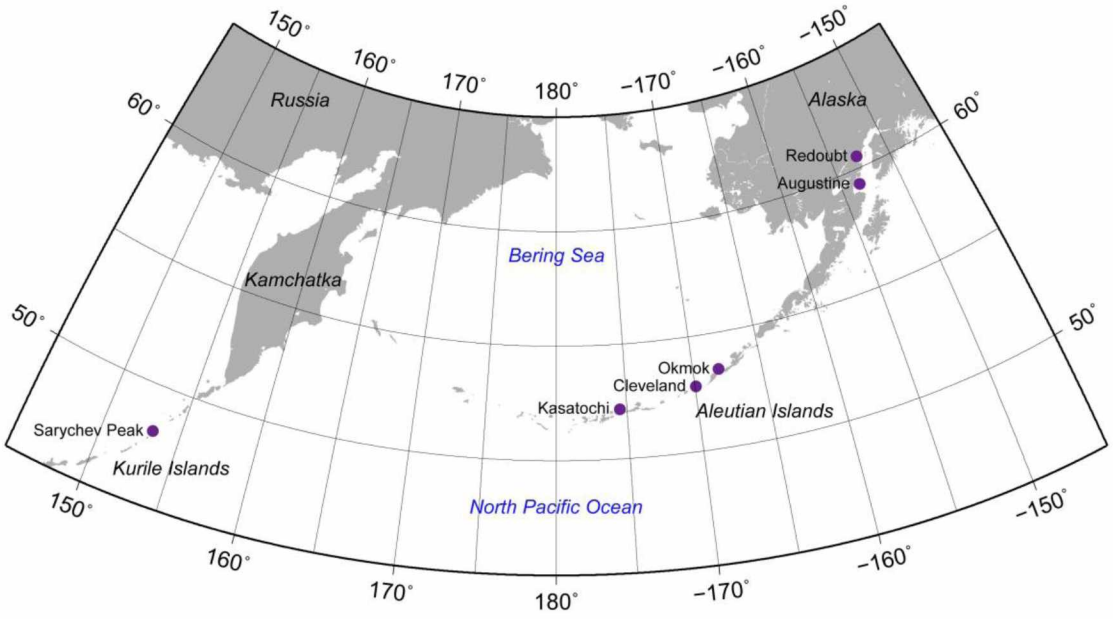

Figure 1.2: Location map of volcanoes in this study. Map area covers Alaska; the Aleutian Islands; Kamchatka, Russia; and the Russian Kurile Islands. Figure from Chapter 3: Ekstrand et al. (submitted).

Table 1.1: Common methods of height determination for volcanic plumes.

Method	Type (platform)	Effective range	Temporal resolution	Assessment of effectiveness in NOPAC
Temperature	Satellite (polar-orbiting: AVHRR, MODIS)	Swath size 2300 to 2700 km. Repeat coverage at nadir within ~1 week.	AVHRR 47-60 passes per day; MODIS 36 passes per day	Frequent data, higher resolution
	Satellite (geostationary: GOES, MTSAT)	Between the two satellites, instantaneous coverage of entire NOPAC.	~15 minutes	Near real time data, poorer resolution
Lidar	Satellite (CALIOP on AURA)	Swath size 64 km. Repeat coverage at nadir within 16 days	Less than 1 pass per day	Data extremely limited
Stereo	Satellite (MISR)	400 km common field of view. Repeat coverage at nadir within ~1 week.	2 passes per volcano per day in NOPAC	Limited data frequency; very accurate
Displacement	Satellite (GOES)	Entire NOPAC	15 minutes	Only effective for large plumes directly over vent; poor spatial resolution
Shadow	Satellite (any image with a shadow)	Depends on satellite	Depends on satellite	Limited to presence of shadows; so daytime
Radar	Ground based (USGS and FAA systems)	For Alaska's Cook Inlet, 240 to 460 km	1 to 10 minutes	Near real time data, very limited effective range
Flight observations	Aircraft; visual estimates	Sight distance	During applicable flights	Limited to times of aircraft flight
Flight measurements	Aircraft; GPS	Aircraft proximity	During applicable flights	Limited to times of commissioned aircraft flight
Ground observations	Ground, person-based	Sight distance	Person acquired based on proximity	Affective only for some volcanoes; Aleutian volcanoes too remote
Photos	Aircraft or ground, person-based or webcam based	Sight/effective camera distance	Person acquired based on proximity; webcam near constant	Person acquired same as for ground observations; Webcams also only at some locations; Both methods limited in quantitative application

Data from: Hoblitt and Schneider, 2009; Webley et al., 2009; Winker et al., 2002, 2004 and 2009; Schneider and Hoblitt, in press.

Chapter 2 A multi-sensor plume height analysis of the 2009 Redoubt eruption[1]

2.1 Abstract

During an explosive volcanic eruption, accurately determining the height of a volcanic plume or cloud is essential to accurately forecast its motion because volcanic ash transport and dispersion models require the initial plume height as an input parameter. The direct use of satellite infrared temperatures for height determination, one of the most commonly employed methods at the Alaska Volcano Observatory, often does not yield unique solutions for height. This result is documented here for the 2009 eruption of Redoubt Volcano. Satellite temperature heights consistently underestimated the height of ash plumes in comparison to other methods such as ground-based radar and Multi-angle Imaging SpectroRadiometer (MISR) stereo heights. For ash plumes below the tropopause, increasing transparency of a plume begins to affect the accuracy of simple temperature height retrievals soon after eruption. With decreasing opacity, plume temperature heights become increasingly inaccurate. Comparison with dispersion models and aircraft gas flight data confirms that radar and MISR stereo heights are more accurate than basic satellite temperature heights. Even in the cases in which satellite temperature results appeared to be relatively accurate (e.g., for plumes below the tropopause), a mixed signal of plume and ground radiation still presented a persistent issue for almost every event studied. This was true regardless of the fact that a band differencing method was used to remove presumably translucent pixels. The data presented here make a strong case for the use of data fusion in volcano

[1] Ekstrand, A.L., Webley, P.W., Garay, M.J., Dehn, J., Prakash, A., Nelson, D.J., Dean, K., Steensen, T., in review. A multi-sensor plume height analysis of the 2009 Redoubt eruption. In: Webley, P., Waythomas, C.F. (Eds.), The 2009 Eruption of Redoubt Volcano, Alaska. J. Volcanol. Geotherm. Res.

monitoring, as there is a need to confirm satellite temperature heights with other height data. If only basic satellite temperature heights are available for a given eruption, then these heights must be considered with a significant margin of error.

2.2 Introduction and background

During an explosive volcanic eruption, a primary goal of volcano monitoring is to predict the regions that may be adversely affected by an ash cloud so that local populations and aviation agencies can be notified of impending hazards. In Alaska, volcano monitoring is performed by the Alaska Volcano Observatory (AVO), a joint program of the United States Geological Survey (USGS), the Geophysical Institute (GI) of the University of Alaska Fairbanks (UAF), and the Alaska Division of Geological and Geophysical Surveys (ADGGS). AVO relies heavily on volcanic ash transport and dispersion (VATD) models which allow scientists to predict the movement of an ash cloud based on wind field data (Webley et al., 2009). Plume height (i.e., altitude above mean sea level) information is used as an input parameter for VATD models, and because wind directions and speeds often vary with altitude (known as wind shear), accurate plume height information is necessary for making accurate cloud movement forecasts (Searcy et al., 1998).

Currently, discrepancies exist between methods for plume height retrieval (Ekstrand et al., 2009; 2010). The basic satellite temperature method, which uses direct comparison of single band thermal infrared (TIR) temperatures to local temperature-altitude profiles to determine plume height (Kienle and Shaw, 1979; Sparks et al., 1997), tends to produce lower heights than methods such as satellite stereo and ground-based radar (Ekstrand et al., 2009; 2010). While this discrepancy is not significant for all eruptions (e.g., Augustine 2006, Bailey et al., 2010), some

recent eruptions in the North Pacific (NOPAC) have displayed significant discrepancies (up to ~10 km; Ekstrand et al., 2009; 2010). These discrepancies, in turn, greatly impact the ability of AVO to accurately constrain plume heights and effectively utilize VATD models.

Located in a region of heavy air traffic, the 100+ active volcanoes in the NOPAC between Alaska and Russia are potential threats to aircraft (Miller and Casadevall, 2000; Dean et al., in press), though most are in remote, difficult to monitor locations. Satellites provide frequent coverage of the entire NOPAC region, so the basic satellite temperature method is heavily used by AVO for volcano monitoring. Ground-based radar and satellite stereo methods, as described in this manuscript, have greater limits on temporal and spatial coverage. Some volcanoes (e.g., Mt. Cleveland in the Aleutians; McGimsey et al., 2011) lack seismic networks, making satellite data sometimes the sole source of information about an active eruption. Because the basic satellite temperature method is heavily relied upon, it is necessary to understand its limitations. This study aims to fulfill that objective by comparing multiple plume height retrieval methods for the 2009 eruption of Redoubt Volcano in Alaska. Redoubt is an excellent case study because of its location in the Cook Inlet region (Figure 2.1). At this location, ground-based radar and aircraft gas flight data are available for comparison with satellite stereo data, VATD models, and temperature method data.

2.2.1 The 2009 Redoubt eruption

Redoubt Volcano (60.485° N, 152.743° W; Figure 2.1) erupted explosively on March 23, 2009 after nearly 20 years of repose, and continued erupting until April 4, 2009 (Schaefer, 2012). Nineteen events were recorded for which a Volcano Activity Notice (VAN) and Volcano Observatory Notice for Aviation (VONA) were issued by AVO (Table 2.1). Seismic analysis by

AVO scientists revealed that there were actually over 30 explosive events (Table 2.1; McNutt et al., in press). After the eruptive phase of activity, the volcano transitioned to a lava dome building phase (Bull and Buurman, in press).

Redoubt is located within a region of heavy air traffic about 175 km southwest of Anchorage (Figure 2.1), which has the largest population of any Alaskan city (nearly 300,000 people in the Anchorage metropolitan area; U.S. Census Bureau, 2010), and has the fifth largest airport in cargo transit in the world (Airports Council International, 2011). During the Redoubt eruption, commercial flights from area airports, as well as activity at Elmendorf Air Force Base in Anchorage, were halted (Dean et al., 2009; Riccardi and Glascock, 2009). Most plumes during this period were products of explosive eruptions, however, on April 4, 2009, an ash plume developed from lava dome collapse (Webley et al., in press), creating a lahar. The lahar traveled down the Drift River Valley towards the Drift River Oil Terminal, threatening the terminal (Carlisle and Nelson, 2009).

2.3 Methods of height determination, datasets, and sensors

In this study, four height retrieval methods are considered: (1) aircraft gas flight observations, (2) ground-based radar, (3) satellite-based stereo height analysis, and (4) the basic satellite temperature method. Of the above, all are used operationally for volcano monitoring purposes within AVO except stereo height analysis, with emphasis on satellite and radar methods. In addition, results from the Puff VATD model (Searcy et al., 1998) are included, which allowed comparisons of model wind results to known volcanic ash trajectories.

2.3.1 Gas flight heights

During the Redoubt 2009 eruption, gas observation flights were conducted in a fixed-wing aircraft at Redoubt Volcano. AVO and the USGS Cascades Volcano Observatory scientists used in-situ and remote instrumentation to measure the plume composition and calculate emission rates of carbon dioxide (CO_2), sulfur dioxide (SO_2), and hydrogen sulfide (H_2S) gases (personal communication, T. Lopez). The gas flight observations described in this manuscript were obtained from Werner et al. (in press). Height information and position from gas flights was obtained from a Global Positioning System (GPS) receiver at 1-second intervals (1 Hz frequency; personal communication, P. Kelly).

2.3.2 Ground-based radar heights

Radar systems send out radio waves and detect the reflected signal from volcanic particles. Such systems are able to provide information about volcanic plumes, including column height, in most weather conditions (Rose et al., 1995; Marzano et al., 2006a, b; 2010; Wood et al., 2007). Larger particle sizes (on the order of 1-2 mm or greater), or higher concentrations, theoretically cause greater reflectivity (Rose et al., 1995; Wood et al., 2007). For volcanic ash, a C-band system (~6GHz or λ=5 cm) loses signal in about 30 minutes (Rose et al., 1995), and an S-band system (~3GHz or λ=10 cm) loses signal in about 90 minutes (Wood et al., 2007). Additionally, Rose et al. (1995) noted that since the top of the eruption column may not contain coarse ash, it may not be detected, and radar may underestimate the overall height.

The ground-based radars used to detect the Redoubt 2009 eruption plumes were the Federal Aviation Administration's (FAA's) Next Generation Radar (NEXRAD) Doppler radar system, and the USGS's Doppler radar system. The USGS radar (a movable system) was located at the

Kenai Municipal Airport, 82 km east of Redoubt (Figure 2.1). The FAA NEXRAD system is located slightly north (~25 km) of the USGS system (Figure 2.1). The USGS radar system operates in the C-band and has a maximum effective range of 240 km. The FAA NEXRAD system operates in the S-band and has a maximum effective range of 460 km (Hoblitt and Schneider, 2009; Schneider and Hoblitt, in press). Further specifications for each system are given by Schneider and Hoblitt (in press).

Both the USGS and NEXRAD systems detected the developing ash plumes during the Redoubt eruption, though the USGS system scanned a 45-degree sector centered on Redoubt Volcano, allowing for higher temporal resolution (Hoblitt and Schneider, 2009; Schneider and Hoblitt, in press). The NEXRAD system scanned a full 360 degrees, taking 4 to 10 minutes to rescan the same location. Only the highest altitude measurement for each major eruptive event was provided for use in this study.

2.3.3 MISR stereo heights

The Multi-angle Imaging SpectroRadiometer (MISR) sensor has been used to study many plume types, including forest fire plumes, and volcanic plumes (Kahn et al., 2007; 2008; Mims et al., 2009; Scollo et al., 2010; Val Martin et al., 2010). The sensor has been acquiring data since early 2000 and is aboard the National Aeronautics and Space Administration's (NASA's) Terra satellite (Diner et al., 1998). MISR acquires near-simultaneous (within 7 minutes) views of a given location via nine different cameras positioned at various view angles (Table 2.2). The MISR INteractive eXplorer (MINX) software is an Interactive Data Language (IDL)-based program designed for the processing and viewing of MISR images, and contains built-in plume

processing utilities (Nelson et al., 2009). The open source software is available from the Open Channel Foundation (2010).

MINX allows the user to manually define a region containing a plume and specify an associated wind direction that represents the expected transport direction of volcanic particles. MINX uses a correlation matcher among six different camera pairs to calculate the best-fitting height and wind speed at 1.1 km spatial resolution, using data from the 275 m resolution MISR red band (Table 2.2). Because feature propagation in the direction of satellite motion (along-track) aliases with the stereo-derived heights (Moroney et al., 2002), the wind speed and direction are used to correct the retrieved (zero wind) stereo heights determined from the stereo matching alone. The vertical resolution of the operational MISR heights, which use a faster but less accurate pattern matcher, is approximately 560 m with good agreement with validation data (e.g., Garay et al., 2008). Based on this, the effective vertical resolution of the MINX height retrievals is expected to be on the order of 100 to 200 m. Studies have shown that MINX works best for relatively dense, well-defined plumes (Mims et al., 2009).

2.3.4 Basic satellite temperature method heights

At AVO, the satellite sensors most commonly used for basic temperature height retrievals are the Advanced Very High Resolution Radiometer (AVHRR) sensors aboard the National Oceanographic and Atmospheric Administration (NOAA) satellites, and the Moderate Resolution Imaging Spectroradiometer (MODIS) sensor on NASA's Terra and Aqua satellites (Table 2.2). For the NOPAC, about 47-60 AVHRR overpasses, and 36 MODIS overpasses, are acquired per day (Webley et al., 2009).

The basic temperature method involves analysis of a single band of TIR satellite imagery – the 11 μm channel – to determine the brightness temperature of the coldest pixel in a volcanic plume. Assuming the plume is in thermal equilibrium with the surrounding atmosphere and the temperature of the atmosphere decreases with height (i.e., the plume is lower in altitude than the tropopause), this coldest pixel is expected to correspond to its maximum height. Local atmospheric temperature profiles are used to determine the relationship of temperature to altitude for a given region. This method is referred to here as the "basic satellite temperature method." It may also be referred to simply as the "temperature method" and the associated heights referred to as "temperature heights" or "temperature retrieved heights."

Temperature measurements of the upper atmosphere are obtained from radiosonde measurements (i.e., soundings). Worldwide observations from various locations transmit data on temperature, pressure, humidity, and winds up to an altitude of ~30 km ASL twice a day at 00 and 12 UTC (Simpson et al., 2000). Radiosonde data used by AVO are obtained from the University of Wyoming's College of Engineering's Department of Atmospheric Science online sounding database. Soundings are used in this study to closely approximate AVO's operational process – they are used during eruption response – and because they represent the observed temperature profile with height rather than a profile produced by a model, which may be overly smooth and contain additional uncertainties (e.g., Garay et al., 2008).

Basic satellite temperature heights may not be accurate for several reasons. Heights may be inaccurate for the initial eruption column above the vent due to possible undercooling (when the initial plume is colder than the surrounding atmosphere; Kienle and Shaw, 1979; Woods and Self, 1992; Sparks et al., 1997). There is also typically a temperature inversion at the tropopause, at

which temperature begins increasing with height (or becomes isothermal), instead of decreasing, making it difficult to determine the basic temperature height of volcanic plumes at stratospheric altitudes (Woods and Self, 1992; Woods, 1995; Graf et al., 1999; Tupper and Wunderman, 2009). Since the tropopause often acts as a barrier to a rising eruption column (Sparks et al., 1997), it has been argued that the altitude of the tropopause may have a significant effect on the maximum altitude plumes will attain. According to Dean et al. (2002), most of the ash clouds observed in the NOPAC in the last 14 years have a maximum altitude less than 10 km ASL, with the maximum height typically constrained by the temperature inversion at the tropopause. During the 2009 eruption of Redoubt, the tropopause was located between about 9 and 10 km ASL based on soundings from Anchorage, Alaska.

If the atmosphere is isothermal (constant temperature), or if there is an inversion present, temperatures may correlate to more than one height (Woods and Self, 1992; Garay et al., 2008). Due to this ambiguity, Woods and Self (1992) argue against the use of the basic temperature method. Theoretically, if it cannot be determined if a plume is stratospheric or tropospheric based on temperature alone, the ambiguity could perhaps be resolved with the shadow method, which uses sun angle and shadow length to calculate the height of a plume (Holasek and Self, 1995). In this study, however, no images contained shadows. Note that Pavolonis (2010) describes a more sophisticated and detailed, but robust, approach to retrieving ash plume and cloud information from satellite IR radiances in multiple spectral bands, but this technique was not explored in this study.

The basic temperature method also depends on the accuracy of the temperature obtained from satellite data, and, thus, only works for opaque plumes or clouds that are dense enough that

underlying ground radiation does not reach the satellite sensor (Schneider et al., 1995; Dean et al., 2002). For example, if ground radiation penetrates an ash plume (i.e., if the plume is transparent or semi-transparent), the temperature of the pixel will be warmer than the ash plume itself, and the heights retrieved will be lower than the true height of the plume for a plume below the tropopause, and higher for a plume above the tropopause (Sparks et al., 1997; Simpson et al., 2000). Volcanic ash plumes undergo a natural evolution from opaque, to semi-transparent, to transparent as they disperse (as they move away from the vent to travel as ash clouds; Schneider et al., 1995; Dean et al., 2002). To account for this effect, in this study a band differencing method of ash detection was used as a proxy for plume opacity, because the method should "detect" ash (i.e., produce a negative signal) only if the ash plume is at least semi-transparent. This method (Prata, 1989a, b) is widely used by volcanologists and is known by various names such as: brightness temperature difference (BTD), apparent temperature difference, split window, and reverse absorption. In this study, the method is referred to as BTD.

In the BTD method, 12 μm band brightness temperatures (TIR values) are subtracted from 11 μm band brightness temperatures (Table 2.2). This technique works because meteorological clouds absorb more radiation in the 12 μm wavelength range than they do in the 11 μm wavelength range, and differencing these temperatures produces a positive BTD (Prata, 1989a, b), while ash absorption behaves in the opposite manner for these wavelengths, so differencing these temperatures produces a negative BTD (Prata, 1989a, b). This technique works best for a plume composed of fine ash, in a relatively dry environment (Simpson et al., 2000). Under these ideal circumstances, a negative BTD is produced only when a volcanic emission is transparent and contains ash. A positive or zero BTD is produced only when the volcanic emission is opaque, or does not contain ash (e.g., steam plumes; Prata 1989a, b; Simpson et al., 2000; Prata et al., 2001).

In this study, pixels with a negative BTD were assumed to be at least semi-transparent, and therefore not suitable for basic temperature height analysis.

The BTD method works well only under certain circumstances, so this technique provides only an approximate indicator of plume and pixel opacity or transparency. Many studies, including Prata (1989a, b), Wen and Rose (1994), and Rose et al., (2000) argue that the method only detects fine ash ~3 to 5 μm or smaller. Rose et al. (2000) also argue that fine ash comprises only a few percent of the total mass of a volcanic plume, meaning that the BTD method will not necessarily detect the plume until coarse ash falls out. Furthermore, water and/or ice coating an ash particle can mask the ash signal and cause the retrieval to report the pixel as water or ice (Prata, 1989a, b; Simpson et al., 2000; Prata et al., 2001; Pavolonis et al., 2006). False signals can also be generated, and Webley et al. (2009) provide an overview of these effects for the NOPAC region. These false signals are well understood (Simpson et al., 2000; Prata et al., 2001), and do not present an issue in this study. Note that the BTD method is only used as a filter for the analyzed images: it removes pixels assumed to be transparent but does not alter the pixels left behind.

2.3.5 Puff VATD model heights

The Puff VATD model is a Lagrangian dispersion model developed for tracking young eruption clouds (less than about 48 hours old; Searcy et al., 1998). Puff models the dispersion of hypothetical particles of a specified grain size distribution, height, and column shape in a 4-dimensional (latitude, longitude, height, and time) gridded wind field, and tracks the movement of these particles (Papp et al., 2005). Because accurate height information is so difficult to acquire (Searcy et al., 1998), the dispersion of ash particles is modeled from the summit altitude to a maximum height specified by the user.

By comparing Puff results with satellite imagery, the height of an ash cloud or plume can be constrained. Satellite imagery that shows the transport direction of the volcanic emission can be compared to a Puff run that outputs possible ash dispersion for particles injected from the surface to the user-specified maximum height. If the wind model used by Puff is accurate, a particular horizontal extent of the ash dispersion area in the Puff results should match the extent of the volcanic emission in the satellite imagery, and this extent will correlate to a range of injection heights in the model. Wind shear must be present for this method to work, or heights will be poorly constrained (Searcy et al., 1998).

2.4 Satellite imagery processing

2.4.1 MISR processing

During the 2009 Redoubt eruption, only two MISR images that contained plumes and lacked cloud cover were available for analysis (Table 2.3). Once acquired, the terrain-projected data were processed using the "Process Plumes" utility in the MINX software. Two versions of the MINX software were used in this analysis: the currently released version 1.2 (Nelson et al., 2009), and a development version 2.0. Results from both are reported here.

2.4.2 AVHRR and MODIS processing

AVHRR and MODIS (TIR) data were subset into predefined sectors (as used operationally at the AVO Tools Website) containing Redoubt Volcano, converted from their storage format to Hierarchical Data Format (HDF), and georeferenced using ENVI, an IDL-based raster data processing package. BTD results were calculated for each image. Satellite images with no

coverage of Redoubt were removed from the dataset. Images which contained plumes that were not noticeably covered by meteorological clouds based on visual analysis, and were not cut off by the edge of the satellite field of view, were retained for analysis (Table 2.3). This included several images in which a plume was visible above the cloud deck in fairly cloudy conditions. Each plume was delineated using the 11 μm data. Band math (mathematical operations performed on entire satellite image bands) was then performed with the following operation to ensure that only opaque pixels were used:

$$(BTD\ band > 0) * 11\ \mu m\ band \quad (1)$$

This operation selects the pixels in the BTD band with values greater than zero. It assigns to those pixels a value of 1, and all other pixels a value of zero. This band of ones and zeroes is multiplied with the 11 μm band, resulting in an 11 μm band in which pixels with a negative BTD (supposedly transparent pixels) have zero values, eliminating them from temperature height analysis. The results of this operation were extracted for the delineated plume area and stored for further analysis.

AVHRR and MODIS overpasses which were close in time to selected MISR overpasses were analyzed for comparison between temperature and stereo height methods. Overpasses with no corresponding MISR image were also retained for in-depth analysis of the basic satellite temperature method. Imagery was selected to correspond to days during the eruption which had significant explosive activity (Tables 2.1, 2.3). Data analyzed include both very large and very small events (based on seismic pressure, see Table 2.1). Select representative results are included here.

Temperature data were converted to height using environmental lapse rates calculated from atmospheric soundings from Anchorage, Alaska (PANC) acquired as close in time to each image as possible. The lapse rate calculation assumes a ground surface temperature of 0°C, which is reasonable for this time of the year in the NOPAC, and in agreement with the sounding data.

2.4.3 Analysis of satellite derived plume heights

To analyze the results, heights and geographic coordinates from AVHRR, MODIS, and MISR were imported together into ArcInfo, a geographic information system (GIS) software package for spatial analysis. The three-dimensional (3D) data were displayed over a digital elevation model (DEM) of the Redoubt area in ArcScene. This DEM was generated using data from the Advanced Land Observing Satellite (ALOS) Panchromatic Remote-sensing Instrument for Stereo Mapping (PRISM) sensor. The data were acquired on September 21, 2009, and have a 2.5 m spatial resolution. The data were obtained from UAF's Alaska Satellite Facility, and are © JAXA 2009.

Three-dimensional GIS analysis was used in combination with analysis of two-dimensional (2D) graphs. These 2D graphs were created by using IDL to calculate the great circle distance between the location of each plume height retrieval and the location of the vent, and then plotting the height retrievals against these distances in Excel. The Hybrid Single Particle Lagrangian Integrated Trajectory (HYSPLIT) model, which uses numerical reanalysis wind field data to determine the origin time and location of a given airborne feature (Draxler and Hess, 1997; Draxler and Hess, 1998; Draxler, 1999), was used to run back trajectories when more than one explosive event may have produced the plume in question. HYSPLIT back trajectories were run

from the NOAA-operated HYSPLIT website (Draxler and Rolph, 2012), and this analysis determined from which explosive event each plume originated (Tables 2.1, 2.4).

2.4.4 Puff VATD model height analysis

A Puff model was run for each eruptive event analyzed by the above methods. HYSPLIT back trajectories confirmed eruption start times, and the corresponding times from seismic analysis were used as input parameters for Puff model runs. These runs used the NOAA NCEP/NCAR reanalysis wind field (Kalnay et al., 1996), a Poisson column distribution, and a column height range from 3.1 km (vent altitude) to 18 km ASL. The results were compared with satellite imagery to determine which portion of the ash cloud in the model corresponded to the observed cloud. The height range of the model with this same extent was then considered to be a reasonable height range for the ash cloud.

2.5 Results

2.5.1 Maximum TIR temperature heights compared to maximum radar heights

Figure 2.2 plots operationally obtained (from daily satellite report data) maximum basic satellite temperature heights and radar heights for each of the 19 official eruptive events. For 12 of 14 events with temperature data, ground-based radar produced higher maximum altitudes than AVHRR and MODIS temperature retrievals. As stated in section 2.3.2, limited radar data were made available to this study, and only the maximum radar height results for each event are shown here, rather than the radar height results obtained closest in time to the satellite overpass.

The coldest temperature was used to retrieve the temperature height for each event. In Figure 2.2, the bottom error bar shows the lowest possible height to which this temperature corresponds, while the top error bar shows the maximum possible height to which this temperature corresponds. The red triangle between the error bars represents the mean of the two temperatures. The tropopause was usually located between the two error bar extremes; when the temperature results were higher than the tropopause altogether (events 8, 10, and 19), it was because the atmosphere displayed an atypical temperature profile with no temperature inversion at the tropopause.

In all cases, the average and tropospheric satellite temperature heights were lower in altitude than the radar results. In some cases, the average or stratospheric heights overlapped the radar results, or were very close to the radar results. However, there was typically a difference of at least a few kilometers between satellite temperature heights and radar heights (Figure 2.2). Note that if the tropopause were indeed a significant barrier to the penetration of ash plumes from Redoubt, there would be no radar retrievals at heights within the stratosphere.

2.5.2 TIR temperature heights compared to stereo heights

On April 1 and 5, time-similar MISR, AVHRR, and MODIS data allowed a detailed comparison of the plume heights from both basic temperature and stereo methods (Tables 2.3, 2.4). On April 1, eruptions occurred at 00:07 UTC and 03:46 UTC (Tables 2.1, 2.4), while satellite imagery was acquired between 21:30 and 22:10 UTC (Tables 2.3, 2.4). On April 5, an eruption occurred at 18:36 UTC (Tables 2.1, 2.4), while satellite imagery was acquired between 21:00 and 21:30 UTC (Tables 2.3, 2.4). For April 5, no MODIS image was available due to processing difficulties. On both days, plumes were fairly small, and the volcano appears to have transitioned to a phase of

continuous ash emission and degassing by the time of image acquisition. Meteorological cloud cover was minimal and satellite views were mostly clear. For the April 5 imagery, a HYSPLIT back trajectory shows that the material at the farthest extent of the plume came from the vent around the time of the initial eruptive blast at 18:36 UTC, roughly three hours prior to image acquisition.

For both the April 1 and April 5 imagery, the heights were most similar near the vent. However, farther away from the vent, MODIS and AVHRR heights were much lower in altitude than the MISR heights (Figures 2.3, 2.4; Table 2.4). For the April 1 plume, retrieved heights are shown in Figure 2.3 and Table 2.4. AVHRR, MODIS, and MISR height retrievals do not align at the vent in Figure 2.3a due to a slight georeferencing issue in AVHRR data; however this is minor and does not affect the comparison here. AVHRR, MODIS, and MISR height retrievals show a similar maximum altitude near the vent of ~3 to 3.5 km ASL, which is close to the altitude of the Redoubt summit, at ~3.1 km ASL. For AVHRR and MODIS imagery, retrieved heights dropped steadily from the vent and leveled out at a distance of ~30 km from the vent to maxima of ~1 km and ~0.7 km ASL, respectively. This leveling off of the retrieved plume heights occurred over an ocean background. For MISR, retrieved stereo heights had a maximum slightly above vent altitude (~3.4 km ASL) and dropped to ~2.4 km ASL at a distance of 40 to 50 km from the vent. Compared to AVHRR and MODIS heights, MISR heights remained relatively constant with downwind distance.

For the April 5 plume, retrieved heights are shown in Figure 2.4 and Table 2.4. For AVHRR imagery, retrieved heights near the vent were at a maximum of ~3.1 km ASL, almost exactly the same height as the summit itself. Retrieved heights dropped steadily from the vent to a distance of

~30 km away from the vent, where they leveled out over an ocean background, similar to the April 1 results, to a maximum retrieved height of ~1.2 km ASL. For MISR, retrieved stereo heights had a maximum altitude over 1 km greater than the AVHRR data (~4.4 km ASL), with the exception of an outlier point at ~5 km ASL. MISR retrieved heights remained relatively constant with downwind distance, dropping to ~4.2 km ASL over the plume length. Airborne photographic imagery was available for the April 5 plume, and this imagery showed no discernable drop in altitude of the eruption plume as it drifted from the vent (Figure 2.4c). The satellite imagery was acquired roughly 5-6 hours after the gas flight and photograph acquisition, and Puff VATD model runs showed that in this time, wind fields remained fairly consistent.

2.5.3 Variations and trends in TIR temperature heights

In none of the following analyzed cases did the basic temperature method analysis retrieve heights greater than 9 to 10 km ASL. The variation of maximum and minimum retrieved plume heights is included in the following results. Note that these results are representative of the larger dataset.

March 23, 2009, AVHRR acquisitions at 13:25 UTC, 14:30 UTC, 16:06 UTC, and 17:44 UTC imaged a plume that originated at 12:30 UTC, based on HYSPLIT back trajectory analysis. Figure 2.5 and Table 2.4 show the March 23 height results. Meteorological cloud cover was significant in all images, though the plume was clearly visible above the cloud deck. The retrieved maximum altitude dropped with each subsequent image (Figure 2.5b-e), and, in all images, the edge of the plume was apparently at a lower altitude than the center of the plume (Figure 2.5a). The retrieved minimum plume height dropped a bit in each image, but not significantly.

Imagery at 13:25 UTC produced maximum retrieved heights of ~9.6 to ~10.2 km ASL, with a low point at ~8.8 km ASL (Figure 2.5b). Retrieved heights for the "bottom" of the plume (the lowest retrieved heights, not necessarily the true plume bottom) were relatively constant, at a height of ~7.7 km ASL. Imagery at 14:30 UTC produced maximum retrieved heights of ~9.3 to ~10 km ASL, with a low point at ~8.8 km (Figure 2.5c). Retrieved heights for the bottom of the plume were relatively constant, at a height of ~8 km ASL. Imagery at 16:06 UTC produced maximum retrieved heights which varied with distance (Figure 2.5d). Retrieved heights for the plume top were ~5.9 km ASL near the vent, ~8.9 km ASL at the maximum height (mid plume), and ~7.4 km ASL at the farthest plume extent. Retrieved heights for the plume bottom varied from a low of ~4.6 km ASL near the vent, to retrieved heights between ~6 km and ~7 km ASL at the farthest plume extent. Retrieved heights varied the most for imagery at 17:44 UTC (Figure 2.5e). Maximum retrieved plume top heights were ~7.5 km ASL near the vent, ~8.4 km ASL at ~175 km from the vent (mid plume), and ~ 7.1 km ASL at the farthest plume extent. Minimum retrieved plume top heights were between ~5.5 and ~6.2 km ASL. Maximum retrieved plume bottom heights were ~6.7 km ASL near the vent, ~5.8 km ASL at ~175 km from the vent (mid plume), and ~5.4 km ASL at the farthest plume extent. Minimum retrieved plume bottom heights ranged from ~4.6 to ~5 km ASL.

Between images, the retrieved maximum plume top height dropped about 2 km in altitude, and the retrieved plume bottom height dropped about 4 km in altitude. With time and distance from the vent, the plume heights displayed some increased scatter, though the scatter was not significant.

April 4, 2009 imagery consisted of one major event which originated from a lava dome collapse (Schaefer, 2012). This eruption contained two pulses, one at 13:57 UTC and another at 14:16 UTC (Tables 2.1, 2.4). Material from both events combined to make a single plume. Figure 2.6 and Table 2.4 show the April 4 height results. The ash was visible in AVHRR images at 14:45 UTC, 16:23 UTC, 17:03 UTC, and 19:17 UTC. The retrieved heights dropped significantly between subsequent images (Figure 2.6c-f). In all images, meteorological cloud cover was sparse, and present only on the east side of the plume.

Imagery at 14:45 UTC produced maximum retrieved heights near the vent of ~9 km ASL, and these heights decreased to ~8.6 km ASL with distance from the vent (Figure 2.6c). Retrieved heights for the plume bottom were fairly consistent at ~5.8 km ASL. Imagery at 16:23 UTC produced maximum retrieved heights of ~5.1 to ~6 km ASL (Figure 2.6d). There was no consistent plume bottom, however, with some height retrievals as low as ~0.9 km ASL, and others as high as ~3.5 km ASL. Imagery at 17:03 UTC produced maximum retrieved heights of ~5 km ASL near the vent, which decreased to ~2.3 km ASL at a distance of ~75 km from the vent, then increased to ~4.8 km ASL at mid plume (200 km from the vent) and decreased again to ~3.1 km ASL at the maximum plume extent (Figure 2.6e). The plume bottom was incredibly variable in retrieved height (displaying significant scatter), with some points as low as 94 m (0.094 km) ASL. Most heights for the plume bottom clustered between 0.6 km and 1.6 km ASL. Imagery at 19:17 UTC produced very scattered results (Figure 2.6f). There was significant variability in the plume bottom and the plume top altitudes. Maximum retrieved plume top heights ranged from ~1.4 km to ~3.2 km ASL. Retrieved heights for the plume bottom ranged from ~0.3 km to ~1.2 km ASL, with most height retrievals between 0.3 and 1 km ASL.

Between images, the retrieved maximum plume top height dropped ~6 km, from ~9 km ASL at 14:45 UTC to ~3 km ASL at 19:17 UTC. The plume bottom dropped from ~5.8 km to (near) ground level. The plume displayed significant scatter, much more than the March 23 plume, and dropped in retrieved height more rapidly, and to lower heights.

Images from 16:23, 17:03, and 19:17 UTC displayed an interesting feature: a quick drop from a higher retrieved altitude to a lower altitude in the first few kilometers of plume length (Figures 2.6b, 2.6d-f). This is very similar to the quick drop in altitude seen in AVHRR and MODIS data from April 1 and 5 (Figures 2.3, 2.4). In 16:23 and 17:03 UTC imagery, the drop was from ~5 km ASL to ~1 and ~2.3 km ASL, respectively. In the 19:17 UTC image, the drop was from ~2.1 to ~0.8 km ASL. Retrieved heights leveled out or changed again where the drops "ended," about 30 km from the vent.

2.5.4 Gas flight heights

Gas flight height results were available for comparison with April 4 and 5, 2009 satellite imagery. Gas flight data were acquired ~5-6 hours after the satellite acquisitions, and for both days, Puff VATD model runs showed that wind fields did not change significantly in this time frame, making a comparison of the two datasets reasonable. Gas flight data provided plume top and bulk ash altitudes. No information was given on plume bottom. For comparison with April 4 satellite imagery from AVHRR (Figure 2.6; Table 2.4), gas flight data from ~00:30 UTC on April 5 showed that the plume top was at least (and not much greater than) 4.1 km ASL in altitude at a distance of 11.8 to 12.3 km from the summit. The bulk of the plume was at ~3.5 km ASL. The latest (AVHRR) image analyzed on April 4 was acquired at 19:17 UTC (later images were available, but the plume was so poorly delineated it was unable to be analyzed). Here, at a similar

distance from the vent to the acquired gas flight height, the AVHRR analysis showed the plume to be no higher than 2 km ASL, with the bulk of the plume concentrated at an even lower altitude of ~1 km ASL. This was significantly lower than the heights reported from the gas flight.

For comparison with April 5 satellite imagery from AVHRR and MISR (Figure 2.4; Table 2.4), gas flight data from ~00:00 UTC on April 6 showed that the plume top was at least (and not much greater than) 4.1 km ASL, at a distance of 26.4 to 27.5 km from the summit (for comparison to these distances, the Cook Inlet is approximately 30 km from the summit of Redoubt). The bulk of the plume was at ~3.8 km ASL. For April 5 satellite imagery, at a similar distance from the vent to the reported gas flight height, MISR showed the plume top to be ~4.1 km ASL, with the bulk of the plume between ~3 and 4.1 km ASL, while AVHRR data showed the plume to be ~1.5 km ASL. The MISR retrievals agreed well with the gas flight heights, while the AVHRR retrievals did not.

2.5.5 TIR temperature heights compared to Puff heights

Puff VATD model results produced a range of heights (Table 2.4). For each event, the range of heights extended to a greater altitude than the maximum satellite temperature heights. For most Puff model runs, significant wind shear was present. This allowed the height to be determined with some precision, and also demonstrated how significantly the dispersion of ash could change with altitude. However, for the April 4 event, wind shear was not significant, and the range of possible heights was poorly constrained.

2.5.6 TIR temperature heights compared to volcanic ash retrieval code

It would be extremely useful to have a quantitative reference by which to judge the reliability of the temperature heights. Without such a reference, the accuracy of a basic temperature height retrieval can only be estimated. Steensen et al. (in press) conducted analysis of the Redoubt 2009 eruption using the Volcanic Ash Retrieval (VAR) code (Wen and Rose, 1994). A comparison of these VAR results (including optical depth, ash mass, pixel mass, and particle radius) with maximum heights was performed for a small number of plumes for which both VAR and temperature method height results were available. A positive, relatively linear, correlation between optical depth and maximum height was obtained, with plumes of higher TIR optical depth giving higher, and presumably more reliable, heights (Figure 2.7). Plumes of lower optical depth gave apparent underestimates of height. The number of data points was extremely limited, and further analysis is necessary to confirm this trend. Furthermore, optical depth itself can depend on many factors. These results may be more complex than they seem, and the results documented here simply suggest a possible relationship that warrants further investigation.

2.6 Discussion

The first, and one of the most important observations made is that the data showed a significant discrepancy between basic satellite temperature method heights and ground-based radar heights (Figure 2.2). Satellite temperature results offered only one certainty: the plume was at least as high as the lowest altitude (the tropospheric altitude) to which the retrieved temperature corresponded. Without another method to determine whether the plume top was in the troposphere or the stratosphere, it cannot be definitively stated that the plume was higher than this tropospheric height, only that it was at least this high. In every case, radar height retrievals were higher than the tropospheric temperature height retrievals. In every case, radar height retrievals

were also higher than the *average* temperature height retrievals (represented by the red triangles in Figure 2.2).

For event 10 in Figure 2.2, the average temperature height retrieval was very close to the radar height result. For events 2, 12, 14, 18, and 19, the stratospheric temperature height retrievals were very close to at least one of the radar results. For event 4, the radar height retrieval fell between the average and stratospheric temperature height retrieved. Event 3 was a combination of the two previous results, with one radar height retrieval between the average and stratospheric temperature height retrievals, and one radar height only slightly above the stratospheric temperature height retrieval. For events 5, 6, 8, 11, 12 (one radar height), and 15, radar height retrievals were significantly greater than even the stratospheric temperature height retrievals. For events 12 and 14, one radar height was similar to the stratospheric temperature retrieval, and another was much greater.

If the only definitive result of a basic temperature height retrieval is to produce a minimum height for the plume, then based on the above analysis, this minimum height (the only definitive one in the absence of other methods) was always lower than radar height retrievals for the same plume. But to what was this difference due?

One possibility is the difference in temporal resolution between sensors; radar may retrieve heights for an overshooting plume not observed by the satellite during its overpass. This suggests that the results would be in better agreement if radar observations closest in time to satellite acquisition (data not available in this study) were used, rather than using maximum radar heights. The satellite and radar acquisitions closest in time (~6 minutes) were for event 10, which showed

good agreement between the basic temperature method and radar height retrievals. However, event 6, similar in time (~10 minutes) for satellite and radar acquisition, had the poorest agreement. Furthermore, event 4, which had a long time interval between satellite and radar acquisitions (~80 minutes), showed good agreement between results.

Thus, there was no clear pattern between temporal resolution and agreement of the two methods. Furthermore, to systematically analyze whether temporal resolution had an effect on these results, a time series of radar data would be needed, rather than the limited data available here. Based on these results, the effect of temporal resolution is, at best, unclear. However, other results, discussed below, suggest that basic temperature method height retrievals indeed underestimated the height of volcanic plumes, and that this discrepancy is, at least in part, inherent to the method. Furthermore, satellite-based Cloud-Aerosol Lidar with Orthogonal Polarization (CALIOP) and Microwave Limb Sounder (MLS) data showed that eruptive material from Redoubt was observed at stratospheric altitudes sometimes days after eruption (personal communication, Mike Fromm; Carn et al., 2011). However, this material was not detected by satellite temperature analysis, and there must be an explanation for this.

Like radar, MISR stereo height retrievals were consistently higher than AVHRR and MODIS temperature method height retrievals. For both April 1 (Figure 2.3, Table 2.4) and April 5 (Figure 2.4, Table 2.4) results, temperature height retrievals were closer to MISR results near the vent, but "dropped" in retrieved altitude away from the vent. No such drop was seen in photographic imagery from April 5 (Figure 2.4), and gas flight data from this day showed that the plume was at least 4.1 km ASL at a distance of 26.4 to 27.5 km from the vent. According to the Puff VATD model, the wind fields did not change significantly in the time between satellite, photographic,

and gas flight acquisition, so this comparison between data sources is a fair one. Thus, this "drop" in altitude was an artifact of the method, not an actual drop in altitude, and these results suggest that MISR retrievals are more likely to retrieve accurate plume heights.

If this drop in height was artificial, the validity of the other significant "drops" in AVHRR data from March 23 and April 4 is then called into question. Based on analyzed imagery, March 23 temperature retrieved maximum plume top heights dropped ~2 km over ~4.5 hours, and April 4 temperature retrieved maximum plume top heights dropped ~6 km over ~4.5 hours. The temperature retrieved heights reached as low as ~2-3 km ASL on April 4 at 19:17, though ~5-6 hours later, gas flight data showed the height of the plume to be greater than 4 km ASL (again, Puff showed little wind field change in this time frame, and there was no new eruptive blast). Furthermore, frequently seen in the data on most days were plumes with edges lower in retrieved height than plume centers (as in Figures 2.5a-c, 2.6a). Additional cases not included here also showed this feature, and this drop in edge height can be seen easily in the 3D figures.

These "drops" in height occurred for plumes on different days, of different extents and thicknesses, with different content and particle sizes (e.g., April 4 fall deposits contained finer ash content than plumes from other events; Wallace et al., in press). The one thing that all plumes had in common is that they were undergoing dispersion and fallout. All plumes analyzed dropped in altitude with time and distance from the vent, whether it occurred over multiple images (March 23, April 4), or within one image (April 1 and 5). Plume edges, which also had lower retrieved heights, were more dispersed than plume centers in many cases, as plume edges are more easily able to disperse, and the ash was likely optically thinner.

Puff results (Table 2.4) confirmed that these basic temperature retrieved heights were not accurate. While March 23 temperature retrieved heights had a maximum of 10.2 km ASL, Puff results showed that the plume extent was likely between 6 and 15 km ASL. While April 4 temperature retrieved heights had a maximum of 9 km ASL, Puff results showed that the plume could have been as high as 15 km ASL. April 1 and 5 plumes showed maximum temperature retrieved heights around 3 km ASL, and significant height drops, while Puff showed results of 4-5 km ASL or less. Puff is, indeed, a model, and while models may not be perfect representations of reality, in these cases the modeled plumes were in better agreement with radar (events 1-5 on March 23, and event 19 on April 4; Figure 2.2), photographic evidence, and gas flight heights than with satellite temperature retrieved heights. In light of this other evidence, the fact that the ash *should* have consistently risen higher in altitude than the satellite temperature heights is further evidence that plume altitude was underestimated by the basic temperature method.

Certainly, the presence of the tropopause affected these temperature height results. It is notable that the retrieval of plume heights using the basic temperature method in this study was limited to the height of the tropopause, at ~9 to 10 km ASL in the NOPAC. This was due to the temperature inversion, which often makes it impossible to retrieve a unique height for plumes that are near the tropopause. Such material could be above or below the tropopause, but will always be retrieved at a (minimum) height below or at the tropopause by the method utilized here (in the absence of another method to resolve this ambiguity). This confirms the findings of Woods and Self (1992). However, as Puff showed, some of the altitudes retrieved by the temperature method likely contained some eruptive material (i.e., the altitudes are not all too low to be within the plume's vertical extent, but may not be high enough to be at the plume top either). At least some of the temperatures could only be attributed to material residing at heights below the tropopause

because there was no corresponding stratospheric height based on local radiosonde data. Yet many height retrievals were clearly not accurate (those displaying artificial drops) even though they were below the tropopause. Thus, not only the effect of the tropopause inversion was at play here; another factor must have influenced the results.

Sparks et al. (1997) argued that a satellite-based measurement of plume temperature corresponds to a point inside the plume at which the plume becomes opaque. They further argue that this point may be several centimeters inside the plume, or several meters for plumes with diffuse margins. However, it appears that centimeters and meters are a vast underestimate: it may actually be several kilometers inside the plume that the plume becomes opaque, and after a certain amount of plume dispersion, it is not opaque at all, and the radiant temperatures of either meteorological cloud cover or the ground surface become detectable by the satellite.

The BTD method was used as a filter before the temperature method was applied to eliminate pixels likely to be transparent. However, since temperatures and heights "dropped" in almost all temperature data studied, this method for the elimination of transparent pixels clearly did not eliminate all pixels with a degree of transparency. First, this may be a result of the content of the plume. The Redoubt 2009 eruption plumes produced rather small negative BTD or ash signals, and this may have been due to the water content of the eruption plumes (Webley et al., in press). Indeed, Schaefer (2012) found that all the tephra deposits from the Redoubt 2009 eruption contained a significant percentage of accretionary lapilli clasts, composed of fine-grained ash particles held together by ice (water) particles. As previously mentioned, the presence of an ice coating can cause the particle to scatter and absorb radiation like water/ice, making the BTD method less effective (Prata, 1989a, b; Simpson et al., 2000; Prata et al., 2001; Pavolonis et al.,

2006). This is one plausible explanation for the lack of a strong BTD signal during the eruption, and a reason it may not have been a good proxy for plume transparency.

However, the limitations of the BTD method as a filter do not fully account for the results presented here. It appears that the plumes analyzed behaved as neither totally transparent (some retrievals appeared to have some accuracy), nor totally opaque (many retrievals were underestimated, despite BTD filtering). The BTD method, limitations aside, should only detect plumes or clouds that are totally transparent. It does not account for varying degrees of optical depth of a cloud that are between complete opacity (detecting cloud top only) and complete transparency (detecting ground radiation rather than a point inside the cloud). The plumes imaged in this study appear to be in this range, and, as such, the temperatures – and thus heights – retrieved were often somewhere inside the plume, though likely not at the plume top. Contrary to the assertion by Sparks et al. (1997) that this retrieved height is centimeters or meters below the plume top, the results here show it to be on the order of kilometers below the plume top – sometimes several kilometers. There is no other explanation thus far that accounts for the results so completely.

In light of this, it is reasonable that the plumes in this study decreased in temperature retrieved height with decreasing optical depth. To act as a completely opaque blackbody, a plume would need an optical depth greater than ~3 (DeSlover et al., 1999), while the optical depths of the few plumes analyzed with the VAR code were less than ~1.3. Surely, these plumes were not acting as blackbodies, meaning that optical depth may have influenced the accuracy of their corresponding temperature height retrievals. As stated before, this comparison is preliminary, and further work is required to fully understand this process. Furthermore, VAR results (and thus optical depths)

were only retrieved for pixels with a negative BTD; heights were only retrieved for pixels with a positive BTD. These results may then appear to be comparing two different types of pixels, and thus perhaps two different portions of the plume. However, this is not necessarily the case: because even plumes with positive BTDs appeared to be behaving as partially transparent bodies, we might assume that the positive BTDs are not necessarily due to transparency, but rather that they may be due to other factors (e.g., masking of particles by ice). In this case, we might also assume that when a plume is found to have decreasing optical depth over time, this decrease in optical depth may apply not only to negative BTD pixels, but to the erroneously positive BTD pixels as well. By extension, the heights from the erroneously positive BTD pixels might then be comparable to VAR optical depths from negative BTD pixels. To confirm this, further study is needed.

Given these assumptions, the optical depth and height comparison fits well with the other lines of evidence presented here, and does not seem unreasonable in light of the other results. That said, the results of the basic temperature method in comparison to stereo, radar, gas flight and photo analyses suggest that varying degrees of opacity (optical depth) produce heights lower than the plume top, even though a plume may not be transparent to ground radiation. Indeed, most plumes are not entirely opaque. Thus, plume *top* height will almost never be retrieved with the basic temperature method. Instead, the most accurate retrieved temperature heights almost always represent a point inside the plume. With increasing transparency (decreasing optical depth), height is increasingly underestimated. Thus, this drop in heights is not real; it is an artifact of the method. Though other factors (particle size, etc.) could also come into play, these factors as analyzed by the VAR code produced no obvious correlation with height, and were not analyzed

further in this study. Note that a more thorough discussion of these and related points with regard to the BTD and IR height retrieval problem can be found in Pavolonis (2010).

We propose that satellite temperature method results and BTD method results can be used together to determine the accuracy of satellite temperature retrievals. A positive BTD may suggest that the plume has some degree of opacity, and that ground radiation is not being detected by the sensor through the plume (Figures 2.5b-c, 2.6c). However, a positive BTD may also be retrieved when ground radiation is visible, but the plume is so dispersed that ash does not comprise a large enough percentage of the integrated pixel temperature to cause a negative BTD, or when significant water/ice is present (Figures 2.3, 2.4, 2.6e-f). Positive BTDs combined with a plume that, in 2D plotting, does not show significant vertical scatter (Figures 2.5b-c, 2.6c) suggest that temperature height results are from some point inside the plume. Significant scatter, on the other hand, regardless of positive BTD, may indicate the presence of ground or meteorological cloud radiation reaching the satellite sensor through the plume (Figures 2.5d-e, 2.6d-f).

The shape of plume height vs. distance plots can indicate the reliability of the results. The plumes with the least significant drop in retrieved height were found in imagery that contained moderate to significant meteorological cloud cover (Figure 2.5). On March 23, minimum retrieved plume heights dropped less than on other days (April 1, 4, and 5; Figures 2.3, 2.4, 2.6), and these minimum temperature heights correlate to the maximum temperature height of the surrounding meteorological cloud deck. The plumes with the most significant drops in retrieved height were within imagery that contained mostly clear views to sparse meteorological cloud cover: April 1, 4, and 5 (Figures 2.3, 2.4, 2.6). On these days, larger drops in minimum retrieved temperature

heights were possible because the ground and water surfaces were largely exposed. In images with a great deal of meteorological cloud cover, these clouds provided a minimum below which the retrieved satellite temperature heights did not drop. Meteorological cloud cover in satellite imagery from these days can be seen in Figure 2.8.

March 23 height retrievals showed minimal scatter in height-distance plots, and even where scatter was present (Figure 2.3d-e), the minimum height of the plume was fairly constant. April 4 height retrievals showed significant scatter in height-distance plots: the scatter in the heights reached all the way to the ground surface, and other than the ground surface itself, there seemed to be no consistent minimum to the height retrievals (Figure 2.6d-f). The difference in these patterns was due to the presence of meteorological cloud cover, and the lack of such cloud cover, respectively. Additionally, April 4 ash content was also the most fine grained of all the eruptions, due to the dome collapse onset (Wallace et al., in press). However, the most consistent explanation for the drop in temperature retrieved heights, based on the evidence in total, appears to be lack of meteorological cloud cover, combined with ash cloud dispersion, not particle size. There is no line of evidence in this study suggesting that particle size may be a factor.

On days when there is a lack of meteorological cloud cover, it is possible to retrieve a height pattern that closely reflects the topography. Significant apparent drops in retrieved temperature heights occurred for the April 1 and 5 plumes (Figures 2.3, 2.4), as well as in three images for the April 4 plumes (Figure 2.6d-f), though the drop here was not as dramatic as in the smaller plumes. Here, retrieved temperature heights dropped sharply from the vent and leveled out over water (~30 km from the summit). In these cases, it is likely the temperature heights corresponded to a land surface temperature gradient rather than a plume gradient; the pattern of the drop in

retrieved altitude followed the shape of the topography, and it appears that the plume was transparent enough that the pixel temperatures were primarily reflecting the temperature of the land, only influenced in very small part by the temperature of the plume. Indeed, other data on these days showed no drop in heights. Furthermore, though MISR and basic temperature heights seemed to agree closer to the vent for April 1 and 5 plumes, temperature heights on both days were nearly the same as, or less than, the altitude of the summit of Redoubt itself (3.1 km ASL). It cannot be conclusively determined whether the plume, or the surface of Redoubt Volcano, was being retrieved on either day.

When patterns are retrieved that show a smooth plume bottom, it is likely that the basic temperature height retrievals are from somewhere inside the plume (Figure 2.9a). When patterns are retrieved that show scatter in the heights, but still a consistent plume bottom altitude, it is likely that there is meteorological cloud cover (Figure 2.9b). Some of the heights retrieved may correspond to the height of this cloud cover; others may correspond to some point inside the plume. When scatter in heights reaches to the ground, heights are very likely to be unreliable (Figure 2.9c). When the pattern retrieved is one of ground topography such as a volcano profile, heights are certainly unreliable (Figure 2.9d).

If retrieved temperature heights appear to be corresponding to a point inside the plume, an alternative method for retrieving the ash plume heights (such as shadow, if conditions allow for it) may be used to resolve whether these temperature heights correspond to a location in the troposphere or the stratosphere. In the absence of an alternative method to resolve the ambiguity, the results of this study suggest that plume heights retrieved by the basic temperature method are minimums only, and are limited to the height of the tropopause, around 9 or 10 km ASL in the

NOPAC. However, this does not mean that plumes *do not go* higher than the tropopause – just that the temperature method *does not retrieve* these higher heights.

The analysis here calls into question previous height results produced by the temperature method. Based on temperature height data, Dean et al. (2002) found that plumes in the NOPAC clustered at ~10 km ASL, with the maximum height constrained by the temperature inversion at the tropopause. As shown in the present study, plumes *do* appear to cluster at this altitude when analyzed with the basic temperature method. However, both plumes which reach maximum altitude at the tropopause, and plumes that reach higher altitudes (perhaps less common, if we assume it is difficult for less energetic plumes to penetrate this layer) will appear to be the same height when analyzed using this approach. For this reason, it is possible that plumes previously thought to have reached a maximum height of ~10 km ASL may have, in fact, been higher, though the basic temperature method was unable to retrieve these higher heights.

In other words, a clustering of retrieved plume heights at 9 or 10 km ASL may be a) an artifact of the temperature method, or b) a true reflection of the presence of a significant atmospheric barrier to higher plume penetration, or c) some combination of the two. As currently implemented, the basic satellite temperature method cannot distinguish between these possibilities. This suggests that previous results, such as the conclusion by Dean et al. (2002), deserve another look. Though Dean et al. (2002) acknowledge the limitations of the satellite temperature method based on the tropopause inversion, they only acknowledge higher than tropopause altitudes for the eruptions which have proof of tropopause penetration from some other method. Furthermore, the evidence presented here shows that even retrieved heights that area below the tropopause may be unreliable, *unless* the plumes were optically thick enough to produce reliable heights. On the

other hand, there are cases in which tropospheric plume temperature results have had relatively good agreement with radar, such as in the 2006 eruption of Augustine Volcano (Bailey et al., 2010).

It is important to note that at the location of the tropopause, there is usually (in a standard atmospheric curve) one unique (and coldest) temperature which appears to offer a unique solution for height. For the material at this temperature, there *is* a unique solution for height. However, the presence of the "coldest" temperature material does not prove that warmer higher altitude material above the tropopause does not exist which cannot be effectively distinguished from warmer lower altitude material below the tropopause.

Based on the results presented here, other methods of height determination have proven to be more reliable than the basic satellite temperature method. Both ground-based radar and MISR stereo height retrievals are preferable to satellite temperature method height retrievals because they are more accurate, and less prone to interpretation errors. The comparison between radar and satellite retrieved heights presented here contradicts the assertion by Rose et al. (1995) that radar may underestimate plume height due to its ability to detect only larger particles. In the present study, compared to the basic satellite temperature method, radar is apparently far more accurate. Though they may be designed to detect larger particles, radar sensors acquire data more frequently, and are theoretically more likely to image a plume close to the start of an eruption, when the plume has the greatest momentum and is most likely to reach its maximum height.

In contrast, TIR satellite sensors appear to be more sensitive to optical depth and transparency issues, in addition to the issues with the tropopause described above. Thus, though fine ash may

indeed go higher, and the satellite temperature method may be more sensitive to fine ash, the data presented here show that the plume height is almost always underestimated by the basic temperature method. Indeed, the theoretical assertion of the underestimate of radar (in comparison to satellite temperature) by Rose et al. (1995) may only hold true for plumes which are opaque enough to act as true blackbodies, which may be very unlikely in real conditions, save for the thickest and freshest of plumes. Whatever limitations the radar height method has with regard to particle size sensitivity, this study shows these limitations to be small compared to the underestimates of the basic temperature method. Certainly, radar retrievals have other limitations that are important to note, including the limited distance range of the sensors and limited number of radar sites. Still another limitation is that radar images the plume in vertical "steps" and the vertical resolution of these steps will limit the ability of the radar to accurately resolve the height of the plume (Rose et al., 1995; Wood et al., 2007; Hoblitt and Schneider, 2009; Arason et al., 2011). Even with these limitations, for the Redoubt eruption, radar proved to be far more able to detect the highest ash than basic satellite temperature height retrievals.

The work here supports the idea that MISR can detect plumes that are relatively thin compared to the detection threshold of other methods. The plumes on April 1 and April 5 were almost transparent in TIR data compared to imagery from other dates (Figure 2.8), with the coastline fairly visible through the plume. However, MISR was able to retrieve heights which agreed with both photographic and gas flight data on April 5. Part of the difference in accuracy between AVHRR/MODIS temperature and MISR stereo heights may be due to the difference in the spatial resolution of the sensors (Table 2.2). However, even at higher resolution, the issue of ash plume transparency in TIR data would not be circumvented.

While a plume must be opaque for the satellite temperature method to reliably retrieve heights, and must contain certain particle sizes for radar to return a signal, stereo methods simply require enough detectable texture in the plume for multiple cameras to image and match on the same features. This means that much smaller or thinner plumes can be detected by MISR than by other methods. Indeed, MISR is used to detect plumes that can be orders of magnitude more diffuse than volcanic plumes, such as plumes from forest and grassland fires (Kahn et al., 2007; Mims et al., 2009). However, limitations to MISR data exist as well: the swath size is relatively narrow, data are acquired infrequently (each volcano is only imaged once every two days in the NOPAC), and the sensor only acquires data during the daytime. These characteristics limit the operational usefulness of the MISR sensor. However, such limitations do not preclude the use of the data whenever they are available. When available, these data are among the most reliable for height determination.

2.7 Conclusions

We have assessed the performance of a variety of different techniques for determining the height of the ash plumes emitted during the eruption of Redoubt Volcano in late March and early April 2009. Based on a comparison of these techniques, we have highlighted their strengths and limitations for determining the height of ash plumes in the North Pacific region.

The basic satellite temperature method has limited application in determination of plume height. Early in the eruption, before significant dispersion occurs and when the plume is more concentrated, height retrievals will be more accurate; and nearer to the vent, where an ash plume is more likely to be highly concentrated and of greater optical depth, height retrievals will also be more accurate. This accuracy of retrieved plume heights may directly correlate to optical depth,

with plumes of greater optical depth producing more accurate temperature heights. These more accurate plume heights may correspond to a layer somewhere inside the plume, but likely not the plume top. Due to the temperature inversion at the tropopause, plume heights based on temperature will reach a maximum at the tropopause, ~10 km ASL in the NOPAC, unless the ambiguity can be resolved by other methods. Plumes will tend to have a minimum temperature retrieved height when meteorological cloud cover is present, and no minimum temperature retrieved height other than ground level in the absence of meteorological cloud cover.

Eruptions producing plumes that reach 10 km ASL and higher in the NOPAC are considered to be large eruptions (Tupper et al., 2004; 2009). Because the tropopause is lower at high latitudes (~9-10 km ASL), and is higher at tropical latitudes (up to 18 km ASL), plume behavior is very different in the two locations. A large eruption column of 18 km ASL in the tropics may, in fact, be analogous in strength to an eruption column that reaches 10 km ASL in the NOPAC; both are significantly large eruptions (Tupper et al., 2004). As shown by radar analysis in this study, volcanic material in the NOPAC can reach much higher than the 10 km ASL threshold of the basic temperature method. Depending on the strength of the eruption, some plumes reach the tropopause, spread laterally, and go no higher (Sparks et al., 1997), and some plumes punch through the tropopause. The basic temperature method will report the same altitude for these two types of plumes. Since even 10 km ASL constitutes a fairly large eruption, it is advised that when eruptions reach 9 or 10 km ASL in the NOPAC, dispersion should be forecast for the range of heights from 9 or 10 to ~20 km ASL, so as to predict the movement of particles at all these locations. If other, more reliable data are available, height information from those data should be utilized instead. In a best case scenario, data fusion would constrain the height of volcanic material, and more precise forecasts could be made. If only basic satellite temperature data are

available for height retrieval, an initial plume trajectory forecast must be quickly refined to a more precise forecast as soon as heights can be further constrained.

To accurately assess plume heights, additional methods other than the basic satellite temperature method are required. MISR is an excellent sensor which is unaffected by the presence of the tropopause because it does not rely on plume temperature for height retrievals. However, the temporal frequency and spatial coverage of the MISR sensor are limited. Still, if and when MISR stereo height data are available during an active eruption, they should be utilized. Certainly, MISR data should always be analyzed in retrospect, when available. Radar is also an excellent source of data; however, the range of ground-based radar is extremely limited. Where radar can be utilized, it is likely to be more reliable than temperature data in reporting plume tops. Whatever the accompanying method to thermal satellite data, data fusion is currently the best way to assess an ash plume's height most accurately. The following points give an assessment of the conditions under which each method best functions:

- For heavily populated areas, which are likely to have radar sensors, a ground-based radar system is best for time-sensitive detection of volcanic plumes. Such systems provide quick detection of activity and the assessment of the eruption column height needed to predict cloud movement and protect local communities.
- For remote locations, satellite methods provide the quickest analysis of plume height. Either MISR stereo or the basic satellite temperature method can be utilized.
- For optically thick plumes, the basic satellite temperature method should be fairly reliable in close proximity to the vent, before the plume has had a chance to disperse, for plumes at or below the tropopause (~10 km ASL in the NOPAC). However, the height of plumes

which are optically thick and actually above the tropopause could be significantly underestimated if no other method is available to resolve the ambiguity due solely to the temperature inversion at the tropopause. Thus, these results should be supplemented, if possible, with MISR stereo analysis, or a method such as the shadow method.

- For optically thin plumes, MISR stereo analysis, if coverage is available, is the most reliable method for ash plume height determination. MISR can determine the heights of plumes for which the basic satellite temperature method will produce very poor results due to optical depth issues.
- For weak (low) plumes that are optically thick, basic satellite temperature analysis of height will suffice, while for weak (low) plumes that are optically thin, MISR stereo analysis will provide much more reliable results.
- For strong (high) plumes, the basic satellite temperature method will only suffice if the plume is below the tropopause (or if the true height can be resolved with another method) and optically thick. If either of these conditions is not met, MISR stereo or ground-based radar will provide much more reliable results.

Lastly, a more complete exploration of height determination methods, and especially temperature methods, which account for the imperfect and varying optical depth of plumes and clouds, is needed. Work along these lines has recently been described by Pavolonis (2010) who has developed a more robust approach for plume analysis using multiple infrared channels. We urge future investigation into such methods, in collaboration with the meteorology community, and the use of subsequently developed methods by volcano observatories for whom accurate heights, and accurate dispersion forecasts, are of the utmost importance.

2.8 Acknowledgements

We would like to thank Lovro Valcic (AVO/UAF-GI) and Scott McFarlane (AVO/UAF-GI) for assistance in obtaining and processing AVHRR and MODIS satellite imagery, David McAlpin (UAF-GI) for processing of the DEM data, Jeremy Harbeck for assistance with programming and computational analysis in IDL, David Schneider (USGS) for providing radar data, Peter Kelly (USGS) for providing gas flight data, and Steve McNutt (AVO/UAF-GI) for providing seismic data. Thanks to Ralph Kahn (NASA GSFC) and Michael Pavolonis (NOAA) and one anonymous reviewer for helpful comments and feedback. This work was supported in part by The American Reinvestment and Recovery Act, as well as the Alaska Space Grant Program. Portions of this work were carried out at the Jet Propulsion Laboratory, California Institute of Technology, under a contract with the National Aeronautics and Space Administration. This publication is the result in part of research sponsored by the Cooperative Institute for Alaska Research with funds from the National Oceanic and Atmospheric Administration under cooperative agreement NA080AR4320751 with the University of Alaska.

2.9 References

Arason, P., Peterson, G.N., Bjornsson, H., 2011. Observations of the altitude of the volcanic plume during the eruption of Eyjafjallajökull, April-May 2010. Earth Sys. Sci. Data 4, 1-25.

Bailey, J.E., Dean, K., Dehn, J., Webley, P., 2010. Integrated satellite observations of the 2006 eruption of Augustine Volcano (Chapter 20). In: Power, J.A., Coombs, M.L., Freymueller, J.T. (Eds.), The 2006 Eruptions of Augustine Volcano. USGS Professional Paper 1769. http://pubs.usgs.gov/pp/1769/

Bull, K., Buurman, H., in press. An overview of the 2009 eruption of Redoubt Volcano. In: Webley, P., Waythomas, C.F. (Eds.), The 2009 Eruption of Redoubt Volcano, Alaska. J. Volcanol. Geotherm. Res.

Carlisle, J., Nelson, K., 2009. Redoubt Volcano eruption/ash synopsis - November 2008 - July 2009. Unpublished Federal Aviation Administration summary document, 39 pp. http://www.avo.alaska.edu/pdfs/cit4547.pdf

Carn S.A., Prata, A.J., Yang, K., Rose, W.I., 2011. A-Train observations of young volcanic eruption clouds. Abstr. V33A-2609 presented at the 2011 Fall Mtg., AGU, San Francisco, Calif., 5-9 Dec.

Dean, K.G., Dehn, J., Engle, K., Izbekov, P., Papp, K., Patrick, M., 2002. Operational satellite monitoring of volcanoes at the Alaska Volcano Observatory. Adv. Environ. Monit. Modell. 1, 70-97.

Dean, K.G., Ekstrand, A.L., Webley, P., 2009. Satellite observations of volcanic clouds from the eruption of Redoubt Volcano, Alaska, 2009. Abstr. V43A-2210 presented at 2009 Fall Mtg., AGU, San Francisco, Calif., 14-18 Dec.

Dean, K.G., Eichelberger, J., Rothery, D., in press. Setting, history, and impact of the North Pacific region (Chapter 1). In: Dean, K.G., Dehn, J. (Eds.), Monitoring Volcanoes in the North Pacific: Observations from Space. Springer.

DeSlover, D.H., Smith, W.L., Piironen, P.K., Eloranta, E.W., 1999. A methodology for measuring cirrus cloud visible-to-infrared spectral optical depth ratios. J. Atmos. Ocean. Tech. 16, 251-262.

Diner, D.J., Beckert, J.C., Reilly, T.H., Bruegge, C.J., Conel, J.E., Kahn, R.A., Martonchik, J.V., Ackerman, T.P., Davies, R., Gerstl, S.A.W., Gordon, H.R., Muller, J.-P., Myneni, R.B., Sellers, P.J., Pinty, B., Verstraete, M.M., 1998. Multi-angle Imaging SpectroRadiometer (MISR) instrument description and experiment overview. IEEE Trans. Geosci. Rem. Sens. 36, 1072–1087.

Draxler, R.R., 1999. HYSPLIT4 user's guide. NOAA Tech. Memo. ERL ARL-230, NOAA Air Resources Laboratory.

Draxler, R.R., Hess, G.D., 1997. Description of the HYSPLIT_4 modeling system. NOAA Tech. Memo. ERL ARL-224, NOAA Air Resources Laboratory, 24 pp.

Draxler, R.R., Hess, G.D., 1998. An overview of the HYSLPIT_4 modeling system for trajectories, dispersion and deposition. Aust. Meteorol. Mag. 47, 295-308.

Draxler, R.R., Rolph, G.D., 2012. HYSPLIT (Hybrid Single-Particle Lagrangian Integrated Trajectory) model access via NOAA ARL READY website (http://ready.arl.noaa.gov/HYSPLIT.php). NOAA Air Resources Laboratory. 8 April 2011.

Ekstrand, A.L., Dean, K.G., Webley, P., Dehn, J., 2009. Plume height analysis of two major Alaskan eruptions: Implications for operational use of satellite data. Abstr. V31A-1945 presented at 2009 Fall Mtg., AGU, San Francisco, Calif., 14-18 Dec.

Ekstrand, A.L., Webley, P., Dehn, J., Nelson, D.L., Garay, M.J., Dean, K.G., 2010. Plume height analysis of the 2009 Redoubt eruption: A comparison of MISR, AVHRR, and MODIS data. Abstr. NH43A-1492 presented at 2010 Fall Mtg., AGU, San Francisco, Calif., 13-17 Dec.

Garay, M.J., de Szoeke, S.P., Moroney, C.M., 2008. Comparison of marine stratocumulus cloud top heights in the southeastern Pacific retrieved from satellites with coincident ship-based observations. J. Geophys. Res. 113, D18204. doi:10.1029/2008JD009975.

Graf, H.-F., Herzog, M., Oberhuer, J.M., Textor, C., 1999. Effect of environmental conditions on volcanic plume rise. J. Geophys. Res. 104, 24309-24320.

Hoblitt, R.P., Schneider, D.J., 2009. Radar observations of the 2009 eruption of Redoubt Volcano, Alaska: Initial deployment of a transportable Doppler radar system for volcano monitoring. Abstr. V43A-2209 presented at 2009 Fall Mtg., AGU, San Francisco, Calif., 14-18 Dec.

Holasek, R.E., Self, S., 1995. GOES weather satellite observations and measurement of the May 18, 1980, Mount St. Helens eruption. J. Geophys. Res. 100, 8469-8487.

Kahn, R.A., Li, W.-H., Moroney, C., Diner, D.J., Martonchik, J.V., Fishbein, E., 2007. Aerosol source plume physical characteristics from space-based multiangle imaging. J. Geophys. Res. 112, D11205. doi:10.1029/2006JD007647.

Kahn, R.A., Chen, Y., Nelson, D.L., Leung, F.-Y., Li, Q., Diner, D.J., Logan, J.A., 2008. Wildfire smoke injection heights: Two perspectives from space. Geophys. Res. Lett. 35, L04809. doi:10.1029/2007GL032165.

Kalnay, E., Kanamitsu, M., Kistler, R., Collins, W., Deaven, D., 1996. The NCEP/NCAR 40-year reanalysis project. Bull. Amer. Meteor. Soc. 77, 437-471.

Kienle, J., Shaw, G.E., 1979. Plume dynamics, thermal energy, and long-distance transport of vulcanian eruption clouds from Augustine Volcano, Alaska. J. Volcanol. Geotherm. Res. 6, 139-164.

Marzano, F.S., Barbieri, S., Vulpiani, G., Rose, W.I., 2006a. Volcanic ash cloud retrieval by ground-based microwave weather radar. IEEE Trans. Geosci. Remote Sens. 44, 3235–3246.

Marzano, F.S., Vulpiani, G., Rose W.I., 2006b. Microphysical characterization of microwave radar reflectivity due to volcanic ash clouds. IEEE Trans. Geosci. Rem. Sens. 44, 313–327.

Marzano, F.S., Marchiotto, S., Textor, C., Schneider, D.J., 2010. Model-based weather radar remote sensing of explosive volcanic ash eruption. IEEE Trans. Geosci. Remote Sens. 48, 3591–3607.

McGimsey, R.G., Neal, C.A., Dixon, J.P., Malik, N., and Chibisova, M., 2011. 2007 Volcanic activity in Alaska, Kamchatka, and the Kurile Islands: Summary of events and response of the Alaska Volcano Observatory. USGS Scientific Investigations Report 2010-5242, 110 pp. http://pubs.usgs.gov/sir/2010/5242/

McNutt, S.R., Thompson, G., West, M.E., Fee, D., Stihler, S., Clark, E., in press. Local seismic and infrasound observation of the 2009 explosive eruptions of Redoubt Volcano, Alaska. In: Webley, P., Waythomas, C.F. (Eds.), The 2009 Eruption of Redoubt Volcano, Alaska. J. Volcanol. Geotherm. Res.

Miller, T.P., Casadevall, T.J., 2000. Volcanic ash hazards to aviation. In: Sigurdsson, H. (Ed.), Encyclopedia of Volcanoes. Academic Press, San Diego, 915-930.

Mims., S.R., Kahn, R.A., Moroney, C.M., Gaitley, B.J., Nelson, D.L., Garay, M.J., 2009. MISR stereo heights of grassland fire smoke plumes in Australia. IEEE Trans. Geosci. Rem. Sens. 48, 25-35.

Moroney, C., Davies, R., Muller, J.-P., 2002. Operational retrieval of cloud-top heights using MISR data. IEEE Trans. Geosci. Rem. Sens. 40, 1532–1540.

Nelson, D.L., Averill, C., Boland, S., Morford, R., Menzies, A., Garay, M., Diner, D., Rheingans, B., Thompson, C., Hall, J., Scholes, M., Campbell, H., 2009. MISR INteractive eXplorer (MINX) v1.2 user's guide. JPL Tech. Rep. D-41552. http://www.openchannelsoftware.com/projects/MINX/

Papp, K.R., Dean, K.G., Dehn, J., 2005. Predicting regions susceptible to high concentrations of airborne volcanic ash in the North Pacific region. J. Volcanol. Geotherm. Res. 148, 295-314.

Pavolonis, M.J., 2010. Advanced in extracting cloud composition information from spaceborne infrared radiances – A robust alternative to brightness temperatures. Part I: Theory. J. Appl. Meteorol. Climatol. 49, 1992–2012.

Pavolonis, M.J., Feltz, W.F., Heidinger, A.K., Gallina, G.M., 2006. A daytime complement to the reverse absorption technique for improved automated detection of volcanic ash. J. Atmos. Oceanic Tech. 23, 1422-1444.

Prata, A.J., 1989a. Infrared radiative transfer calculations for volcanic ash clouds. Geophys. Res. Lett. 16, 1293-1296.

Prata, A.J, 1989b. Observations of volcanic ash clouds in the 10-12 μm window using AVHRR/2 data. Int. J. Rem. Sens. 10, 751-761.

Prata, A.F., Bluth, G., Rose, B., Schneider, D., Tupper, A., 2001. Comments on "Failures in detecting volcanic ash from a satellite-based technique." Rem. Sens. Environ. 78, 341-346.

Riccardi, N., Glascock, S., March 24, 2009, Alaska's Mt. Redoubt erupts five times overnight. Los Angeles Times. http://articles.latimes.com/2009/mar/24/nation/na-alaska-volcano24. 14 July 2010.

Rose, W.I., Kostinski, A.B., Kelley, L., 1995. Real time C band radar observations of 1992 eruption clouds from Crater Peak, Mount Spurr Volcano, Alaska. USGS Bull. 2139, 19-28.

Rose, W.I., Bluth, G.J.S., Ernst, G.G.J., 2000. Integrating retrievals of volcanic cloud characteristics from satellite remote sensors: a summary. Philos. Trans. Royal Soc. Lond. A 358, 1585-1606.

Schaefer, J.R.G., 2012. The 2009 eruption of Redoubt Volcano, Alaska. Alaska Div. Geol. Geophys. Survey Rep. Invest. 2011-5, 45 pp. http://www.dggs.alaska.gov/pubs/id/23123

Schneider, D.J., Rose, W.I., Kelley, L., 1995. Tracking of the 1992 eruption clouds from Crater Peak vent of Mount Spurr Volcano, Alaska, using AVHRR. In: Keith, T. (Ed.), The 1992 Eruptions of Crater Peak Vent, Mt. Spurr Volcano, Alaska. USGS Bull. 2139, 27-36.

Schneider, D., Hoblitt, R., in press. Doppler weather radar observations of the 2009 eruption of Redoubt Volcano, Alaska. In: Webley, P., Waythomas, C.F. (Eds.), The 2009 Eruption of Redoubt Volcano, Alaska. J. Volcanol. Geotherm. Res.

Scollo, S., Folch, A., Coltelli, M., Realmuto, V.J., 2010. Three-dimensional volcanic aerosol dispersal: A comparison between Multiangle Imaging Spectroradiometer (MISR) data and numerical simulations. J. Geophys. Res. 115, D24210. doi:10.1029/2009JD013162

Searcy, C., Dean, K., Stringer, W., 1998. PUFF: A high-resolution volcanic ash tracking model. J. Volcanol. Geotherm. Res. 80, 1-16.

Simpson, J.J., Hufford, G., Pieri, D., Berg, J., 2000. Failures in detecting volcanic ash from a satellite-based technique. Rem. Sens. Environ. 72, 191-217.

Sparks, R.S.J., Bursik, M.I., Carey, S.N., Gilbert, J.S., Glaze, L.S., Sigurdsson, H., Woods, A.W., 1997. Volcanic Plumes. Wiley, Chichester, 574 pp.

Steensen, T., Stuefer, M., Webley, P.W., Grell, G., Freitas, S., in press. Analysis of ash distribution of the Redoubt 2009 eruption based on satellite observations and model estimates. In: Webley, P., Waythomas, C.F. (Eds.), The 2009 Eruption of Redoubt Volcano, Alaska. J. Volcanol. Geotherm. Res.

Tupper, A., Wunderman, R., 2009. Reducing discrepancies in ground and satellite-observed eruption heights. J. Volcanol. Geotherm. Res. 186, 22-31.

Tupper, A., Carn, S., Davey, J., Kamada, Y., Potts, R., Prata, F., Tokuno, M., 2004. An evaluation of volcanic cloud detection techniques during recent significant eruptions in the western 'Ring of Fire.' Rem. Sens. Environ. 91, 27-46.

Tupper, A., Textor, C., Herzog, M., Graf, H.-F., Richards, M.S., 2009. Tall clouds from small eruptions: the sensitivity of eruption height and fine ash content to tropospheric instability. Nat. Hazards 51, 375-401.

U.S. Census Bureau, 2010. Alaska – 2010 census results: Total population by county equivalent (map). April 25 2012. http://2010.census.gov/news/pdf/cb11cn83_ak_totalpop_2010map.pdf

Val Martin, M., Logan, J.A., Kahn, R.A., Leung, F.-Y., Nelson, D.L., Diner, D.J., 2010. Smoke injection heights from fires in North America: Analysis of 5 years of satellite observations. Atmos. Chem. Phys. 10, 1491–1510.

Wallace, K., Schaefer, J., Coombs, M., in press. Character, mass, distribution, and origin of tephra-fall deposits from the 2009 eruption of Redoubt Volcano, Alaska. In: Webley, P., Waythomas, C.F. (Eds.), The 2009 Eruption of Redoubt Volcano, Alaska. J. Volcanol. Geotherm. Res.

Webley, P.W., Dehn, J., Lovick, J., Dean, K.G., Bailey, J.E., Valcic, L. 2009. Near-real-time volcanic ash cloud detection: Experiences from the Alaska Volcano Observatory. J. Volcanol. Geotherm. Res. 186, 79-90.

Webley, P.W., Lopez, T.M., Dean, K.G., Rinkleff, P., Dehn, J., Cahill, C.F., Wessels, R., Schneider, D.J., Ekstrand, A., Bailey, J.E., Izbekov, P., and Worden, A., in press. Remote observations of eruptive clouds and surface thermal activity during the 2009 eruption of Redoubt Volcano. In: Webley, P., Waythomas, C.F. (Eds.), The 2009 Eruption of Redoubt Volcano, Alaska. J. Volcanol. Geotherm. Res.

Wen, S., Rose, W.I., 1994. Retrieval of sizes and total masses of particles in volcanic clouds using AVHRR bands 4 and 5. J. Geophys. Res. 99, 5421-5431.

Werner, C., Kelly, P.J., Doukas, M., Lopez, T., Pfeffer, M., McGimsey, R.G., Neal, C.A., in press. Degassing associated with the 2009 eruption of Redoubt Volcano, Alaska. In: Webley, P., Waythomas, C.F. (Eds.), The 2009 Eruption of Redoubt Volcano, Alaska. J. Volcanol. Geotherm. Res.

Wood, J., Scott, C., Schneider, D., 2007. WSR-88D radar observations of volcanic ash. 4th Int. Workshop on Volcanic Ash, World Meterol. Org, Int. Civil Aviation Org., and Civil Aviation Authority New Zealand, Rotorua, New Zealand, 26-20 Mar., 9 pp.

Woods, A.W., 1995. The dynamics of explosive volcanic eruptions. Rev. Geophys. 33, 495-530.

Woods, A.W., Self, S., 1992. Thermal disequilibrium at the top of volcanic clouds and its effect on estimates of the column height. Nature 355, 628-630.

2.10 Websites referenced

Airports Council International, 2011. Cargo traffic 2010 final. http://www.airports.org/cda/aci_common/display/main/aci_content07_c.jsp?zn=aci&cp=1-5-54-4819_666_2__. 20 February 2012.

AVO Tools webpage, 2007. http://avo.images.alaska.edu/tools/

NASA Langley Research Center Atmospheric Sciences Data Center, 2011. http://eosweb.larc.nasa.gov/. 14 April 2011.

Open Channel Foundation, 2010. MINX software. http://www.openchannelsoftware.com/projects/MINX/. 5 March 2010.

University of Wyoming's College of Engineering, Department of Atmospheric Science database. http://weather.uwyo.edu/upperair/sounding.html. 22 February 2011.

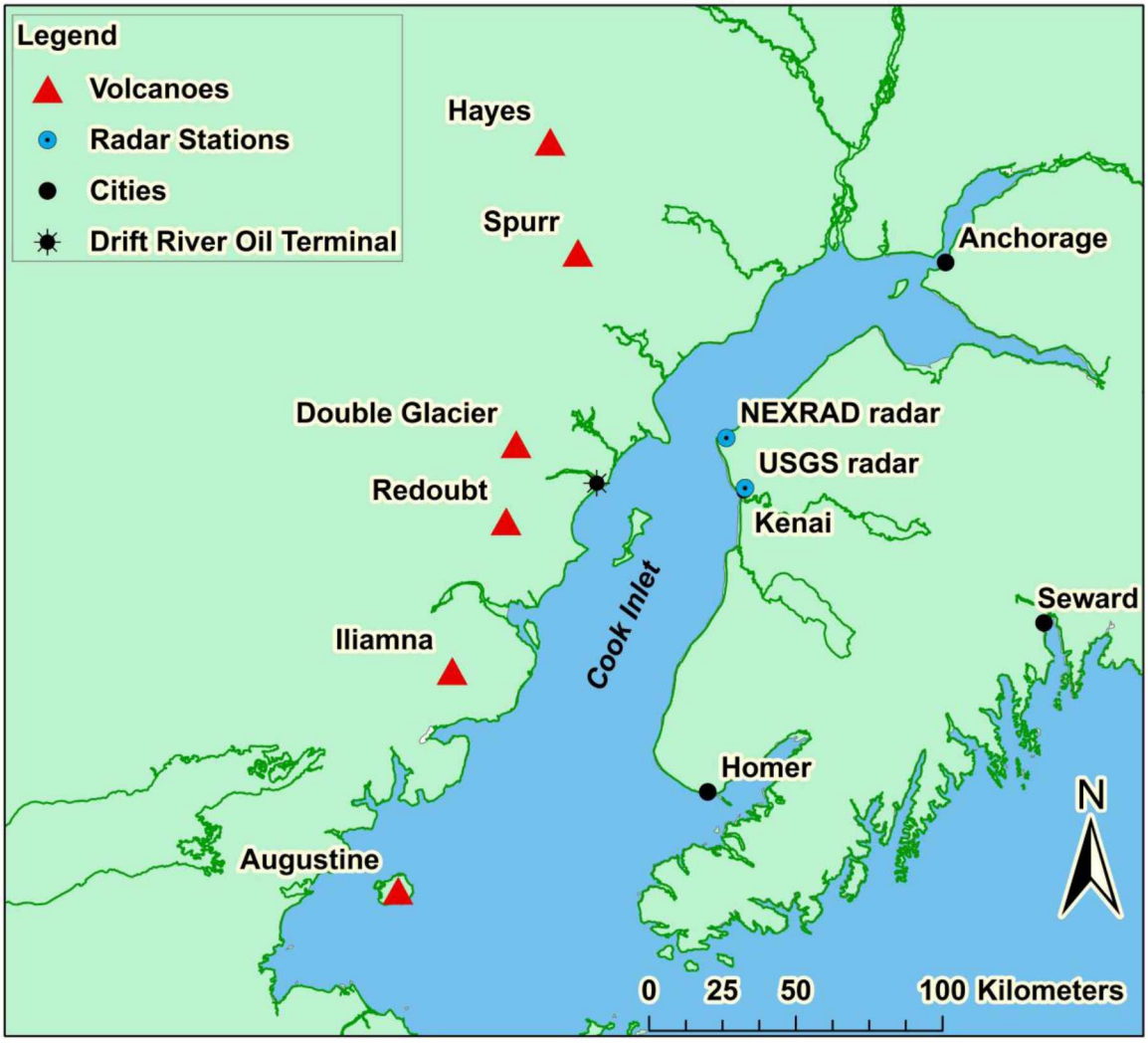

Figure 2.1: Location of Redoubt Volcano relative to Anchorage and surrounding area. The summit of Redoubt is approximately 160 km from Anchorage, and 30 km from the Cook Inlet. Radar locations from Hoblitt and Schneider (2009) and Schneider and Hoblitt (in press).

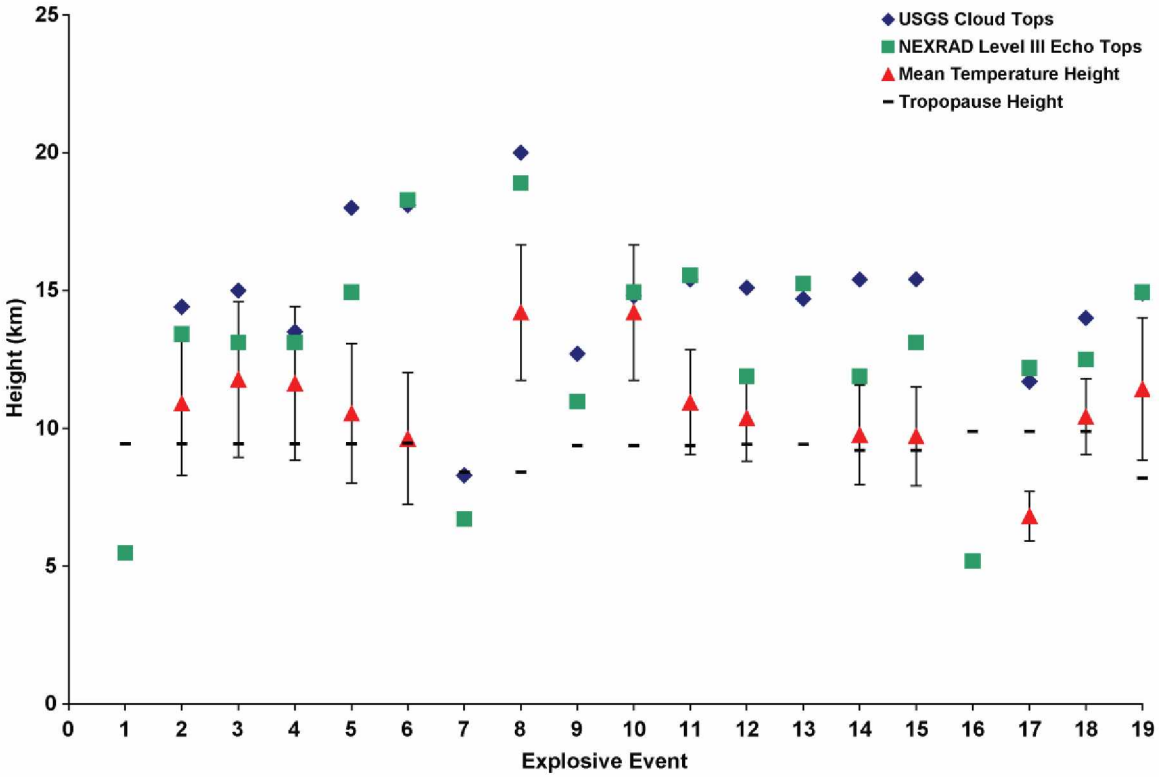

Figure 2.2: Plume heights for the 19 official Redoubt events. USGS and NEXRAD radar heights are consistently higher than the temperature heights. Temperature heights (mean height from radiosonde) are shown with error bars as follows: the top of the error bar represents the coldest temperature corresponding to the stratosphere, and the bottom of the error bar represents the coldest temperature corresponding to the troposphere, and the symbol between them represents the average. Radar data from Dave Schneider (AVO/USGS). Figure adapted from Ekstrand et al. (2009).

Figure 2.3: MISR/AVHRR/MODIS comparisons for April 1, 2009. Shown with 3x vertical exaggeration. A) ArcScene 3D representation of height results relative to Redoubt, B) 2D plot of height results with distance from vent. AVHRR and MODIS heights are consistently lower than MISR heights. For scale, Redoubt has a height of ~3 km. The distance from the Redoubt summit to the Cook Inlet (i.e., nearest coastline) is ~30 km, and the distance from Redoubt to Anchorage is ~160 km. DEM and overlain image are © JAXA 2009.

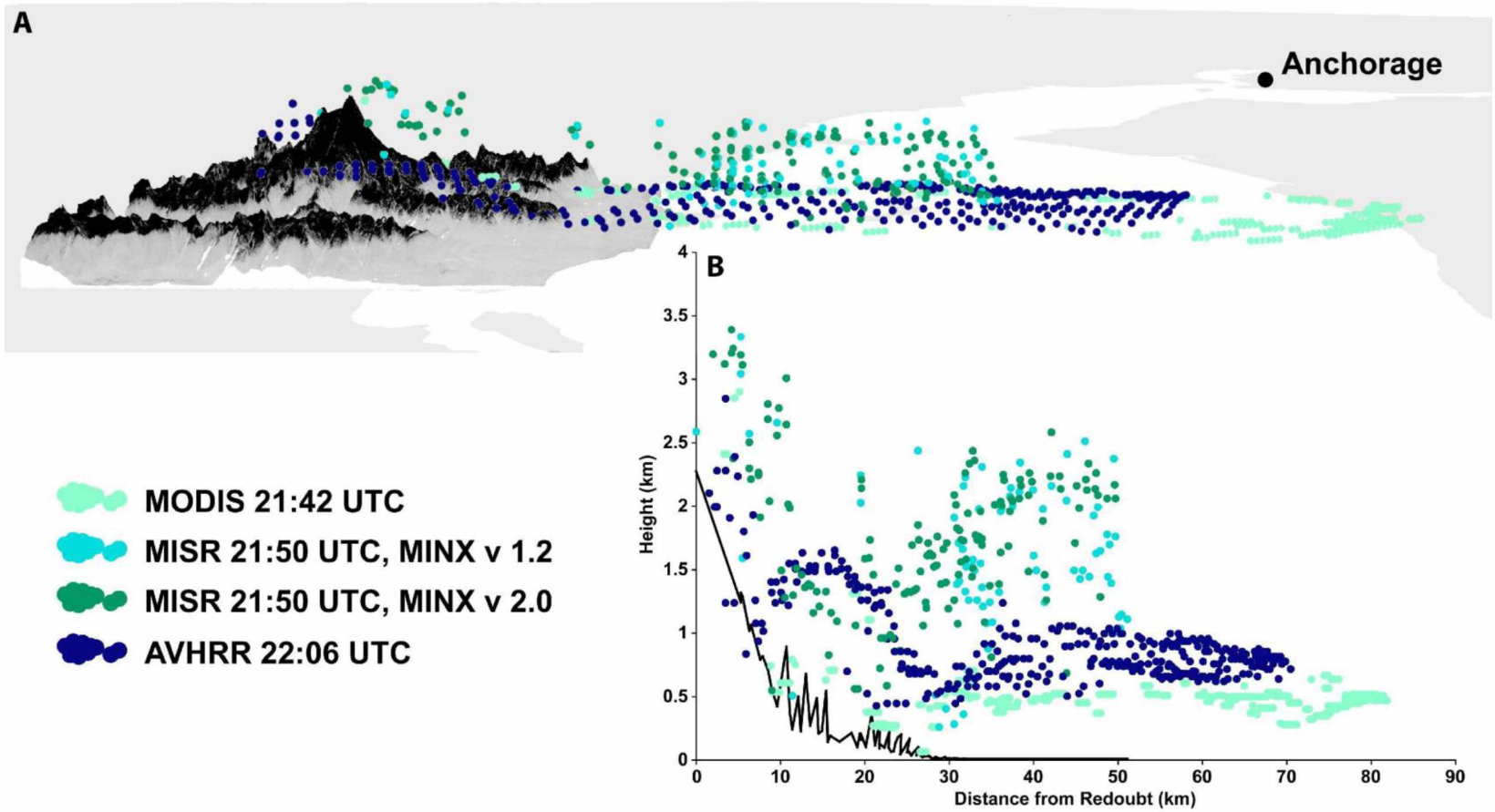
A
Anchorage
B
MODIS 21:42 UTC
MISR 21:50 UTC, MINX v 1.2
MISR 21:50 UTC, MINX v 2.0
AVHRR 22:06 UTC
Height (km)
Distance from Redoubt (km)
0
0.5
1
1.5
2
2.5
3
3.5
4
0
10
20
30
40
50
60
70
80
90

Figure 2.4: MISR/AVHRR comparison for April 5, 2009. A) ArcScene 3D representation of height results relative to Redoubt, shown with 3x vertical exaggeration, B) 2D plot of height results with distance from vent, C) Redoubt Volcano during an observation and gas collection overflight on April 5, 2009. AVHRR and MODIS heights are consistently lower than MISR heights, and the photo shows no "drop" in heights. Photographer: Leslie Holland-Bartels. Image courtesy of AVO/USGS. Image obtained from http://www.avo.alaska.edu/. For scale, Redoubt has a height of ~3 km. The distance from the Redoubt summit to the Cook Inlet (i.e., nearest coastline) is ~30 km, and the distance from Redoubt to Anchorage is ~160 km. DEM and overlain image are © JAXA 2009.

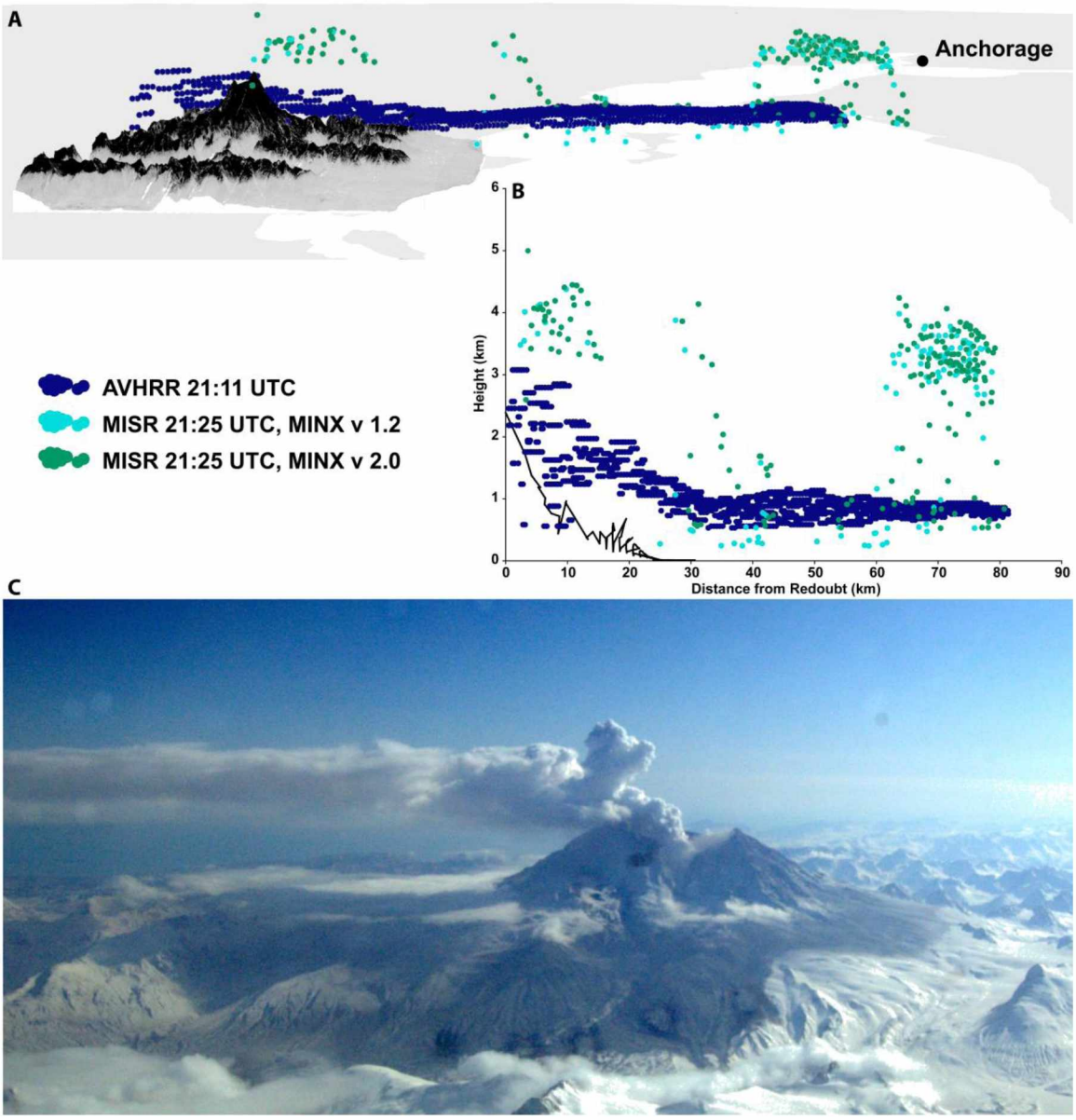
A
Anchorage
B
AVHRR 21:11 UTC
MISR 21:25 UTC, MINX v 1.2
MISR 21:25 UTC, MINX v 2.0
Height (km)
Distance from Redoubt (km)
C

Figure 2.5: Plumes from March 23, 2009. Imagery from 13:25, 14:30, 16:06 and 17:44 UTC. A) ArcScene 3D representation of height results relative to Redoubt, shown with 3x vertical exaggeration, B-E) 2D plot of height results with distance from vent for B) 13:25 UTC, C) 14:30 UTC, D) 16:06 UTC, and E) 17:44 UTC. Plume "drops" artificially between satellite images. For scale, Redoubt has a height of ~3 km. The distance from the Redoubt summit to the Cook Inlet (i.e., nearest coastline) is ~30 km, and the distance from Redoubt to Anchorage is ~160 km. DEM and overlain image are © JAXA 2009.

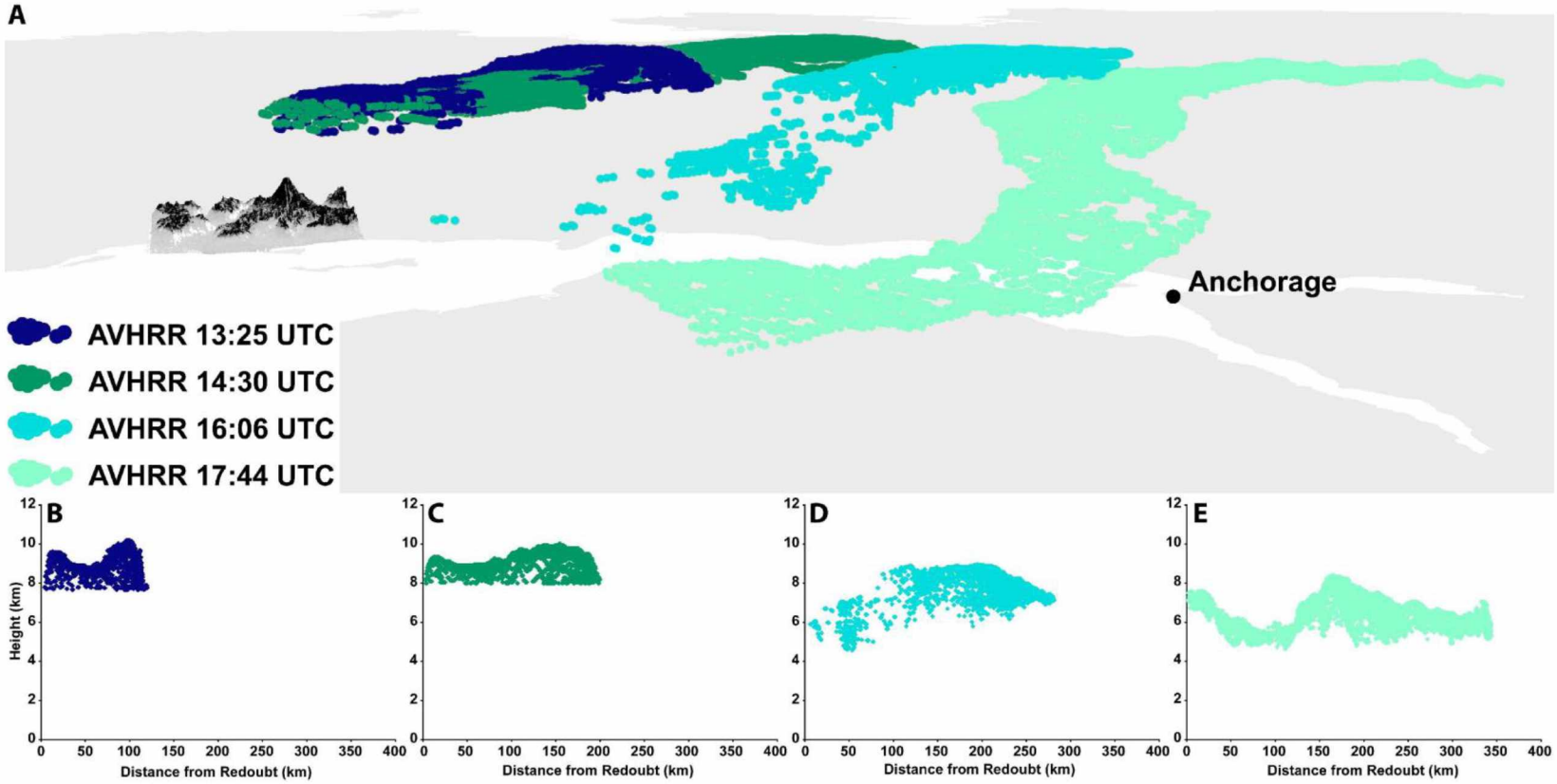
A
Anchorage
AVHRR 13:25 UTC
AVHRR 14:30 UTC
AVHRR 16:06 UTC
AVHRR 17:44 UTC
B
C
D
E
Height (km)
Distance from Redoubt (km)
Distance from Redoubt (km)
Distance from Redoubt (km)
Distance from Redoubt (km)

Figure 2.6: Plumes from April 4, 2009. Imagery from 14:45, 16:23, 17:03, and 19:17 UTC. A) ArcScene 3D representation of height results relative to Redoubt, shown with 3x vertical exaggeration, zoomed out view, B) ArcScene 3D representation of height results relative to Redoubt, shown with 3x vertical exaggeration, zoomed in view, more clearly showing drop in altitude near the vent, C-F) 2D plot of height results with distance from vent for C) 14:45 UTC, D) 16:23 UTC, E) 17:03 UTC, and F) 19:17 UTC. Plume "drops" artificially between satellite images. For scale, Redoubt has a height of ~3 km. The distance from the Redoubt summit to the Cook Inlet (i.e., nearest coastline) is ~30 km, and the distance from Redoubt to Anchorage is ~160 km. DEM and overlain image are © JAXA 2009.

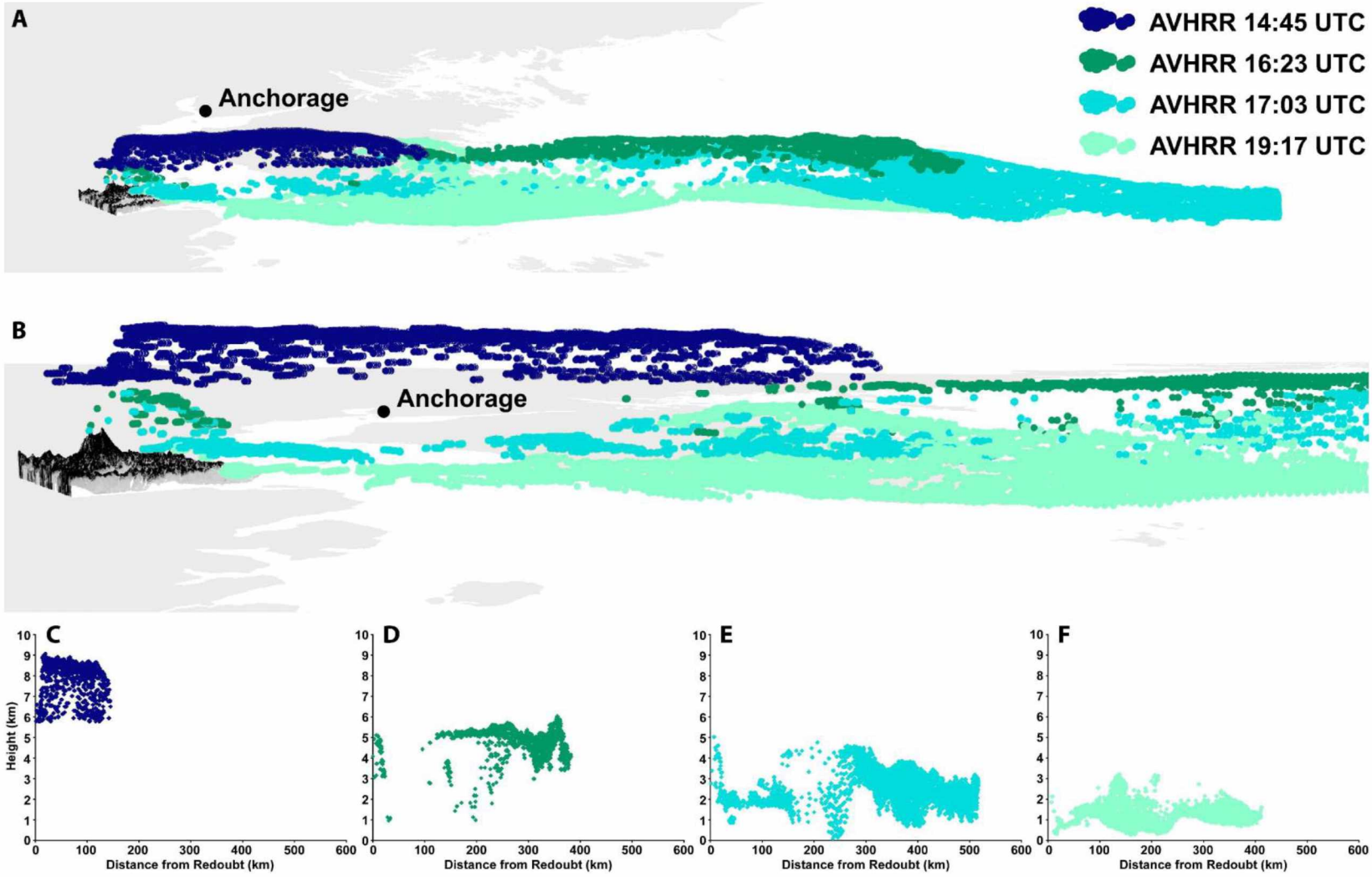
A
Anchorage
AVHRR 14:45 UTC
AVHRR 16:23 UTC
AVHRR 17:03 UTC
AVHRR 19:17 UTC
B
Anchorage
C
D
E
F
Height (km)
Distance from Redoubt (km)

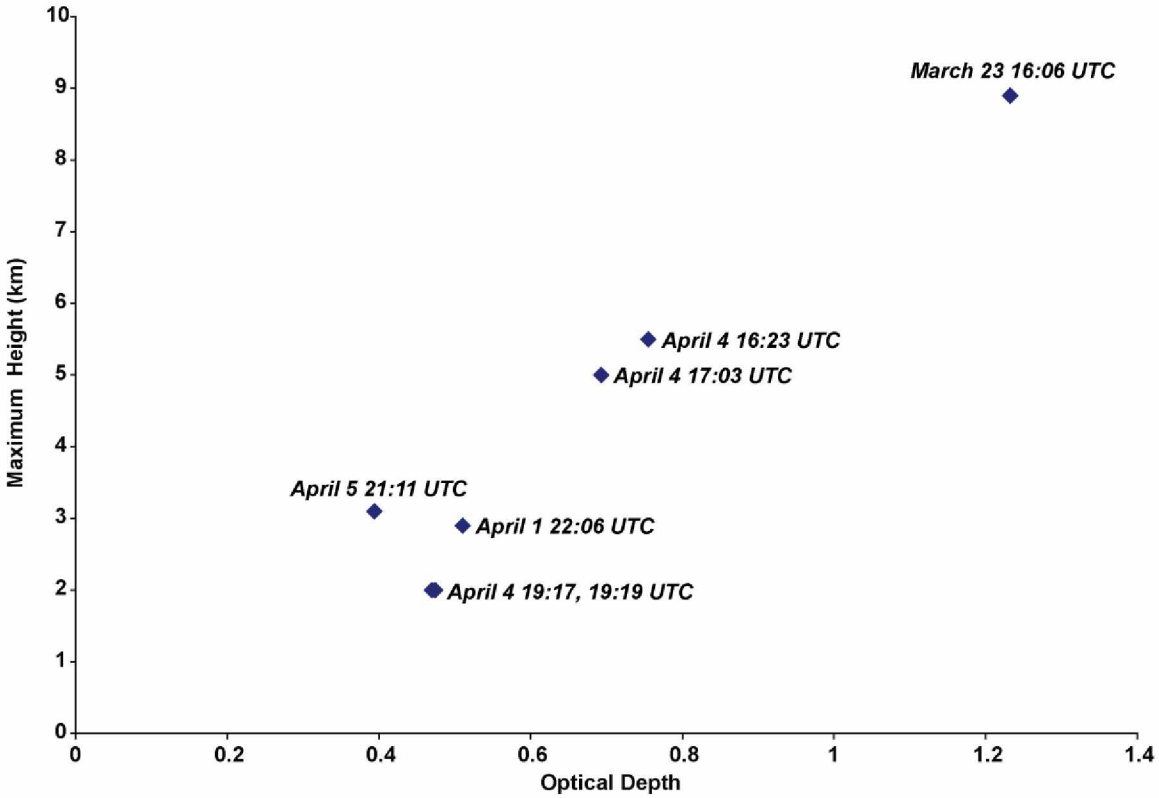

Figure 2.7: Comparison of VAR-obtained mean optical depth and maximum temperature height. Shown is a positive correlation between optical depth and height based on preliminary analysis. Labels specify the imagery to which each data point corresponds. The points for April 4, 19:17 and 19:19 UTC should be considered to effectively represent a single data point. In this case, two files were available for the same satellite pass. The VAR code was run for both files with nearly identical results. Height for the 19:17 pass was used, and was assumed to be identical for both images, as the files should have only differed due to processing error.

Figure 2.8: Select satellite imagery for this study. Imagery shows meteorological cloud cover and plume extent. All images shown are 11 μm band (AVHRR band 4) images from which plume temperatures were determined. Note the small size of the plumes on April 1 and April 5 in comparison to the larger size of the plumes on other days studied. Scale bar, north arrow and temperature scale on the left side of the image are applicable to all satellite images, except for the zoomed in version of 04/05 21:11 UTC, which has its own scale bar.

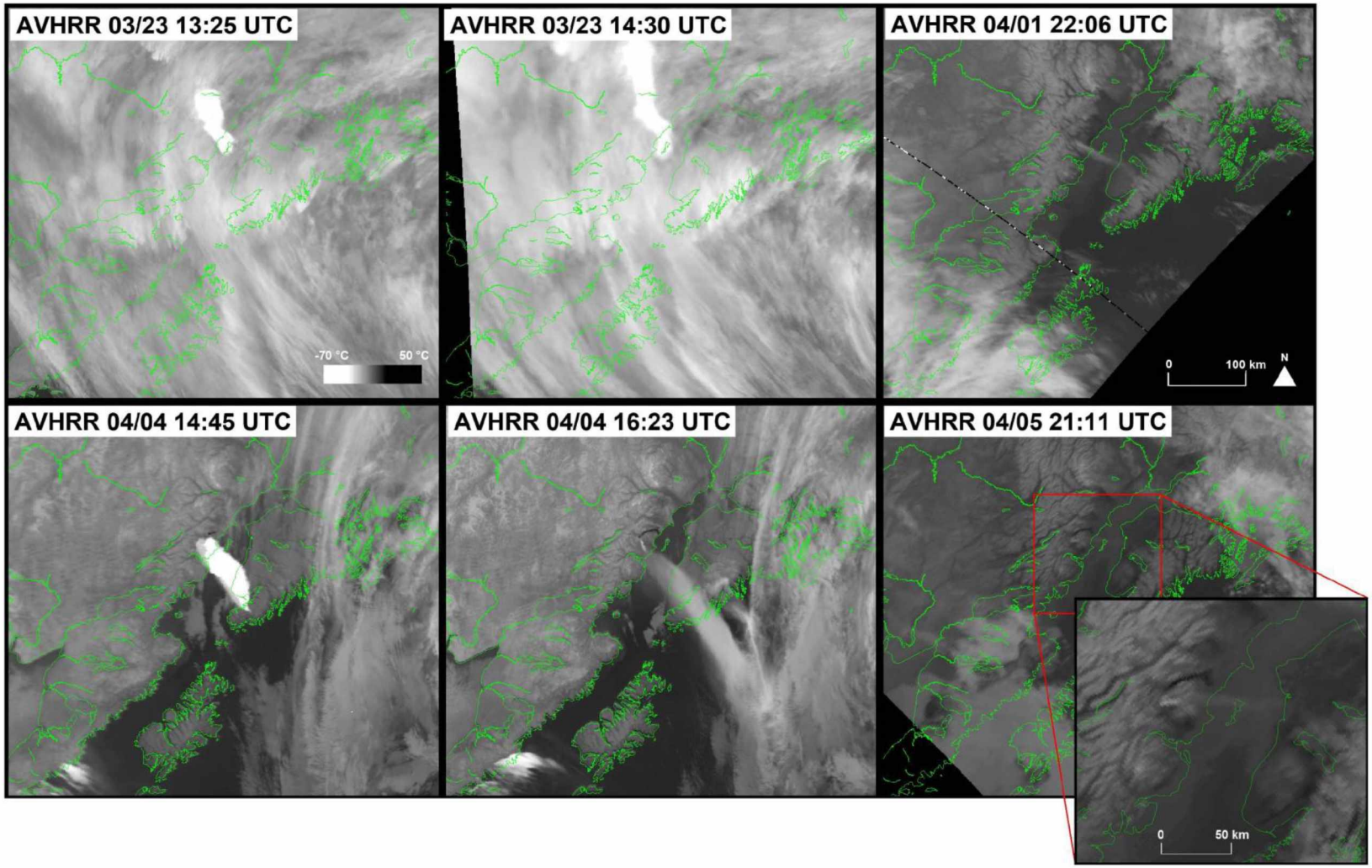
AVHRR 03/23 13:25 UTC
-70 °C
50 °C
AVHRR 03/23 14:30 UTC
AVHRR 04/01 22:06 UTC
0
100 km
N
AVHRR 04/04 14:45 UTC
AVHRR 04/04 16:23 UTC
AVHRR 04/05 21:11 UTC
0
50 km

Figure 2.9: Idealized 2D profiles of temperature height results. A) Smooth plume bottom with height retrievals somewhere inside the plume, B) Scatter in plume, but constant minimum plume bottom showing height retrievals that correspond to underlying weather cloud layer, C) Scatter in plume reaching to ground showing height retrievals that correspond to underlying ground surface, D) Height retrieval that reflects the topography.

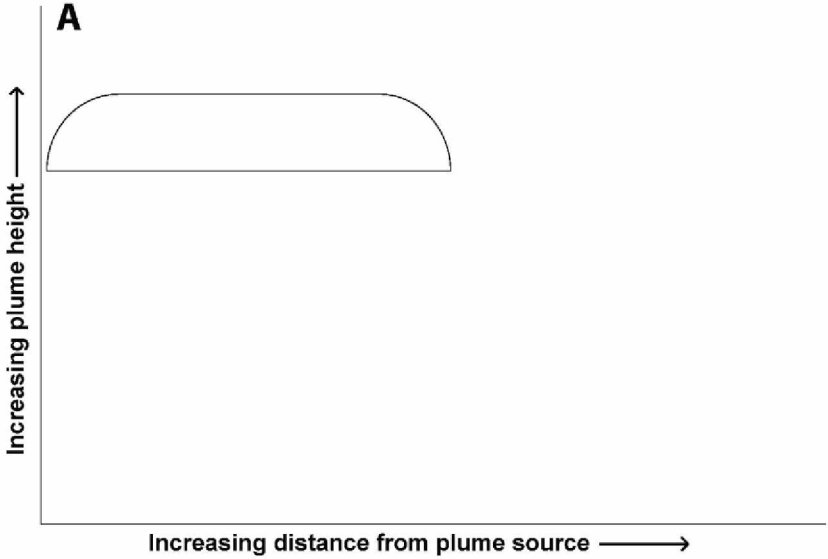
A
Increasing plume height
Increasing distance from plume source

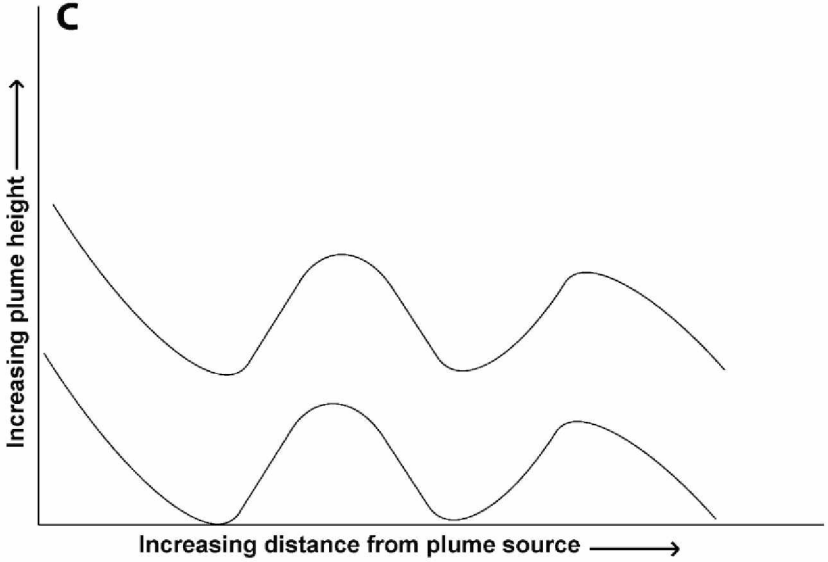
C
Increasing plume height
Increasing distance from plume source

B

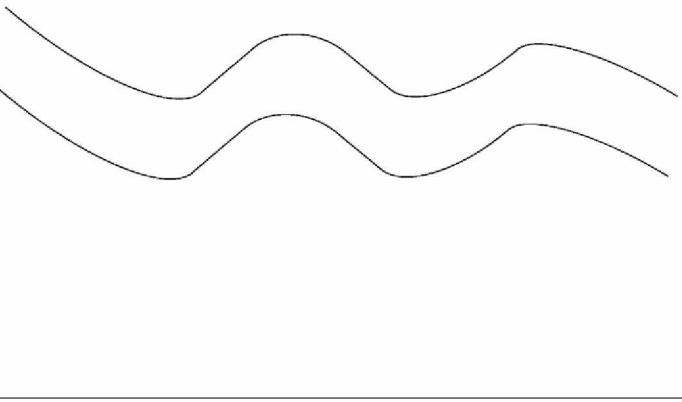

Increasing distance from plume source ⟶

D

Increasing distance from plume source ⟶

Table 2.1: Redoubt explosive events based on AVO seismic analysis

Event number[a]	Date *UTC*[b]	Time *UTC*[b]	Date *AKDT*[b]	Time *AKDT*[b]	Pressure at DFR station 0-p Pa[c]
1	03/23/2009	06:34	03/23/2009	22:34	25
2	03/23/2009	07:02	03/23/2009	23:02	151
3	03/23/2009	08:14	03/23/2009	00:14	38
4	03/23/2009	09:38	03/23/2009	01:38	70
reanalysis	03/23/2009	09:48	03/23/2009	01:48	90
reanalysis	03/23/2009	10:52	03/23/2009	02:52	12
5	03/23/2009	12:30	03/23/2009	04:30	250[d]
reanalysis	03/23/2009	12:58	03/23/2009	04:58	14
6	03/24/2009	03:40	03/24/2009	19:40	76
7	03/26/2009	16:34	03/26/2009	08:34	7
8	03/26/2009	17:24	03/26/2009	09:24	100
9	03/27/2009	07:47	03/27/2009	23:47	31
10	03/27/2009	08:28	03/27/2009	00:28	54
reanalysis	03/27/2009	08:43	03/27/2009	00:43	8
reanalysis	03/27/2009	16:11	03/27/2009	08:11	4.1
11	03/27/2009	16:39	03/27/2009	08:39	83
12	03/28/2009	01:34	03/28/2009	17:34	146
13	03/28/2009	03:24	03/28/2009	19:24	138
14	03/28/2009	07:19	03/28/2009	23:19	78
15	03/28/2009	09:19	03/28/2009	01:19	59
reanalysis	03/28/2009	10:00	03/28/2009	02:00	10
reanalysis	03/28/2009	16:10	03/28/2009	08:10	2
16	03/28/2009	21:40	03/28/2009	13:40	28
reanalysis	03/28/2009	23:09	03/28/2009	15:09	5.9
17	03/28/2009	23:29	03/28/2009	15:29	67
18	03/29/2009	03:23	03/29/2009	19:23	49
reanalysis	03/29/2009	19:19	03/29/2009	11:19	4.3
reanalysis	03/30/2009	07:10	03/30/2009	23:10	1.6
reanalysis	03/30/2009	17:44	03/30/2009	09:44	1
reanalysis	03/30/2009	18:50	03/30/2009	10:50	1
reanalysis	03/31/2009	07:30	03/31/2009	23:30	1.3
reanalysis	03/31/2009	07:41	03/31/2009	23:41	0.25
reanalysis	04/01/2009	00:07	04/01/2009	16:07	1.9
reanalysis	04/01/2009	03:46	04/01/2009	19:46	0.4
19	04/04/2009	13:57	04/04/2009	05:57	38
reanalysis	04/04/2009	14:16	04/04/2009	06:16	88
reanalysis	04/05/2009	18:36	04/05/2009	10:36	3.7

[a] *Event numbers are assigned for explosions for which a VAN/VONA was issued.*
[b] *UTC: Coordinated universal time, or Greenwich mean time; AKDT: Alaska daylight time*
[c] *Seismic pressure is included as an indicator of the strength of each eruption. The data from the DFR station is from an infrasound sensor at DFR. This sensor is a Chaparral Physics model 25 unit with flat response from 0.1 to 200 Hz and a dynamic range of 119 dB (McNutt et al., in press).*
[d] *This pressure is an estimate, as the event was clipped.*
Data in this table from McNutt et al. (in press)

Table 2.2: Specifications of satellite sensors

Sensor	AVHRR	MODIS	MISR
Satellite	NOAA 15, 16, 17, 18, 19	NASA Terra and Aqua	NASA Terra
Number of cameras/sensors	1	1	9
Viewing angles	Near nadir	Near nadir	70.5°, 60.0°, 45.6°, 26.1° forward- and aft-looking, and nadir
Resolution	1100 m	250 m in red, NIR 500 m in visual, SWIR 1000 m in TIR[a]	275 m in red bands of all nine cameras, and all bands of nadir camera; other bands 1100 m
Swath size	~2700 km	2300 km	~400 km common field of view
Bands	5: Visible, MIR, TIR[a]	36: Visible – TIR[a]	4: B/G/R (446, 558, and 672 nm) and NIR (855 nm)[a]
Bands of interest	Temperature: 11 μm (band 4) Ash: 11 & 12 μm (bands 4 & 5)	Temperature: 11 μm (band 31) Ash: 11 & 12 μm (bands 31 & 32)	Heights retrieved using red cameras; 672 nm
Data acquired from	AVO regular data feed; UAF-GINA[b]	AVO regular data feed; UAF-GINA[b]	NASA Langley Research Center Atmospheric Sciences Data Center

[a] *B/G/R: blue, green, red; NIR: near infrared; SWIR: short wave infrared; MIR: mid infrared; TIR: thermal infrared*

[b] *GINA: Geographic Information Network of Alaska*

Table 2.3: Analyzed imagery

Date	UTC time	Sensor	Radiosonde used
03/23/2009	13:25	AVHRR	03/23/2009, 12:00 UTC
03/23/2009	14:30	AVHRR	03/23/2009, 12:00 UTC
03/23/2009	16:06	AVHRR	03/23/2009, 12:00 UTC
03/23/2009	17:44	AVHRR	03/23/2009, 12:00 UTC
04/01/2009	21:42	MODIS	04/02/2009, 00:00 UTC
04/01/2009	21:50	MISR	04/02/2009, 00:00 UTC
04/01/2009	22:06	AVHRR	04/02/2009, 00:00 UTC
04/04/2009	14:45	AVHRR	04/04/2009, 12:00 UTC
04/04/2009	16:23	AVHRR	04/04/2009, 12:00 UTC
04/04/2009	17:03	AVHRR	04/04/2009, 12:00 UTC
04/04/2009	19:17	AVHRR	04/05/2009, 00:00 UTC
04/05/2009	21:11	AVHRR	04/06/2009, 00:00 UTC
04/05/2009	21:25	MISR	04/06/2009, 00:00 UTC

Table 2.4: Summary of results

Date	Sensor	Time of satellite overpass (UTC)	Eruption time (UTC)	Approx. max. plume top height (km ASL)	Approx. avg. plume bottom height (km ASL)	Height from Puff model (ASL)	Altitude drops or varies?[a]
03/23/2009	AVHRR	13:25	12:30 and 12:58	10.2	7.7	6 to 15 km; material lower than ~6 km hidden by cloud cover	varies across plume
03/23/2009	AVHRR	14:30		10	8		varies across plume
03/23/2009	AVHRR	16:06		8.9	6		drops steadily with distance
03/23/2009	AVHRR	17:44		8.4	5		varies irregularly along distance
04/01/2009	MODIS	21:42	0:07 and 3:46, continuous ash emission	3	n/a	~4-5 km or less	drops at 30 km from vent to ~0.7 km ASL
04/01/2009	MISR	21:50		3.4	n/a		drops at 40-50 km from vent to ~2.4 km ASL
04/01/2009	AVHRR	22:06		2.9	n/a		drops at 30 km from vent to ~1 km ASL
04/04/2009	AVHRR	14:45	13:57 and 14:16	9	5.8	Likely 15 km or less	drops steadily to 8.6 km ASL with distance
04/04/2009	AVHRR	16:23		6	~0.9 to ~3.5		varies across plume
04/04/2009	AVHRR	17:03		5	0.6 to 1.6		varies across plume
04/04/2009	AVHRR	19:17		3.2	03 to 1.2		varies irregularly across plume
04/05/2009	AVHRR	21:11	18:36, continuous ash emission	3.1	n/a	~4-5 km or less	drops at 30 km from vent to ~1.2 km ASL
04/05/2009	MISR	21:25		4.4	n/a		drops at 70-80 km from vent to ~4.2 km ASL

[a] *This column is meant to convey the changes in an individual plume as it moves from the vent. The maximum altitude may drop or vary across the plume, and this is detailed here.*

Chapter 3 Application of MISR data to volcanic plumes in the North Pacific: Case studies for Augustine, Okmok, Cleveland, Redoubt, and Sarychev Peak volcanoes[2]

3.1 Abstract

Recent work has shown the Multi-angle Imaging Spectroradiometer (MISR) sensor to be of great utility in the study of volcanic plumes, and this study confirms that MISR stereo height analysis using the software package MINX produces reliable volcanic plume heights under most circumstances. This study analyzes MISR data from the eruptions of Augustine Volcano in 2006, Okmok, Cleveland, and Kasatochi volcanoes in 2008, and Redoubt and Sarychev Peak volcanoes in 2009, all located in the North Pacific on the Alaska mainland (Augustine and Redoubt), in the Alaskan-Aleutian Islands (Okmok, Cleveland and Kasatochi), or in Russia's Kurile Islands (Sarychev Peak). Based on these analyses, this manuscript details circumstances under which reliable MISR height retrievals are possible, such as for plumes of low optical depth, when accurate height retrievals by other methods (e.g., infrared temperature) are not possible. Accurate retrievals are especially likely for plumes of even low optical depth over dark backgrounds such as water. Over bright (highly reflective) backgrounds, such as a layer of meteorological clouds, MISR retrievals at the edges of low optical depth volcanic plumes near the vent, or for dispersed plumes some distance from the vent, may correspond to the underlying land or cloud layer, though these cases were the exception rather than the rule. When MISR retrievals are accurate, MISR stereo heights can replicate textures in clouds that reveal plume dynamics, such as local

---

[2] Ekstrand, A.L., Webley, P.W., Nelson, D.J., Garay, M.J., Dehn, J., submitted. Application of MISR data to volcanic plumes in the North Pacific: Case studies for Augustine, Okmok, Cleveland, Redoubt, and Sarychev Peak volcanoes. J. Volcanol. Geotherm. Res.

transport directions of ash within a plume. Furthermore, MISR stereo height retrievals are of high enough spatial resolution (1.1 km) to detect height gradients and oscillating height patterns within volcanic plumes. MISR aerosol data also allow for confirmation of ash content in most volcanic plumes for which the MISR standard aerosol product is available.

3.2 Introduction and background

The Multi-angle Imaging SpectroRadiometer (MISR) satellite sensor has been used to study many plume types, including forest fire plumes, grassland fire plumes, and volcanic plumes (Kahn et al., 2007; 2008; Mims et al., 2009; Scollo et al., 2010; 2012; Val Martin et al., 2010). By examining the 2009 Redoubt Volcano eruption, Ekstrand et al. (in review) found that the MISR sensor produced more accurate volcanic plume heights than the more commonly used basic infrared (IR) temperature method (Kienle and Shaw, 1979; Sparks et al., 1997; Dean et al., 2002). In this study, volcanic plumes from a variety of eruptions were analyzed using data from the MISR sensor to determine the strengths and limitations of MISR's application to volcanic plumes. These plumes are from the eruptions of Augustine Volcano in 2006; Okmok, Cleveland, and Kasatochi volcanoes in 2008; as well as Redoubt and Sarychev Peak volcanoes in 2009. All of these volcanoes are located in the North Pacific (NOPAC): Augustine and Redoubt are located in Alaska's Cook Inlet region; Okmok, Cleveland, and Kasatochi are located in the Alaskan-Aleutian Islands; and Sarychev Peak is located in Russia's Kurile Islands (Figure 3.1).

The data presented here were analyzed with two goals: 1) to determine if height retrievals were successful for different types of plumes (optically thin vs. thick, ash rich vs. ash poor, higher vs. lower altitude, and in cloudy vs. clear conditions), and 2) to examine if MISR aerosol data provided any insight into the composition of the plume.

3.2.1 Augustine Volcano 2006

Augustine Volcano forms Augustine Island and is located in Alaska's Cook Inlet (Figure 3.1). It is a dome complex of andesite and dacite composition that has a summit elevation of ~1.3 km above sea level (ASL). The volcano is 280 km southwest of Anchorage, Alaska (Bailey et al., 2010). Augustine erupted in January 2006 after a 20-year period of repose (Power et al., 2006). Beginning on January 11, the volcano erupted explosively 13 times, until entering a phase of continuous gas and ash emission from January 28 to February 2. The volcano subsequently had a two-week period of effusive activity that ended in mid-March. This eruption was typical of Augustine Volcano, and analyses closely match those from the eruptions of 1976 and 1986 (Swanson and Kienle, 1988; Power et al., 2006). Overview and details of this eruption are provided in Power et al. (2006) and Bailey et al. (2010).

3.2.2 Okmok Volcano 2006

Okmok Volcano is located on Umnak Island in Alaska's Aleutian Islands (Figure 3.1). It is a basaltic shield complex containing a relatively young (~2050 years old) caldera, and has a summit elevation of ~1.1 km ASL. It is a very active volcano, with 14 confirmed eruptions since 1817, and the most recent (before 2008) was in 1997. Okmok erupted explosively on July 12, 2008, beginning an eruption that lasted 5 weeks. Typical eruptions at Okmok include modest ash clouds of fairly low altitude (5-6 km ASL) and lava flows across the caldera. The 2008 eruption departed from the typical pattern, and was a sudden, violent phreatomagmatic eruption with little (~5 hours) of precursory seismic activity (Larsen et al., 2009). Satellite detection of volcanic ash was difficult during this eruption because the eruption was very water rich (Larsen et al., 2009), which masked ash signals detected by traditional methods (Larsen et al., 2009). Abundant

accretionary lapilli (particles of smaller ash which are held together by water to form larger lapilli) were found in fine-grained fall deposits. Other eruption deposits included tephra and lahar deposits (Larsen et al., 2009). An overview of this eruption is provided in Larsen et al. (2009).

3.2.3 Cleveland Volcano 2008

Cleveland Volcano is located on Chuginadak Island in Alaska's Aleutian Islands (Figure 3.1). It is a stratovolcano of basaltic andesite composition, and stands at ~1.7 km ASL. It produced infrequent and sudden ash explosions in 2008, with the most vigorous activity occurring in late July of 2008 (Neal et al., 2011). The eruption was characterized by the presence of steam and gas plumes and thermal anomalies (areas of elevated temperature) in satellite data. This behavior – intermittent explosions throughout the year with a period of more concentrated activity – is typical of Cleveland's eruptive behavior in recent years (Neal et al., 2011). From 2005-2011, there have been 13 reports of activity at Cleveland from the Smithsonian's Bulletin of the Global Volcanism Network (2011). Cleveland is unmonitored by seismic equipment, but because of its frequent activity, is closely monitored by satellite remote sensing (Neal et al., 2011). An overview of the 2008 eruption is provided in Neal et al. (2011).

3.2.4 Kasatochi Volcano 2008

Kasatochi Volcano is a 3 km wide, 314 m (0.314 km) ASL island volcano located in the Aleutian Islands (Figure 3.1). It is a small stratovolcano of basaltic and andesitic composition. Kasatochi had no confirmed historical eruptions, and was previously unstudied before the 2008 eruption (Waythomas et al., 2010). It erupted explosively August 7-8, 2008 in a very large, sudden explosive eruption which contained three primary pulses: the first two gas-rich and ash-poor, and the third ash- and gas-rich. These pulses were followed by 17 hours of continuous emission

(Waythomas et al., 2010). The ash cloud produced by the Kasatochi eruption was very large, reaching stratospheric altitudes. The ash cloud reached the western coast of North America before entirely dispersing (Waythomas et al., 2010). The eruption also released a large sulfur dioxide (SO_2) cloud on the order of 2 Tg which was observed to circle the globe (Heue et al., 2010; Kristiansen et al., 2010; Krotkov et al., 2010; Waythomas et al., 2010). An overview of this eruption is provided in Waythomas et al. (2010).

3.2.5 Redoubt Volcano 2009

Redoubt Volcano is located on the Alaska mainland near the Cook Inlet, about 175 km southwest of Anchorage (Figure 3.1). It is an andesitic stratocone standing ~3.1 km ASL. The volcano erupted explosively on March 23, 2009 after nearly 20 years of repose, and these explosive ash eruptions continued until April 4, 2009 (Schaefer, 2012). After the eruptive phase of activity, the volcano transitioned to a lava dome building phase (Bull and Buurman, in press). This eruption was similar in some ways to the previous eruption in 1989, but different in others: the 2009 eruption had months of precursory activity, where the 1989 eruption had ~22 hours, and though the 2009 eruption produced a lava dome, there were few periods of lava dome collapse in the 2009 eruption, and many in the 1989 eruption (Miller and Chouet, 1994; Schaefer, 2012). This eruption also had high explosivity due to high water content: water content obscured ash signals in satellite data, and a high proportion of accretionary lapilli were found in fall deposits (Schaefer, 2012). An overview of this eruption is provided in Schaefer (2012). Plume height analysis of this eruption is provided in Ekstrand et al. (in review).

3.2.6 Sarychev Peak Volcano 2009

Sarychev Peak is a volcano located on the northwest side of Ostrov Matua (Matua Island) in the Kurile Islands, Russia (Figure 3.1). It is one of the most active volcanoes in the Kuriles, with 10 eruptions since 1760. It is a stratovolcano that grew within Matua caldera (an older submarine shield volcano), filling it almost completely. It is composed of basaltic andesite and rare andesite (Rybin et al., 2011). After a 33 year period of repose, the eruption began on June 12, 2009, though activity was indicated in thermal satellite data from the previous day (Rybin et al., 2011). The eruption was imaged by satellite sensors and by the International Space Station, but was not captured with any seismic monitoring equipment, as there was limited seismic equipment in the area (Haywood et al., 2010; Matoza et al., 2011). There were at least 23 explosions between June 11 and 16, 2009, and the eruption was more explosive than the volcano's previous eruptions, which included explosive eruptions of slightly smaller volcano explosivity index (VEI) as well as some effusion of lava (Rybin et al., 2011). The high crystallinity of the erupted magma may have contributed to the high explosivity of the eruption, according to petrological analyses (Rybin et al., 2011). Details of satellite and ground observations are provided in Rybin et al. (2011). Other details are provided in Haywood et al. (2010) and Matoza et al. (2011).

3.2.7 The MISR sensor

The MISR sensor has been acquiring data since early 2000, and flies aboard the National Aeronautics and Space Administration's (NASA's) Terra satellite. It was specifically designed for providing stereo data, and processing of the data is capable of retrieving stereo heights for plume features such as volcanic plumes and forest and grassland fire plumes (Diner et al., 1998; Kahn et al., 2007; 2008; Mims et al., 2009; Scollo et al., 2010; 2012; Val Martin et al., 2010). Data from the MISR sensor is also used to produce aerosol products, which give information such

as optical depth and particle size and shape fractions (Kahn et al., 2010). The sensor acquires views of a given location from nine different cameras positioned at various view angles within a window of seven minutes. It provides global coverage once every 9 days, and more frequently at the poles (Diner et al., 1998). Sensor specifications are provided in Table 3.1.

3.3 Methods

Different datasets were analyzed for each volcanic eruption, as shown in Table 3.2. Only two MISR passes were evaluated for height in comparison to the basic satellite temperature method (described in section 3.3.3), since the temperature method was treated thoroughly in Ekstrand et al. (in review). All passes were compared with the Puff volcanic ash transport and dispersion (VATD) model (Searcy et al., 1998; described in section 3.3.2) to determine if height results were reasonable. Two MISR passes were analyzed in comparison to gas flights or airborne photography. Four MISR passes provided aerosol results which were included in analysis.

3.3.1 MISR and MINX

All MISR data were processed using MISR Interactive eXplorer (MINX), an IDL-based program that features built-in plume processing utilities, including utilities for volcanic plumes (Nelson et al., 2009). MINX is open source software that is available from the Open Channel Foundation (2010). MINX asks the user to manually define a plume area and specify an associated wind direction that represents the expected transport direction of volcanic particles (this is referred to as digitizing the plume). Using a correlation matcher among six different camera pairs, including subpixel accuracy, MINX calculates the best-fitting height and wind speed at 1.1 km spatial resolution, using data from the 275 m resolution MISR red band (see Table 3.1). Due to the fact that feature propagation in the direction of satellite motion (along-track) aliases with the stereo-

derived heights (Moroney et al., 2002), the wind speed and direction are used to correct the retrieved (zero wind) stereo heights determined from the stereo matching alone. Unlike the operational MISR stereo height retrieval algorithm described by Moroney et al. (2002), MINX uses a locally derived wind speed and solves a simpler set of equations, because the true wind direction is specified by the user (Nelson et al., 2009). The vertical resolution of the operational MISR stereo-derived cloud top heights is approximately 560 m with good agreement with validation data (e.g., Garay et al., 2008), but the subpixel matching used in MINX provides vertical resolution on the order of 200 m, although extensive validation is ongoing. Studies have shown that MINX works best for relatively dense, well-defined plumes (Mims et al., 2009).

MINX also reads aerosol retrievals from the MISR standard level 2 aerosol product, which is generated routinely as new images are required. This retrieval uses a look up table that contains 74 predefined mixtures of "pure" aerosol particle types. This is done so that matching is based on candidate aerosols whose physical and chemical (and therefore optical) properties are well known. These particle types fall into a small number of compositional categories including: sea spray, sulfate/nitrate, mineral dust, biogenic particles and urban soot (Kahn et al., 2010). Retrievals are performed for 17.6 km regions, as this area is assumed to correspond to a locally homogenous atmosphere (Kahn et al., 2010). If a retrieval exists for a portion of the user-defined plume area analyzed by MINX (i.e., if the plume area overlaps one or more 17.6 km regions), the aerosol retrievals (if any) for the corresponding locations analyzed by MINX are provided in the MINX text and graphical output, whether or not MINX retrieves a height for the pixels that correspond to these locations.

Aerosol results from the MISR standard level 2 aerosol product that are reported in the MINX output include aerosol optical depth (AOD) and optical depth (tau) fraction by particle type, reported on 17.6-km regions. Optical depth is reported for each band – red, green, blue, and near infrared (NIR). Tau fraction by particle type represents the fraction of the green-band optical depth value that is attributable to small (<0.35 μm radius), medium (radius 0.35 to 0.7 μm) and large (>0.7 μm radius) particle sizes with the sum of these weighted fractions equaling 1, as well as the fraction of the green-band optical depth value that is attributable to spherical particles (the non-spherical fraction is simply 1 minus the spherical fraction). Optical depth, and all other aerosol parameters, will not have valid values when optical depth is very high (greater than ~2.5) or when there is significant cloud contamination within the 17.6-km region (Nelson et al., 2009; Kahn et al., 2010).

MISR imagery in this study was processed using terrain-projected data files, with the exception of an image containing an ash cloud from Kasatochi Volcano, which contained no land and was processed using an ellipsoid-projected data file. These data were processed for height retrievals and aerosol output using the "Process Plumes" utility in MINX. Height data were plotted for analysis using Excel. If available, aerosol data were mapped and compared to the analyzed plume area using ArcGIS, to determine the regions of the plume which contained the most representative aerosol data. Both the currently released MINX version 1.2 (Nelson et al., 2009) and a development version 2.0 were used in this study, with emphasis on the development version. The aerosol data were taken from the currently operational (V22) L2 MISR aerosol product (Kahn et al., 2010).

3.3.2 Puff VATD model

Puff is a volcanic ash transport and dispersion (VATD) model developed at the University of Alaska Fairbanks Geophysical Institute (UAF-GI) for tracking the dispersion of young eruption clouds (less than 48 hours old; Searcy et al., 1998), and is the primary dispersion model in use by the Alaska Volcano Observatory (AVO). Hypothetical particles of a user-specified grain size distribution, height, and column shape are modeled in a 4-dimensional (latitude, longitude, height, time) gridded wind field. The movement of these particles is then tracked according to advection, Lagrangian diffusion, and Stokes' law of settling (Papp et al., 2005). Ash particles are incorporated from the vent altitude to a maximum height specified by the user (Searcy et al., 1998). By comparison with satellite imagery, the height of an eruption cloud can be determined. An observed ash cloud distribution from satellite imagery is compared with the ash cloud distribution in the model; heights can be read from the model for the area that agrees best with the satellite observations. This method always produces a range of heights, and wind shear (differing wind directions at different atmospheric altitudes) must be present for this method to constrain heights well (Ekstrand et al., in review).

Puff model runs were compared to each MISR image. Puff was run several times until it produced a plume that matched the MISR image as closely as possible. This was done to determine if the heights retrieved by MINX were reasonable based on local wind fields at the time of eruption.

3.3.3 Satellite temperature method

The basic satellite temperature method is a simple approach that compares temperatures from satellite data directly to atmospheric data to determine plume height. Satellite data used for the

temperature method is from the Advanced Very High Resolution Radiometer (AVHRR) and the Moderate Resolution Imaging Spectroradiometer (MODIS) sensors. Thermal infrared (TIR) temperatures from the 11 μm channel of each satellite (channel 4 for AVHRR; channel 31 for MODIS) are analyzed for the coldest pixel in the eruption plume. This temperature is then compared to local temperature-altitude atmospheric profiles (soundings) to determine height (Sparks et al., 1997). Assuming that the plume is in thermal equilibrium with the surrounding atmosphere, and that the temperature of the atmosphere generally decreases with height (i.e., the plume is lower in altitude than the tropopause), this coldest pixel should correspond to the highest height of the plume. Atmospheric sounding data from radiosondes (described in Simpson et al., 2000) are used for this method, and are obtained from the University of Wyoming's College of Engineering's Department of Atmospheric Science online sounding database.

This method may produce inaccurate heights in cases of undercooling (when the temperature of the plume is lower than the surrounding atmosphere; Sparks et al., 1997), and the plume or cloud must be opaque to ground radiation for the method to work well (Kienle and Shaw, 1979; Sparks et al., 1997). To account for plume transparency, pixels with a negative brightness temperature difference (BTD; supposedly semi-transparent or transparent pixels; Prata, 1989a, b; Simpson et al., 2000; Prata et al., 2001) were removed from subsequent analysis. This method is detailed in Ekstrand et al. (in review). Not all transparent pixels will be accounted for by this method if the cloud has high water content (Prata, 1989a, b; Simpson et al., 2000; Prata et al., 2001; Ekstrand et al., in review). Satellite temperatures are most accurate for very young, very opaque eruption clouds near the vent; varying degrees of optical thickness result in retrievals of height corresponding to a point inside the plume that may sometimes be several kilometers lower than the cloud top (Ekstrand et al., in review).

AVHRR data was used for temperature height analysis of the Redoubt eruption, and MODIS data was used for analysis of the Okmok eruption. For those images analyzed for temperature heights, the following method was used (described in greater detail in Ekstrand et al., in review). This data was imported into ENVI, an Interactive Data Language (IDL)-based raster data processing package, and the files were georeferenced. Each plume was delineated using the 11 μm data and optimized to contain the maximum extent of the plume. Band math following the method of Ekstrand et al. (in review) was performed to ensure only opaque pixels were used. Temperatures were converted to height using temperature-altitude relationships (lapse rates) defined by atmospheric soundings acquired as close in time as possible to the eruption. These soundings were from Anchorage, Alaska (PANC) for Redoubt, and from Cold Bay (PACD) and St. Paul (PASN) for Okmok. PACD and PASN were roughly equidistant from Okmok, so these lapse rates were averaged. For Redoubt, calculations assumed a ground temperature of 0°C, while calculations for Okmok assumed a ground temperature of 6 or 7°C, taking into account a y-intercept in the lapse rate equation. Temperature results were plotted in Excel for comparison with MISR data. The 2D graphs were created by using IDL to calculate the great circle distance between the location of each plume height retrieval (corresponding to the center of the pixel containing the retrieval), and the location of the vent, and then plots of height against distance were produced for each analyzed plume in Excel.

3.3.4 Observation flight data and airborne photographs

Airborne photographs of Augustine were taken on January 30, 2006 by scientists at AVO during an observation flight (personal communication, Tom Miller and Dave Schneider, USGS). These photographs were used to visually compare the plume shape to that in MISR data. The MISR

overpass and the photographs were acquired within about an hour of each other. Reports from the flight also included estimates of plume height (Table 3.2). Some estimated plume heights exceeded the maximum altitude of the aircraft, and these heights were estimated with attention to the aircraft altitude, and in consultation with the pilot (personal communication, Tom Miller).

During the Redoubt eruption, gas observation flights were conducted in a fixed-wing aircraft by scientists at AVO and the Cascades Volcano Observatory. The gas observation flights collected data about volcanic aerosols, but also collected altitude and position information using a GPS receiver at 1-second intervals (1-Hz frequency; Werner et al., in press). Data is available for April 5, 2009 (Table 3.2). Airborne photographs of Redoubt Volcano were also taken on April 5, 2009. Photography and gas observations were acquired about 4 hours after the MISR overpass for this day, and Puff VATD model runs show that the wind fields did not change significantly in this time, and that any material continuously emitted during this period would likely continue to travel in the same trajectory, at the same altitudes.

3.4 Results

3.4.1 Augustine Volcano 2006

For Augustine on January 30, 2006, MINX retrieved a very flat plume top that was about 5.2 to 5.7 km ASL in maximum height, with the bulk of the cloud ~5 km ASL (Figures 3.2a, 3.3a). The plume was over an ocean background, and retrievals are very good, with heights retrieved for 88 percent of digitized pixels. Notably, for MISR to produce a flat plume top, the two "sides" or "halves" of the plume had to be digitized separately with diverging wind directions. Puff VATD runs that produced an output closest to the MISR results modeled a plume of similar trajectory

(Puff bearing 58.94°; MISR bearing 56.25°; Figure 3.4a), and a plume height distribution reasonably similar to the one in the MISR retrievals at ~6 km ASL (Figure 3.2a).

Airborne photographs from this date also showed a very flat plume top (Figure 3.5a-b). Descriptions from the observation flight on which airborne photographs were obtained estimated that the top of the column was at ~4.9 km ASL, with white segments strongly convecting to an altitude of ~4.5 km ASL, and a brownish ash-rich segment "hung in space" below ~3.6 km ASL (personal communication, Tom Miller, USGS). Compared to MISR, these appear to be slight underestimates, but not by much (less than 1 km).

3.4.2 Okmok Volcano 2008

Okmok produced a plume with decoupled (bifurcated) ash and steam portions during its eruption on July 13, 2008 (Figures 3.2b, 3.3b). The background (beneath the plumes) was comprised mostly of water. The assessment of content of the plumes (ash vs. steam) was conducted visually, it being assumed the white portion was comprised mostly of steam, and that the brown portion was comprised mostly of ash. For Okmok imagery from this date, MINX retrieved heights for 91 percent of digitized ash plume pixels, and 79 percent of digitized steam plume pixels. Some oscillation was seen in MINX heights for the steam plume, but not for the ash plume. The ash plume had a relatively flat top at ~2 km ASL (Figure 3.3b). The steam plume's height oscillated along its length, with maximum heights at ~10.4 km, 9.3 km, and ~11.5 km ASL with increasing distance from the vent. The closest Puff VATD model simulation was not an exact match in plume trajectory (Figure 3.4b), but showed lower altitude material at ~2 km ASL traveling in a more southerly direction (Puff bearing 143.83°, MISR bearing 150.51°; Figures 3.2b, 3.4b), and

higher altitude material at ~6 to 10 km ASL traveling in a more southeasterly direction (Puff bearing 138.95°, MISR bearing 127.36°; Figures 3.2b, 3.4b).

Temperature heights for these plumes only partially matched MISR heights (Figure 3.3b). The ash portion of the temperature heights (the thick concentration of heights denoted by the arrow in Figure 3.3b) was slightly higher than the MINX retrieved heights, with plume top heights ranging from ~2 km ASL to ~2.5 km ASL for temperature retrieved heights compared to ~2 km ASL for MINX heights. The heights for the steam portion (lower portion of these heights denoted by the bracket in Figure 3.3b) were in relatively good agreement near the vent (~11.1 km ASL compared to MISR heights ~10.4 km ASL), and farther away from the vent were much lower than the MINX retrieved heights (maximums at ~6.5 km to ~7.1 km ASL compared to MISR heights maximums at 9.3 km to 11.5 km ASL).

Okmok imagery was also available for July 22, 2008, and the plume was visible above meteorological clouds (Figure 3.2c). Retrievals were good, with 95 percent of digitized pixels producing heights. MINX retrievals for this day showed variable heights over the length of the plume (Figure 3.2c, 3.3c). These height oscillations were relatively regular along the length of the plume (about every 10-15 km or so). The bulk of the plume was between 1.5 and 4.5 km ASL, with plume top maximums ranging from 3 km to 5 km ASL, and plume minimum heights around 0.5 km to 1.5 km ASL (Figure 3.3c). The closest Puff run produced a similar trajectory (Puff trajectory 112.73°, MISR bearing 117.40°; Figure 3.4c), and heights around 2 to 5 km ASL (Figure 3.2c).

Another notable feature from the MINX height retrievals for July 22 is that different retrievals were produced when the edges of the Okmok ash plume were not digitized. In the inset in Figure 3.3c, there is a layer of heights at about 0.5 to 1.5 km ASL. This layer is very dense, with many height retrievals. These points correspond to the ash plume edges. When the ash plume is digitized without these edges, this lower height layer disappears.

Okmok imagery was also available for July 29, 2008, another day when the plume was visible over meteorological clouds (Figure 3.2d). Retrievals were good for this plume, with heights retrieved for 97 percent of digitized pixels. MINX retrievals for this plume showed a mostly flat plume with a fairly consistent maximum plume top altitude ~4 km ASL (Figure 3.2d, 3.3d). There were some portions of the plume that displayed higher altitudes, up to 5 or 6.5 km ASL (Figure 3.3d). Based on visual analysis of the MISR oblique camera images, these portions of the plume also appeared to be of volcanic origin. The closest Puff run produced a plume with a fairly consistent maximum altitude around 3 to 5 km ASL (Figure 3.2d), and a similar trajectory (Puff trajectory 112.97°, MISR bearing 110.44°; Figure 3.4d).

3.4.3 Cleveland Volcano 2008

MISR imagery was available for Cleveland Volcano on July 22, 2008, and the plume was visible above meteorological cloud cover (Figure 3.6a). Height retrievals were good for Cleveland, with 95 percent of digitized pixels producing heights. Height retrievals from MINX showed a fairly consistent maximum plume altitude ranging from 2.7 km to 3.6 km ASL, with the center of the plume at the lower end of this range, and the farthest plume extent and near vent portions at the higher end of this range (Figure 3.6a, 3.7a). Height retrievals from this day also showed a similar phenomenon to the July 22 Okmok data, in which a lower altitude area of heights ranging from

~0 to 1.5 km ASL, was retrieved when the digitized area is too large (Figure 3.7a inset). When the narrowest range of the plume was digitized, this layer almost disappeared (Figure 3.7a). The closest Puff VATD model run produced a plume with a fairly consistent maximum altitude between 2 and 4 km ASL (Figure 3.6a), and a fairly similar trajectory (Puff trajectory 109.04°, MISR trajectory 110.95°; Figure 3.4e).

3.4.4 Kasatochi Volcano 2008

Heights for an ash cloud from Kasatochi were not successfully retrieved by MINX processing in the present study. The extremely thin brown ash cloud was visible over meteorological clouds as a brown "tint" to the image (this does not appear clearly on small images, so no figure is included). Puff VATD model runs and other satellite data (unpublished GOES and AVHRR data from AVO; some imagery available at www.avo.alaska.edu) confirm that the ash cloud was in this location during the time of MISR acquisition. However, when MINX was run for the particular location, only one zero-wind height was retrieved (at 10 km) ASL and after wind correction, no valid heights remained, only heights for the underlying meteorological cloud layer at 0 to 2 km ASL.

3.4.5 Redoubt Volcano 2009

A comparison between MISR, AVHRR, photographic, and gas flight data was available for April 5, 2009. This comparison was detailed in Ekstrand et al. (in review). However, reruns of the MISR data presented here showed that MINX produced even more (and higher) retrievals near the vent than were reported in Ekstrand et al. (in review; Figure 3.6b, 3.7b).

MINX retrievals were poor for Redoubt Volcano plumes; with heights produced for only 16 percent of digitized pixels. These retrievals showed a plume that was, at its highest, 6 km ASL near the vent, and then dropped in altitude from 5 km ASL mid-plume to 4 km ASL at the farthest plume extent (Figure 3.6b, 3.7b). Temperature retrieved heights, in contrast, showed a maximum of just over 3 km ASL near the vent (recall that the summit altitude itself is ~3.1 km ASL), and dropped to between ~0.5 and 1.2 km ASL over the length of the plume (this drop levels at ~30 km from the vent, over an ocean background). Puff VATD model runs, which produced a maximum altitude of about 4 to 5 km ASL (with more modeled points toward the higher end of this range near the vent) were in better agreement with the MINX retrievals (Figure 3.6b), and the trajectory of the Puff results agreed very well with MISR results (Puff trajectory 88.01°, MISR trajectory 92.01°; Figure 3.4f). Airborne photographs did not show a drop in altitude, and gas flight estimates put the bulk of the plume at 3.8 km ASL and the plume top at above 4.1 km ASL (Figure 3.5c). There was no cloud cover on this day, and all retrievals occurred over land or an ocean background.

3.4.6 Sarychev Peak Volcano 2009

MISR imagery was available for Sarychev Peak on June 14, 2009. The plume was visible above meteorological cloud cover. MINX retrievals were good, producing heights for 85 percent of digitized pixels. MINX height retrievals showed an area of very high altitude material (>9 or 10 km ASL) on the east side of the plume, and, in contrast, decreasing heights away from the vent to the west (Figure 3.6c, 3.7c). These heights decreased steadily from ~10 km to ~6 km ASL for the plume top, and ~8 km ASL to near ground level for the plume bottom (Figure 3.6c, 3.7c). Puff VATD model runs showed that the material to the west of the vent was lower altitude (no more than 12 km ASL with most points near 11 km ASL) than the material to the east of the vent

(closer to 15 to 18 km ASL; Figure 3.6c). However, this material to the east of the vent was cut off in the MISR image by the edge of the swath. The altitude at which material begins to travel east instead of west is, however, different between MINX retrieved heights and Puff modeled heights – about 9 or 10 km ASL for MINX heights and ~15 km ASL in Puff runs (Figure 3.6c). The trajectory for the plumes was the same in overall direction, but Puff showed a much smaller plume area than MISR data, making comparison of bearings difficult (Puff trajectory 278.32°, MISR trajectory 269.40°; Figure 3.4g).

MISR imagery was also available for June 16, 2009. The plume was visible over ocean and partial meteorological cloud cover backgrounds. Retrievals were good, and MINX produced heights for 92 percent of the digitized pixels. The height of the material on the north/northeast side of the plume, according to MINX retrievals, was ~4 km ASL near the vent, and increased to ~7 km ASL at the farthest extent of the plume (Figure 3.6d, 3.7d). The south/southwest side of the plume was close to ~8.5 or 9 km ASL near the vent, and remained at this altitude along the length of the plume. (Figure 3.6d, 3.7d). Puff runs also showed lower altitude material on the north side of the plume (about 2-3 km ASL) and higher altitude material (up to 10 km ASL) at the south side of the plume (Figure 3.6d). The trajectory for the plumes was very similar (Puff trajectory 316.13°, MISR trajectory 313.14°; Figure 3.4h).

3.4.7 Aerosol results

Representative values are presented here for plumes which had aerosol results (Table 3.3). Optical depth of the plumes varied depending on plume thickness; however, all were fairly low (<1.0) as MISR does not perform optical depth retrievals for clouds with high optical depth (above ~2.5; Kahn et al., 2009) For the eruption of Okmok Volcano in 2008, it is notable that the

plume center had a higher optical depth than the edges, though the tau fraction particle size and spherical percentages were the same for both areas. For Sarychev Peak Volcano plumes, retrievals at plume edges had lower optical depth than retrievals near the vent, though this comparison is between two eruptive events.

Aerosol results for particle fraction and shape were quite similar for most plumes, except for the plume from the eruption of Redoubt Volcano in 2009. Most results had a spherical fraction of about 0.4. Small, medium, and large fractions were in the range of approximately 0.2 to 0.4 (fairly statistically similar) with only a few outliers. Redoubt Volcano's plume displayed unique results, with a spherical fraction of 1.0, and predominantly large and small particles, fractions of 0.67 and 0.3, respectively.

3.5 Discussion

3.5.1 Puff VATD model height validation

Overall, comparison between MINX retrieved heights and Puff VATD model runs showed that the MINX retrieved heights were within a reasonable range for the eruptions in this study. Puff matched very well in trajectory and height pattern, if not in exact heights, for all plumes studied. For trajectory, most bearings for MINX height retrievals and Puff model results were within 1 to 5 degrees of each other. Only three bearings had greater differences: the ash and steam portions of the July 13, 2008 Okmok Volcano plume had bearing differences of 6.7° and 11.6°, respectively, between the Puff model and MISR results, and the June 14, 2009 Sarychev Peak Volcano plume had an 8.9° difference between the Puff model and MISR results. Despite differences in trajectory and bearing, the July 13 Okmok Puff model showed lower altitude

material closer to the ash plume as seen in MISR data, and higher altitude material closer to the steam plume as seen in MISR data, making the overall height pattern similar (Figure 3.2b).

Likewise, the July 14 Sarychev Peak MISR pass showed a plume that dispersed in opposite directions – west at low altitude, and east at high altitude. Puff model runs replicated this (as detailed in section 3.4.6), despite the fact that the modeled dispersion area in Puff and actual dispersion area in MISR were different (as shown in Figure 3.4g). That Puff showed this directional change at ~15 km ASL instead of 10 km ASL as in MISR data (Figure 3.6c), may have been due to the use of reanalysis model winds rather than real-time measured wind data. Modeled winds, rather than measured data, may be overly smooth and contain additional uncertainties (e.g., Garay et al., 2008). For example, the NOAA NCEP/NCAR reanalysis wind model determines wind speed and direction based on 17 pressure levels for which these parameters are determined, and the vertical resolution of these pressure levels for a given set of atmospheric conditions is a limit on the accuracy of the Puff model output (Kalnay et al., 1996). This NOAA NCEP/NCAR reanalysis wind model is the only option available for running Puff simulations for past dates (see Puff at AVO Tools Website; Kalnay et al., 1996). Despite this, Puff was able to model some height changes and gradients within plumes: Puff replicated the height gradient in the June 16 Sarychev Peak imagery, with the north/northeast side of the plume lower than the south/southwest side of the plume (Figure 3.6d). However in the June 16 case, the trajectory of material matched very well (as shown in Figure 3.4h).

Heights between MISR retrievals and Puff model runs were compared visually and in ArcScene, and all runs overlapped in height significantly (within ~1 km margin of error), though input height in Puff runs was the determining variable of this result. Between both height and the

trajectory, despite the minor differences described for the passes above, the comparison between these two datasets inspires reasonable confidence in the MISR height retrievals. This will be revisited later in section 3.5.5.

3.5.2 Temperature height comparisons

The temperature height comparison for Redoubt Volcano on April 5, 2009 (Figure 3.6b) was treated thoroughly in Ekstrand et al. (in review). They concluded that temperature heights artificially "dropped off," following the temperature gradient, and thus profile, of the land rather than the plume, due to the low optical depth of the plume (Table 3.3 shows optical depth was 0.2 at the farthest extent of the plume, the lowest of the plumes analyzed). However, a question left unanswered in this previous study was whether the temperature heights near the vent were from temperature detection of the plume or the vent itself (at ~3.1 km altitude). In the present work, data are included that show MISR heights up to 6 km ASL (Figures 3.6b, 3.7b), instead of 4.5 – 5 km ASL, as in the original published dataset (Ekstrand et al., in review). Airborne photographs showed no "drop" in heights, and gas flight heights were in agreement with MISR data indicating a plume top >4.1 km ASL (Figure 3.5c; Table 3.4). This significant discrepancy of up to 1.5 km in height between MISR (and gas flight), and temperature retrieved heights indicates that the temperature heights near the vent were produced by the surface temperature of the top of the volcano, rather than the plume. The data also suggest that while MISR retrieved few heights for the whole of the plume (16 percent of digitized pixels), the sensor is still capable of retrieving reliable, if few, heights for at least some optically thin plumes.

Temperature heights give slightly better, but not perfectly matched, results for the July 13, 2008 Okmok eruption (Figure 3.3b). Steam plume temperature retrievals near the vent matched MISR

retrieved heights very well (within ~1 km for maximum height), but then these temperature heights "dropped" and were lower than MISR retrieved heights by about 3 to 4 km ASL. This is consistent with the findings of Ekstrand et al. (in review) that optical depth, and thus temperature height retrieval accuracy, decreases further away from the vent. However, temperature retrieved heights for the ash portion of the plume did not drop and were of a consistent altitude, suggesting this portion of the plume was of reasonably high optical depth, though these heights were slightly higher than the MINX retrieved heights (~0.5 km higher). This was possibly due to the presence of a surface temperature inversion seen in sounding data for July 13. This temperature inversion means that there was more than one possible height for temperatures near the ground. There are three options for choosing a temperature-altitude lapse rate when there is a temperature inversion: above, below, or within the inversion. The lapse rate used in this analysis corresponded to a median value within the inversion, meaning there was a possibility for lower or higher altitudes below and above the chosen lapse rate. While the results for temperature and MISR retrieved heights were close, the temperature heights were overestimated, and thus the points plotted high in comparison to MISR data, suggesting the temperatures actually corresponded to lower altitudes. A similar effect has been seen when temperature heights are plotted against MISR for marine stratocumulus clouds which also occur below a strong temperature inversion (Garay et al., 2008). However, there is no way to confirm based on temperature data alone that the bulk of the material in the plume is actually lower without another source, such as MISR retrieved heights, to confirm this. Because the material is only at ~2 km ASL, this is not a huge discrepancy, but this result indicates the difficulty of retrieving accurate temperature based heights using only this basic technique. However, the consistency of the temperature heights also indicates a case in which slightly larger optical depths allowed for temperature heights to be retrieved that did not "drop" artificially in altitude.

3.5.3 Airborne photographs and gas flight heights

Airborne photographs are very useful for determining that the shape of the plume seen in MISR height retrievals is indeed the true shape of the plume, even if a quantitative height cannot be estimated from them. For the eruption of Augustine Volcano in 2006, airborne photos (Figure 3.5a-b) confirmed the flat, consistent height and shape of the plume, indicating that the MISR heights were reasonable. In addition, height estimates from this flight were within 0.5 km of the MISR height retrievals, also providing evidence that the MISR height retrievals were likely accurate.

Airborne photos for the eruption of Redoubt Volcano in 2009 (Figure 3.5c) confirmed that the plume did not "drop" significantly in altitude though the portion of the plume closest to the vent was indeed slightly higher in altitude than the rest of the plume. Gas flight heights that put the top of the plume >4.1 km ASL also support this conclusion, and were consistent with MISR retrieved heights.

3.5.4 Transparency and ash dispersion effects in MISR data

MISR height results in the present study do demonstrate limits on the transparency (optical depth) of ash plumes where height retrievals are possible, and the results suggest that the background (the surface beneath the ash plume) plays a rather large role in whether height retrievals are possible. Specifically, optically thinner clouds are more likely to be retrieved if they are over a dark (less reflective) background such as water, than if they are over a bright (more reflective) background such as meteorological cloud cover or land.

Height retrievals for Okmok Volcano on July 22, 2008 (Figure 3.2c, 3.3c), as well as for Cleveland Volcano on the same day (Figures 3.6a, 3.7a), produced lower altitudes for the edges of the plume than for the plume centers. These lower altitudes were eliminated when digitization of the plume did not include the edges of these plumes. In these cases, the edges of the plumes were diffuse, and these lower retrievals corresponded to the meteorological cloud layer beneath the plume, rather than the plume itself. For Okmok Volcano on July 29, 2008, however, plume edges were not diffuse, but were easily identified with the naked eye in MISR visible imagery (Figure 3.2d), and retrievals were produced up to these plume edges at heights consistent with plume altitude (Figures 3.2d, 3.3d). This means that in this case, the plume was thick enough at the edges that it, rather than the underlying cloud layer, was retrieved.

The Kasatochi volcanic plume demonstrates a more extreme example of plume transparency. The cloud in the MISR imagery had no detectable texture, having dispersed significantly with distance from the vent, and simply amounted to a brown color visible against the white of the underlying meteorological clouds (note that the eruption occurred on August 7, and the MISR overpass was on August 8, allowing for significant dispersion). Because the texture of the overlying ash cloud was no longer detectable to the sensor, the texture of the underlying meteorological clouds was the feature for which heights were retrieved.

These results suggest a transparency or optical depth limit to the ash clouds for which MISR will retrieve heights. Why, then, was the very thin plume for Redoubt retrieved on April 5, 2009 (Figure 3.6b, 3.7b)? It is because this plume was over a monochromatic ocean background. The ocean had little discernable texture, allowing the sensor to retrieve the texture of the ash plume more clearly. Were this thin plume over a layer of meteorological clouds, its remaining texture

may not have been enough to produce height retrievals, and this hypothetical underlying cloud layer may have been detected instead, as in the above cases of Okmok, Cleveland, and Kasatochi volcano plumes.

This transparency limit, however, is distinctly different from the phenomenon that happens when temperature heights fail to produce reasonable altitudes for volcanic plumes or clouds. For a satellite image, temperature is converted from radiance values, and observed radiance is dependent on several things, including emissivity ε and effective temperature T_{eff} of a volcanic plume (Pavolonis, 2010). Emissivity ε relates to effective absorption optical depth $\tau_{\text{abs,eff}}$ by the following equation:

$$\ln[1 - \varepsilon(\lambda)] = \tau_{\text{abs,eff}}(\lambda) \tag{2}$$

Emissivity of the ash cloud related to R_{obs}, the observed radiance, by the following equation:

$$R_{\text{obs}}(\lambda) = \varepsilon(\lambda)R_{\text{ac}}(\lambda) + T_{\text{ac}}(\lambda)\,\varepsilon(\lambda)B(\lambda,T_{\text{eff}}) + R_{\text{clr}}(\lambda)[1 - \varepsilon(\lambda)] \tag{3}$$

In this equation, λ is the wavelength, R_{obs} is the observed radiance, R_{clr} is the clear-sky radiance (the radiance that would be detected by the sensor as the R_{obs} if there were no plume or cloud), R_{ac} and T_{ac} are the above-cloud upwelling atmospheric radiance and transmittance, respectively. T_{eff} is the effective cloud temperature, and B is the Planck function. Both of the above equations are detailed in Pavolonis (2010). Note that if the clear-sky radiance term is replaced with the upwelling top of atmosphere radiance from a blackbody cloud layer, then the existence of a lower meteorological cloud layer, as opposed to land surface, can be modeled (Pavolonis, 2010).

When a volcanic plume disperses, its optical depth decreases, lowering its emissivity. Its effective temperature also decreases, as there is less plume-temperature (i.e., colder than surface or low-altitude cloud) material contained in each pixel for which a radiance is observed. Thus, the proportion of the observed radiance, R_{obs}, that comes from the plume is lessened with increased ash cloud dispersion compared to the proportion that comes from the clear-sky or cloud radiance, R_{clr}. In this way, the observed radiance of a pixel will begin to correspond to a lower altitude land or cloud layer rather than the plume as the plume disperses.

To demonstrate this, Figure 3.8 is a schematic of how the optical depth of a volcanic plume affects the radiation transmitted to an infrared satellite sensor. This schematic shows what portion of the radiant signal is received by the infrared sensor (e.g., radiative signal from the plume or ground) under different optical depth circumstances, as well as the effect of optical depth on temperature height retrievals and plume height-distance profiles. Ekstrand et al. (in review) argued that when height-distance profiles show a smooth, even plume bottom, height retrievals are likely from somewhere inside the cloud. However, when profiles show scatter or shapes corresponding to topography, the temperature height of a layer below the plume, such as meteorological clouds or land, is likely being retrieved. High thermal infrared optical depth is required for a plume or cloud to appear opaque, a circumstance in which no portion of the radiative signal below the plume top is received by the satellite sensor (Figure 3.8a). This produces a temperature retrieved height result corresponding to the plume top, and a relatively smooth (possibly even, flat-bottomed) plume profile corresponding to the shape of the plume top, without the "scatter" in the plume profile shape as documented by Ekstrand et al. (in review) for inaccurate height retrieval cases. Ekstrand et al. (in review) observed no cases of this kind of

plume. For a less optically thick plume, a radiant signal is detected at the sensor corresponding to some layer within the plume (Figure 3.8b). A smooth-bottomed height-distance profile is produced, but the temperature altitude comes from a layer inside the plume. Here, a positive BTD (recall, this is the ash differencing method used as an indicator of cloud transparency for the temperature method in this study) could still be observed because the cloud is not fully opaque. For very optically thin plumes, radiation from the ground likely reaches the sensor (Figure 3.8c), so retrieved temperature profiles are too low and show scatter relative to the cloud's true altitude and shape. The first two circumstances (Figure 3.8a-b) produce positive BTD results, but the third circumstance (Figure 3.8c) may not. The exception is that the third, low-optical depth, circumstance may produce a positive BTD signal when ash concentrations are too low for a pixel to be interpreted as containing ash by the sensor, or when a great deal of water is present (Ekstrand et al., in review).

In contrast to temperature techniques, MISR's stereo height retrieval techniques (both the standard retrievals and MINX retrievals) are strictly geometric techniques that are not sensitive to radiometric calibration uncertainties (Marchand et al., 2010) or the emissivity of the plume material (Scollo et al., 2012). However, as a plume disperses (resulting in decreasing optical depth; in this case the effect is to visible texture rather than emissivity), the volcanic plume layer becomes transparent, and the plume becomes optically inhomogeneous, allowing for the sensor to detect clouds or ground features below (Scollo et al., 2012). Because this is a texture and transparency, but not an emissivity, issue, MISR is capable of retrieving heights for much thinner clouds than the basic satellite TIR temperature method. However, the optical depth threshold is higher for plumes over brightly textured features (weather clouds or bright land surfaces), than over dark smooth backgrounds (such as water). This threshold, however, does not seem to be

affected by plume composition based on the present data, since Okmok Volcano produced relatively water-rich plumes, and Cleveland Volcano produced relatively ash-rich plumes, and both volcanoes exhibited transparency issues at plume edges relatively near the vent (in plumes not yet detached from the volcano).

3.5.5 Height methods in comparison

Representative results for average maximum MISR retrieved height, Puff VATD model height, basic temperature height, and observation flight height were chosen for comparison (values given in Table 3.4) in order to confirm that the above conclusions were statistically accurate. The latter three heights were plotted against MISR retrieved heights for comparison of each dataset to MISR heights (Figure 3.9). These were compared to a $y=x$ (one-to-one) line, with points that fall closest to the line displaying the best statistical agreement between methods.

As previously discussed, Puff and MISR heights were well within agreement, all falling very close to or on the one-to-one line (within ~1 km). A significant fraction of Puff heights fell below the line, indicating that Puff overestimated the maximum plume top slightly (by ~1 km or less). However, since Puff produces a modeled range of heights rather than a flat retrieved surface, ~1 km constitutes fairly good agreement. Also very close to this line were the heights from observation flights, though these points both plotted above the line, indicating that the observation flight heights were slight underestimates, and as they were subject to observer error, this is also very good agreement (within ~1 km).

Temperature heights, in contrast, plotted much above the line, indicating that the temperature estimates were vast underestimates of height – by as much as 4 km below the plume top. The

exception was the point that corresponded to the Okmok ash plume, which was subject to error due to the surface temperature inversion discussed above in section 3.5.2.

This graph confirms the conclusions above and demonstrates statistically that MISR, Puff VATD model, and observation flight heights are in good agreement, while temperature heights (save for anomalous cases) significantly underestimate plume height.

3.5.6 Dynamic texture within ash plumes

The results presented here demonstrate a number of cases in which dynamic texture within an ash plume was detected, or affected the outcome of the height retrieval. First, both the Augustine Volcano (Figure 3.2a) and July 13 Okmok Volcano (Figure 3.2b) plumes exhibited varying degrees of bifurcation (Ernst et al., 1994). The Augustine plume exhibited different particle transport directions on each "side" of the plume (described in the paragraph below), which could eventually cause the plume to split into two lobes. The Okmok plume split into distinct lobes near the vent, with separate ash and steam portions.

The plume produced by Augustine on January 30, 2006, contained "ribs" or "waves" (Figure 3.2a). These are visible to the naked eye in MISR visible imagery (Figure 3.2a) and suggest a strong local transport of ash from the plume center to the plume edges. They were a result of a shear flow-instability at the interface between the atmosphere and the top of the plume (Gondret and Rabaud, 1997). The presence of this texture, and the fact that this texture was specific to each side of the plume (suggesting bifurcation; Ernst et al., 1994), required that the plume be digitized in two halves, with diverging wind directions. If not digitized in this manner, the plume appeared to have had two different maximum altitudes for its two halves, though airborne photography

suggested a flat, even plume on this day (Figure 3.5a-b). This may be because the local transport direction in one half of the plume paralleled the along-track motion of the MISR sensor. In cases in which plume transport direction aliases with along-track motion, height retrievals can be negatively affected as parallax between cameras cannot be entirely corrected with knowledge of wind direction alone, since the sensor's along-track motion contributes to the apparent parallax of particles in these cases (Moroney et al., 2002; Scollo et al., 2012). Thus, this is a case in which plume texture (corresponding to plume behavior) affected the retrieval of heights.

There were three other cases in which retrieval of heights provided data that allowed insight into plume behavior or shape, though these phenomena did not require any change or correction in the processing of the MISR heights. For all three MISR images containing plumes from the Okmok Volcano 2008 eruption, heights varied with distance from the source (Figures 3.2b-d, 3.3b-d). These were least dramatic in the results from July 29, 2008 (Figure 3.2d, 3.3d), and were most dramatic in the results from July 22, 2008. In the July 22 plume, oscillations were frequent and regular, occurring every ~10 to 15 km along the plume's length (Figures 3.2c, 3.3c). De Angelis et al. (2011) documented height variations in MODIS data produced by gravity waves at the Okmok 2008 eruption, and an associated seismic signature that is sometimes produced in the presence of these waves. Atmospheric waves with periods from a few to several minutes can be produced by volcanic eruptions, and can propagate as acoustic and gravity modes (De Angelis et al., 2011). Gravity modes arise from perturbations to the hydrostatic equilibrium of a cloud and are likely to propagate in fluids with stable density stratification due to vertical temperature and/or density gradients, such as the atmosphere. This results in the perturbed fluid oscillating under the effects of the restoring force of gravity (De Angelis et al., 2011). However, significant eruption strength is required to form these waves, and De Angelis et al. (2011) observed such

waves on the first day of the Okmok 2008 eruption during the strongest eruptive pulse. It may be unlikely that gravity waves formed on a day with a much weaker eruption, such as July 22 (personal communication, Silvio De Angelis). Another possibility is that pulses in eruptive activity led to the oscillations in height, and further investigation of seismic data is required to confirm this.

3.5.7 MISR aerosol results

Scollo et al. (2012) found that, for the eruption of Mt. Etna Volcano in Italy from 2002 to 2006, ash dominated plumes mostly contain large particles (large tau fractions 0.46-0.49, small tau fractions 0.31 to 0.4, medium tau fractions 0.11 to 0.23) which are predominantly non-spherical (most non-spherical fractions about 0.42, but ranging up to 0.76). Sulfate or water dominated plumes mostly contain small particles (small tau fractions 0.56 to 0.77, medium tau fractions 0.03 to 0.24, large tau fractions 0.12 to 0.36) which are predominantly spherical (spherical fractions 0.87 to 1.0).

Most of the results shown in Table 3.3 are in reasonable agreement with the results for Etna Volcano ash plumes in Scollo et al. (2012) – non-spherical (mostly a fraction of 0.4) and with a high fraction of large particles (most with fractions between ~0.28 and ~0.43). However, the plumes presented here were dominated by a bimodal size distribution of *both* large and small particles (Okmok Volcano on July 13, 2008 and Sarychev Peak Volcano on June 16, 2009 as shown in Table 3.3), and sometimes by a trimodal size distribution of relatively similar proportions of all three sizes of particles (Sarychev Peak on June 14, 2009 as shown in Table 3.3). Both Okmok and Sarychev Peak eruptions were considered highly explosive, presumably due to high crystallinity of the eruptive magma for Sarychev Peak (Rybin et al., 2011), and to presence

of a high water fraction for Okmok (Larsen et al., 2009). Some water vapor plumes were also recognized at Sarychev Peak (Rybin et al., 2011). Highly explosive eruptions, especially those containing water, can produce a higher fraction of very, very fine material (Sparks et al., 1997). This may be seen here as higher fractions of small material for the Okmok plumes and for the June 16, 2009 Sarychev Peak plume, and a higher fraction of small and medium material for the June 14, 2009 Sarychev Peak plume. In light of this, aerosol results showed a fairly consistent match with those of Scollo et al. (2012) for relatively ash-rich plumes.

Notably, the steam plume from Okmok Volcano did not produce many aerosol retrievals of its own. Those produced were from a 17.6 km retrieval region that overlapped significantly with the ash portion of the plume, and was thus dominated by the optical properties of the ash particles, based on visual ArcGIS analysis of the aerosol data distribution for these plumes. Thus, these results from digitization of the steam plume actually can be attributed to the edge of the ash plume, as the spherical fractions and particle size fractions were identical to other results for the ash plume aerosols (Table 3.3).

Results for the plume from the eruption of Redoubt Volcano do not fit the model proposed by Scollo et al. (2012). Particles were entirely spherical (spherical fraction of 1.0), but were mostly large, not small (large fraction 0.67, small fraction 0.30; Table 3.3). These results were from a portion of the ash plume above the water and very near the shoreline across the Cook Inlet from Redoubt Volcano. The plume was very thin here (mean AOD 0.2), and only the very edge of the 17.6 km retrieval region was included in the plume digitization. We hypothesize that these detected aerosols either comprised just the leading edge of the plume, or were due to another retrieved feature across the Cook Inlet. Notably, due to the high water content of the Redoubt

eruption, the ash fallout was dominated by accretionary lapilli ranging in size from 1 mm to 2 cm (Schaefer, 2012). However, it is unlikely that particles of this size would be carried across the Cook Inlet, as particles of such large size should fall out within about 30 minutes from 14 km ASL (Rose et al., 1995; Searcy et al., 1998), and this far portion of the ash plume was due to the first eruptive pulse at 18:36 UTC (3 hours prior to the MISR overpass) on April 5, 2009 based on trajectory analysis (Ekstrand et al., in review). Furthermore, the MISR aerosol retrieval algorithm may be sensitive only to particles with radii less than 2.5 μm in size due to the sensor's spectral range (Scollo et al., 2012). However, smaller accretionary material might have been carried this far, and might have been detected by the sensor, and due to the high water content of the plume, these detected particles might have appeared to be quite spherical. It is also possible that the detected aerosols had nothing to do with the eruption, and that these results are anomalous. If these aerosols are associated with the eruption, we hypothesize they must be accretionary particles predominantly of a size range that can be detected as "large" particles by the MISR aerosol retrieval algorithm (0.7 to 2.5 μm radius).

3.6 Conclusions

The MISR sensor provides an excellent tool for accurately analyzing the height and shape of volcanic plumes. The sensor is capable of retrieving reliable heights for plumes that are very optically thin when such plumes are over an ocean background. However, height retrievals have a transparency limit when plumes are over a bright or textured background, such as meteorological clouds (this limit is related to ash cloud dispersion, but is dependent on textural, not thermal plume properties). This issue is especially prominent in ash clouds that have traveled a significant distance from the vent (on the order of hundreds of kilometers for Kasatochi Volcano) and dispersed significantly, or in plumes with very diffuse edges near the vent. In both cases, cloudy

weather conditions will affect the accuracy of retrievals more than clear weather conditions. The content of plumes does not affect whether or not MISR will retrieve heights, nor does the altitude; height retrievals were good for both ash-rich (e.g., Sarychev Peak) and water-rich eruptions (e.g., most Okmok cases), and height retrievals were good for plumes in which heights varied (e.g., Okmok on July 13, 2008 and Sarychev on June 14 and 16, 2009). Heights retrieved may provide insight into plume behavior, such as in the observation of local ash transport directions within a plume that affect height retrievals by aliasing with along-track motion as in the case of Augustine Volcano.

The findings in this work support the argument by Ekstrand et al. (in review) that the MISR sensor is one of the most powerful sensors available for volcanic plume height analysis. Furthermore, when aerosol retrievals are available, the method of Scollo et al. (2012) is very reliable for determining the overall composition of a volcanic plume, at least for the examples of ash-rich plumes documented here. Lastly, the use of MINX is an easy, accessible way for volcano observatories to process MISR height data and acquire aerosol results.

The limitations of the MISR sensor have mostly to do with its limited coverage due to its small swath size; it will never have the frequent coverage that AVHRR and MODIS provide (recall, these are the sensors that provide TIR temperature data). Furthermore, the sensor only acquires data during the daytime. However, we urge volcanologists to utilize MISR data whenever available for volcanic plumes. Furthermore, we argue that similar multi-camera technology would be extremely useful to have on future satellites, and that such technology should be included as part of future satellite designs.

3.7 Acknowledgements

We would like to thank Lovro Valcic (AVO/UAF-GI) and Scott McFarlane (AVO/UAF-GI) for assistance in obtaining and processing AVHRR and MODIS satellite imagery, Dave Schneider (USGS) for providing Augustine airborne photographs, Jeremy Harbeck for assistance with IDL processing, Ralph Kahn (NASA GSFC) and Simona Scollo (INGV) for assistance with the analysis of MISR aerosol data, and Peter Kelly (USGS) for providing gas flight data. This work was supported in part by the Alaska Space Grant Program. Portions of this work were carried out at the Jet Propulsion Laboratory, California Institute of Technology, under a contract with the National Aeronautics and Space Administration. This publication is the result in part of research sponsored by the Cooperative Institute for Alaska Research with funds from the National Oceanic and Atmospheric Administration under cooperative agreement NA080AR4320751 with the University of Alaska.

3.8 References

Bailey, J.E., Dean, K., Dehn, J., Webley, P., 2010. Integrated satellite observations of the 2006 eruption of Augustine Volcano (Chapter 20). In: Power, J.A., Coombs, M.L., Freymueller, J.T. (Eds.), The 2006 Eruptions of Augustine Volcano. USGS Professional Paper 1769. http://pubs.usgs.gov/pp/1769/

Bull, K., Buurman, H., in press. An overview of the 2009 eruption of Redoubt Volcano. In: Webley, P., Waythomas, C.F. (Eds.), The 2009 Eruption of Redoubt Volcano, Alaska. J. Volcanol. Geotherm. Res.

Dean, K.G., Dehn, J., Engle, K., Izbekov, P., Papp, K., Patrick, M., 2002. Operational satellite monitoring of volcanoes at the Alaska Volcano Observatory. Adv. Environ. Monit. Modell. 1, 70-97.

De Angelis, S., McNutt, S.R., Webley, P.W., 2011. Evidence of atmospheric gravity waves during the 2008 eruption of Okmok Volcano from seismic and remote sensing observations. Geophys. Res. Let. 38, L10303. doi:10.1029/2011GL047144.

Diner, D.J., Beckert, J.C., Reilly, T.H., Bruegge, C.J., Conel, J.E., Kahn, R.A., Martonchik, J.V., Ackerman, T.P., Davies, R., Gerstl, S.A.W., Gordon, H.R., Muller, J.-P., Myneni, R.B., Sellers, P.J., Pinty, B., Verstraete, M.M., 1998. Multi-angle Imaging SpectroRadiometer (MISR) instrument description and experiment overview. IEEE Trans. Geosci. Rem. Sens. 36, 1072–1087.

Ekstrand, A.L., Webley, P.W., Garay, M.J., Dehn, J., Prakash, A., Nelson, D.J., Dean, K., Steensen, T., in review. A multi-sensor plume height analysis of the 2009 Redoubt eruption. In: Webley, P., Waythomas, C.F. (Eds.), The 2009 Eruption of Redoubt Volcano, Alaska. J. Volcanol. Geotherm. Res.

Ernst, G.G.J., David, J.P., Sparks, S.J., 1994. Bifurcation of volcanic plumes in a crosswind. Bull. Volc. 56, 159-169.

Garay, M.J., de Szoeke, S.P., Moroney, C.M., 2008. Comparison of marine stratocumulus cloud top heights in the southeastern Pacific retrieved from satellites with coincident ship-based observations. J. Geophys. Res. 113, D18204. doi:10.1029/2008JD009975.

Gondret, P., Rabaud, M., 1997. Shear instability of two-fluid parallel flow in a Hele-Shaw cell. Phys. Fluids 9, 3267-3274.

Haywood, J.M., Jones, A., Clarisse, L., Bourassa, A., Barnes, J., Telford, P., Bellouin, N., Boucher, O., Agnew, P., Clerbuax, C., Coheur, P., Degenstein, D., Braesicke, P., 2010. Observations of the eruption of the Sarychev Volcano and simulations using the HadGEM2 climate model. J. Geophys. Res. 115, D21212. doi:10.1029/2010JD014447.

Heue, K.-P., Brenninkmeijer, C.A.M., Wagner, T., Mies, K., Dix, B., Frieb, U., Martinsson, B.G., Slemr, F., van Velthoven, P.F.J., 2010. Observations of the 2008 Kasatochi volcanic SO_2 plume by CARIBIC aircraft DOAS and the GOME-2 satellite. Atmos. Chem. Phys. 10, 4699-4713. doi:10.5194/acp-10-4699-2010.

Kahn, R.A., Li, W.-H., Moroney, C., Diner, D.J., Martonchik, J.V., Fishbein, E., 2007. Aerosol source plume physical characteristics from space-based multiangle imaging. J. Geophys. Res. 112, D11205. doi:10.1029/2006JD007647.

Kahn, R.A., Chen, Y., Nelson, D.L., Leung, F.-Y., Li, Q., Diner, D.J., Logan, J.A., 2008. Wildfire smoke injection heights: Two perspectives from space. Geophys. Res. Lett. 35, L04809. doi:10.1029/2007GL032165.

Kahn, R.A., Nelson, D.L., Garay, M.J., Levy, R.C., Bull, M.A., Diner D.J., Martonchik J.V., Paradise, S.R., Hansen, E.G., Remer, L.A., 2009. MISR aerosol product attributes and statistical comparisons with MODIS. IEEE Trans. Geosci. Rem. Sens. 47, 4095-4114.

Kahn, R.A., Gaitley, B.J., Garay, M.J., Diner, D.J., Eck, T.F., Smirnov, A., Holben, B.N., 2010. Multiangle Imaging SpectroRadiometer global aerosol product assessment by comparison with the Aerosol Robotic Network. J. Geophys. Res. 115, D23209. doi:10.1029/2010JD014601.

Kalnay, E., Kanamitsu, M., Kistler, R., Collins, W., Deaven, D., 1996. The NCEP/NCAR 40-year reanalysis project. Bull. Amer. Meteor. Soc. 77, 437-471.

Kienle, J., Shaw, G.E., 1979. Plume dynamics, thermal energy, and long-distance transport of vulcanian eruption clouds from Augustine Volcano, Alaska. J. Volcanol. Geotherm. Res. 6, 139-164.

Kristiansen, N.I., Stohl, A., Prata, A.J., Richter, A., Eckhardt, S., Seibert, P., Hoffmann, A., Ritter, C., Bitar, L., Duck, T.J., Stebel, K., 2010. Remote sensing and inverse transport modeling of the Kasatochi eruption sulfur dioxide cloud. J. Geophys. Res. 115, D00L16. doi:10.1029/2009JD013286.

Krotkov, N.A., Schoeberl, M.R., Morris, G.A., Carn, S., Yang, K., 2010. Dispersion and lifetime of the SO_2 cloud from the August 2008 Kasatochi eruption. J. Geophys. Res. 115, D00L20. doi:10.1029/2010JD013984.

Larsen, J., Neal., C., Webley, P., Freymeuller, J., Haney, M., McNutt, S., Schneider, D., Prejean, S., Schaefer, J., Wessels, R., 2009. Eruption of Alaska Volcano breaks historic pattern. EOS Trans. 90, 173-180.

Marchand, R., Ackerman, T., Smyth, M., Rossow, W.B., 2010. A review of cloud top height and optical depth histograms from MISR, ISCCP, and MODIS. J. Geophys. Res. 115, D16206. doi:10.1029/2009JD013422.

Matoza, R.S., Le Pichon, A., Vergox, J., Herry, P., Lalande, J.-M., Lee, H.-i., Che, I.-Y., Rybin, A., 2011. Infrasonic observations of the June 2009 Sarychev Peak eruption, Kuril Islands: Implications for infrasonic monitoring of remote explosive volcanism. J. Volcanol. Geotherm. Res. 200, 35-38.

Miller, T.P., Chouet, B.A., 1994. The 1989-1990 eruptions of Redoubt Volcano: An introduction. J. Volcanol. Geophys. Res. 62, 1-10.

Mims., S.R., Kahn, R.A., Moroney, C.M., Gaitley, B.J., Nelson, D.L., Garay, M.J., 2009. MISR stereo heights of grassland fire smoke plumes in Australia. IEEE Trans. Geosci. Rem. Sens. 48, 25-35.

Moroney, C., Davies, R., Muller, J.-P., 2002. Operational retrieval of cloud-top heights using MISR data. IEEE Trans. Geosci. Rem. Sens. 40, 1532–1540.

Neal, C.A., McGimsey, R.G., Dixon, J.P., Cameron, C.E., 2011. 2008 volcanic activity in Alaska, Kamchatka, and the Kurile Islands: Summary of events and response of the Alaska Volcano Observatory. USGS Sci. Invest. Rep. 2010-5243. http://pubs.usgs.gov/sir/2010/5243/pdf/sir20105243.pdf

Nelson, D.L., Averill, C., Boland, S., Morford, R., Menzies, A., Garay, M., Diner, D., Rheingans, B., Thompson, C., Hall, J., Scholes, M., Campbell, H., 2009. MISR INteractive eXplorer (MINX) v1.2 user's guide. JPL Tech. Rep. D-41552. http://www.openchannelsoftware.com/projects/MINX/

Papp, K.R., Dean, K.G., Dehn, J., 2005. Predicting regions susceptible to high concentrations of airborne volcanic ash in the North Pacific region. J. Volcanol. Geotherm. Res. 148, 295-314.

Pavolonis, M.J., 2010. Advanced in extracting cloud composition information from spaceborne infrared radiances – A robust alternative to brightness temperatures. Part I: Theory. J. Appl. Meteorol. Climatol. 49, 1992–2012.

Power, J.A., Nye, C.J., Coombs, M.L., Wessels, R.L., Cervelli, P.F., Dehn, J., Wallace, K.L., Freymeuller, J.T., Doukas, M.P, 2006. The reawakening of Alaska's Augustine Volcano. EOS Trans. 87, 373-377.

Prata, A.J., 1989a. Infrared radiative transfer calculations for volcanic ash clouds. Geophys. Res. Lett. 16, 1293-1296.

Prata, A.J, 1989b. Observations of volcanic ash clouds in the 10-12 μm window using AVHRR/2 data. Int. J. Rem. Sens. 10, 751-761.

Prata, A.F., Bluth, G., Rose, B., Schneider, D., Tupper, A., 2001. Comments on "Failures in detecting volcanic ash from a satellite-based technique." Rem. Sens. Environ. 78, 341-346.

Rose, W.I., Kostinski, A.B., Kelley, L., 1995. Real time C band radar observations of 1992 eruption clouds from Crater Peak, Mount Spurr Volcano, Alaska. USGS Bull. 2139, 19-28.

Rybin, A., Chibisova, M., Webley, P., Steensen, T., Izbekov, P., Neal, C., 2011. Satellite and ground observations of the June 2009 eruption of Sarychev Peak Volcano, Matua Island, Central Kuriles. Bull. Volc. 73, 1377-1392.

Schaefer, J.R.G., 2012. The 2009 eruption of Redoubt Volcano, Alaska. Alaska Div. Geol. Geophys. Survey Rep. Invest. 2011-5, 45 pp. http://www.dggs.alaska.gov/pubs/id/23123

Scollo, S., Folch, A., Coltelli, M., Realmuto, V.J., 2010. Three-dimensional volcanic aerosol dispersal: A comparison between Multiangle Imaging Spectroradiometer (MISR) data and numerical simulations. J. Geophys. Res. 115, D24210. doi:10.1029/2009JD013162

Scollo, S., Kahn, R.A., Nelson, D.L., Coltelli, M., Diner, D.J., Garay, M.J., Realmuto, V.J., 2012. MISR observations of Etna volcanic plumes. J. Geophys. Res. 117, D06210. doi:10.1029/2011JD016625.

Searcy, C., Dean, K., Stringer, W., 1998. PUFF: A high-resolution volcanic ash tracking model. J. Volcanol. Geotherm. Res. 80, 1-16.

Simpson, J.J., Hufford, G., Pieri, D., Berg, J., 2000. Failures in detecting volcanic ash from a satellite-based technique. Rem. Sens. Environ. 72, 191-217.

Sparks, R.S.J., Bursik, M.I., Carey, S.N., Gilbert, J.S., Glaze, L.S., Sigurdsson, H., Woods, A.W., 1997. Volcanic Plumes. Wiley, Chichester, 574 pp.

Swanson, S.E., Kienle, J., 1988. The 1986 eruption of Mount St. Augustine: Field test of a hazard evaluation. J. Geophys. Res. 93, 4500-4520.

Val Martin, M., Logan, J.A., Kahn, R.A., Leung, F.-Y., Nelson, D.L., Diner, D.J., 2010. Smoke injection heights from fires in North America: Analysis of 5 years of satellite observations. Atmos. Chem. Phys. 10, 1491–1510.

Waythomas, C.F., Scott, W.E., Prejean, S.G., Schneider, D.J., Izbekov, P., Nye, C.J., 2010. The 7-8 August 2008 eruption of Kasatochi Volcano, central Aleutian Islands, Alaska. J. Geophys. Res. 115, B00B06. doi:10.1029/2010B007437.

Werner, C., Kelly, P.J. Doukas, M., Lopez, T., Pfeffer, M., McGimsey, R.G., Neal, C.A., in press. Degassing associated with the 2009 eruption of Redoubt Volcano, Alaska. In: Webley, P., Waythomas, C.F. (Eds.), The 2009 Eruption of Redoubt Volcano, Alaska. J. Volcanol. Geotherm. Res.

3.9 Websites referenced

AVO Tools webpage, 2007. http://avo.images.alaska.edu/tools/

NASA Langley Research Center Atmospheric Sciences Data Center, 2011. http://eosweb.larc.nasa.gov/. 20 July 2011.

Open Channel Foundation, 2010. MINX software. http://www.openchannelsoftware.com/projects/MINX. 5 March 2010.

Smithsonian Bulletin of the Global Volcanism Network, 2011. Cleveland Index of Monthly Reports. http://volcano.si.edu/world/volcano.cfm?vnum=1101-24-&volpage=var. 10 February 2011.

University of Wyoming's College of Engineering, Department of Atmospheric Science database. http://weather.uwyo.edu/upperair/sounding.html. 17 August 2011.

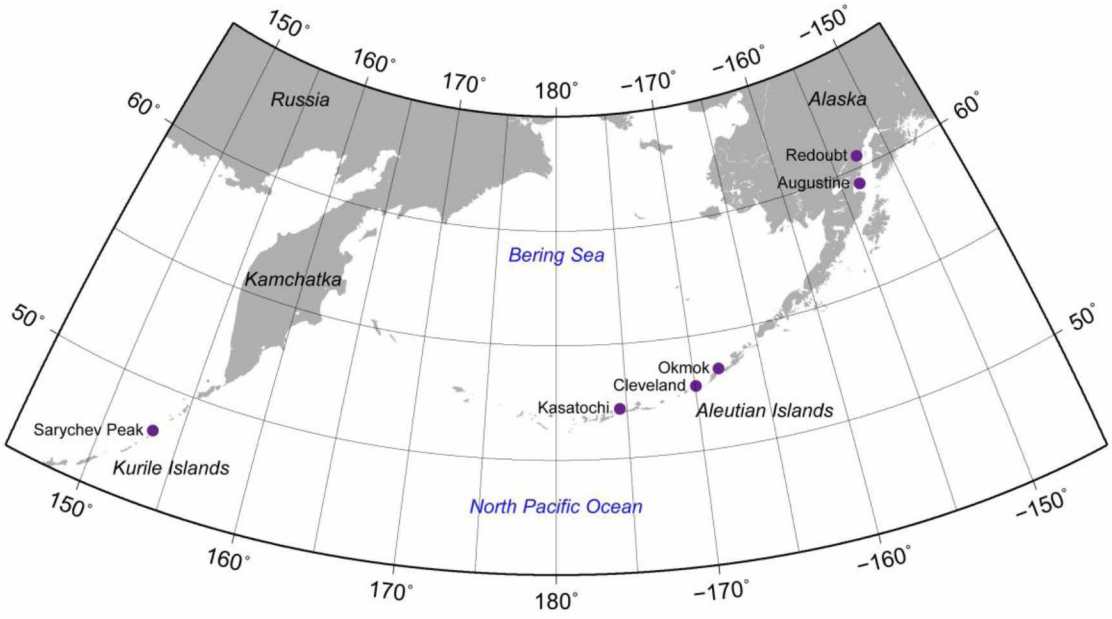

Figure 3.1: Location map of volcanoes in this study. Shown are Alaska, the Aleutian Islands, Kamchatka, Russia, and the Russian Kurile Islands.

Figure 3.2: MISR height map, Puff VATD model output, and MISR visual image for Augustine and Okmok eruptions. A) Augustine on January 30, 2006, showing relatively flat plume top with "ribs" or "vortices" visible in the MISR visual image. For scale, the MISR plume is ~70 km long. B) Okmok on July 13, 2008, showing separated ash (lower altitude) and steam (higher altitude) plumes. For scale, the MISR plume is ~120 km long. C) Okmok on July 22, 2008, showing plume with diffuse edges and oscillating height pattern. For scale, the MISR plume is ~110 km long. D) Okmok on July 29, 2008, showing relatively flat plume. For scale, the MISR plume is ~130 km long.

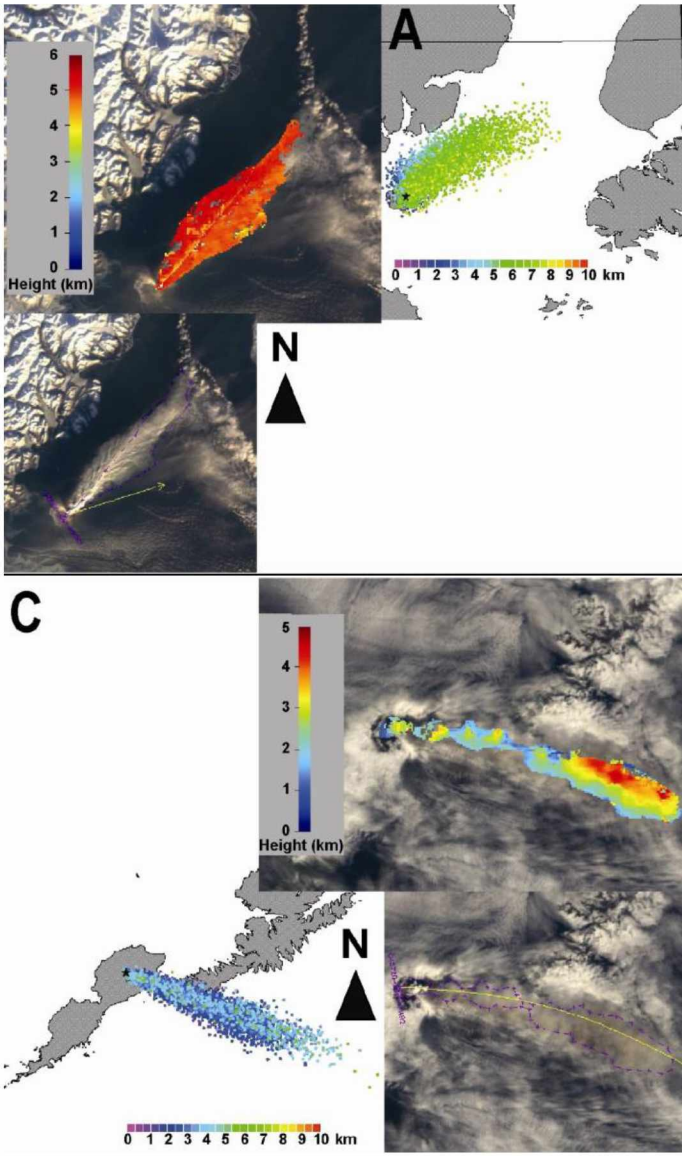
A
6
5
4
3
2
1
0
Height (km)
0 1 2 3 4 5 6 7 8 9 10 km
N
C
5
4
3
2
1
0
Height (km)
N
0 1 2 3 4 5 6 7 8 9 10 km

B
10
8
6
4
2
0
Height (km)
0 1 2 3 4 5 6 7 8 9 10 km
2.5
2.0
1.5
1.0
0.5
0.0
Height (km)
N
D
5
4
3
2
1
0
Height (km)
N
0 1 2 3 4 5 6 7 8 9 10 km

Figure 3.3: Two-dimensional height-distance results for Augustine and Okmok eruptions. A) Augustine on January 30, 2006 showing MISR heights for relatively flat plume; B) Okmok on July 13, 2008 showing MISR and temperature heights for ash plume (lower altitude) and steam plume (higher altitude), though temperature heights are in poor agreement for ash plume and for steam plume after ~40 km from vent; C) Okmok on July 22, 2008, showing MISR heights in oscillating height pattern, with inset showing altitude of weather cloud retrievals; and D) Okmok on July 29, 2008, showing MISR heights for relatively flat plume. MISR zero-wind heights are shown by green (lighter) squares, and MISR wind-corrected heights are shown by blue (darker) squares. Temperature heights are shown by purple (darkest) triangles for ash heights and teal (lightest) diamonds for steam heights.

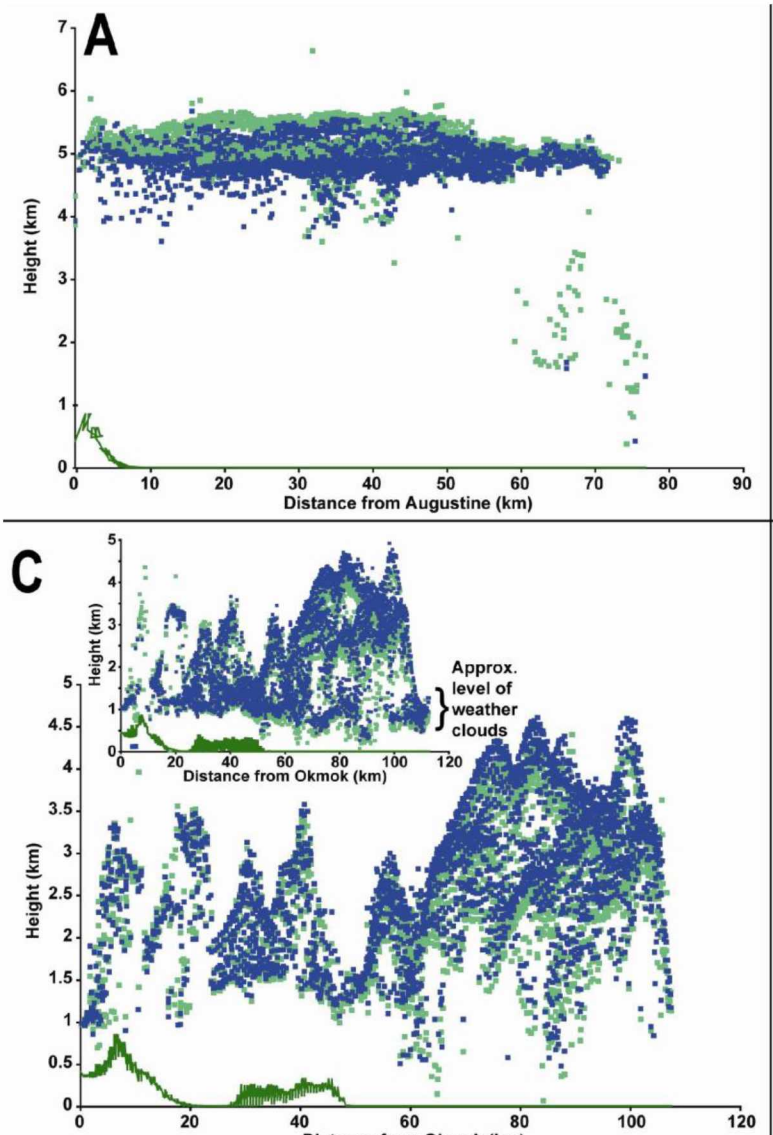
A
Height (km)
Distance from Augustine (km)
C
Height (km)
Distance from Okmok (km)
Approx.
level of
weather
clouds
Height (km)
Distance from Okmok (km)

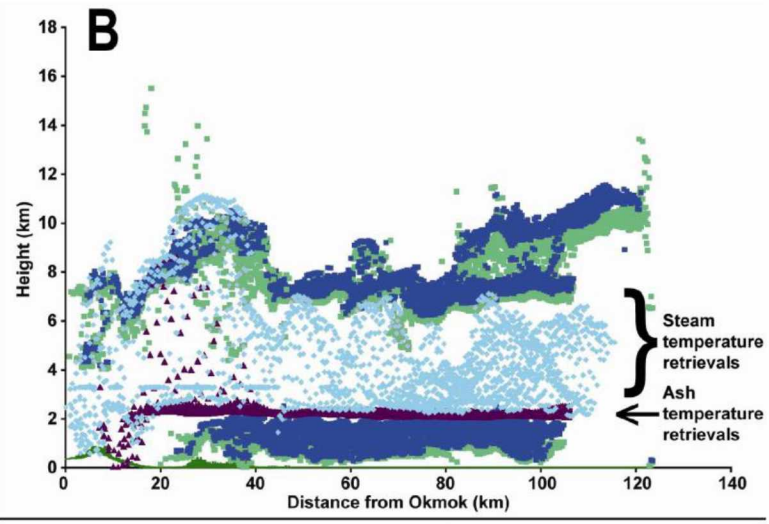
B
Height (km)
Distance from Okmok (km)
Steam temperature retrievals
Ash temperature retrievals

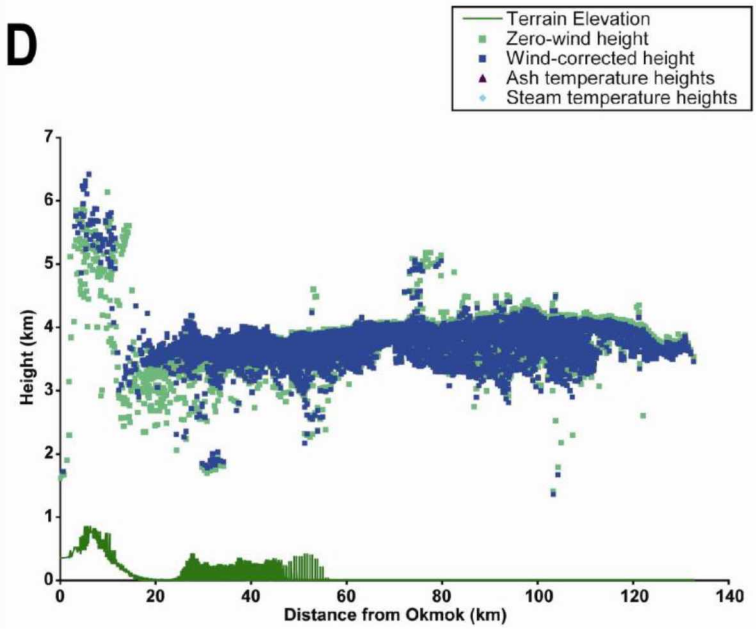
D
Terrain Elevation
Zero-wind height
Wind-corrected height
Ash temperature heights
Steam temperature heights
Height (km)
Distance from Okmok (km)

Figure 3.4: Puff VATD model and MISR retrieved height 2D (top down) comparison of trajectories for all eruptions analyzed. Puff often appears as a more "v" shaped, dispersed result, and is blue in color, whereas MISR often appears as a broader, flatter retrieval region, and is purple in color. A) Augustine on January 30, 2006 showing good trajectory agreement. For scale, the MISR plume is ~70 km long. B) Okmok on July 13, 2008 showing poor trajectory agreement. For scale, the MISR plume is ~120 km long. C) Okmok on July 22, 2008 showing good trajectory agreement. For scale, the MISR plume is ~110 km long. D) Okmok on July 29, 2008 showing good trajectory agreement. For scale, the MISR plume is ~130 km long. E) Cleveland on July 22, 2009 showing good trajectory agreement. For scale, the MISR plume is ~75 km long. F) Redoubt on April 5, 2009 showing good trajectory agreement. For scale, the MISR plume is ~80 km long. G) Sarychev Peak on June 14, 2009 showing good trajectory agreement. For scale, the MISR plume is ~120 km long. H) Sarychev Peak on June 16, 2009 showing poor trajectory agreement. For scale, the MISR plume is ~ 180 km long.

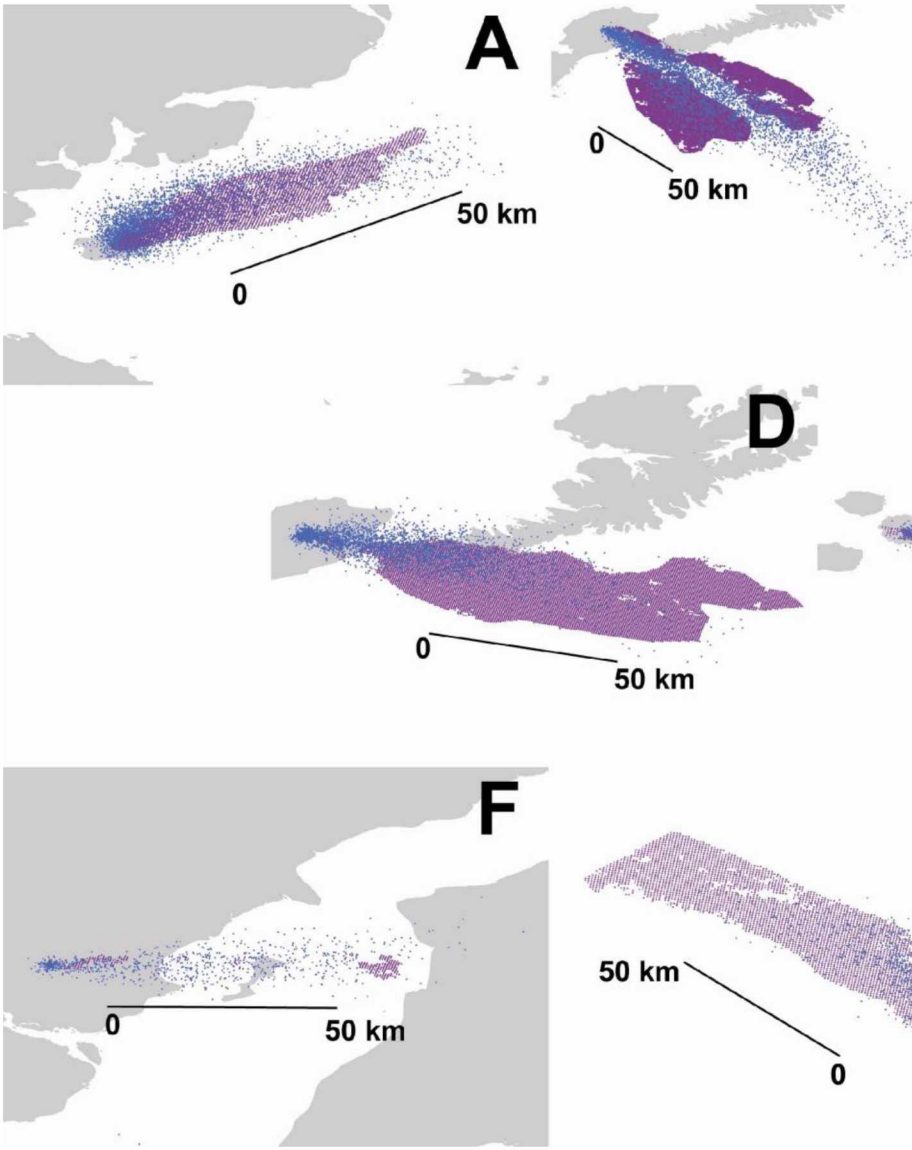
A
0
50 km
0
50 km
D
0
50 km
F
0
50 km
50 km
0

B
C
0
50 km
E
0
50 km
N
G
H
50 km
0

Figure 3.5: Airborne photographs for Augustine and Redoubt. A) Augustine on January 30, 2006 looking to the northeast, along the plume; B) Augustine on January 30, 2006 looking to the northwest at the plume profile; and C) Redoubt on April 5, 2009. On both days, for both volcanoes, relatively flat plumes were observed, though Redoubt photo shows some higher altitude material just above the vent. Photograph for Augustine courtesy of Dave Schneider, AVO/USGS. Photograph for Redoubt taken by Leslie Holland-Bartels. Image courtesy of AVO/USGS and obtained from http://www.avo.alaska.edu/.

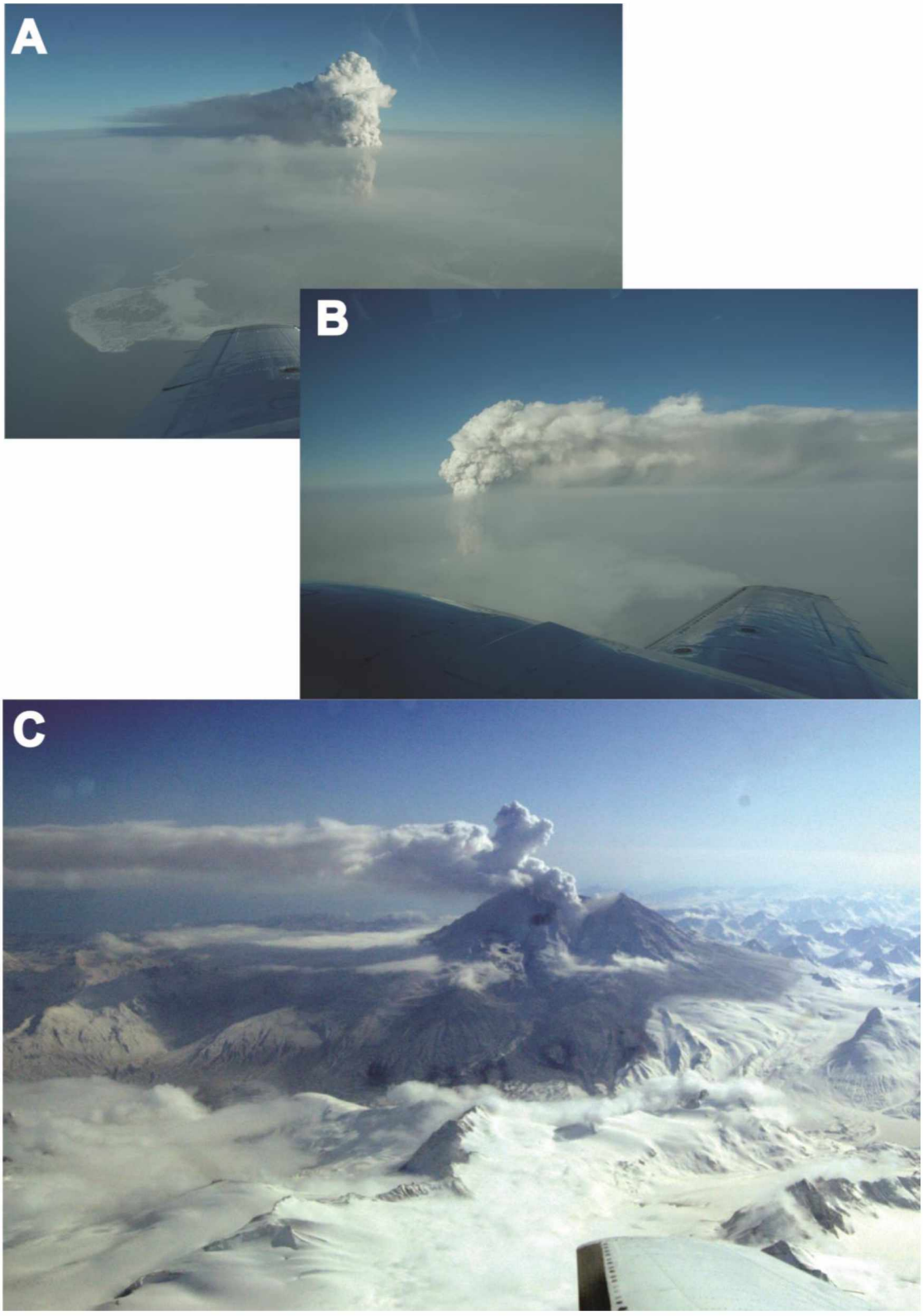
A
B
C

Figure 3.6: MISR height map, Puff VATD model output, and MISR visual image for Cleveland, Redoubt, and Sarychev Peak eruptions. A) Cleveland on July 22, 2009 showing relatively flat plume with only slight height variation. For scale, the MISR plume is ~75 km long. B) Redoubt on April 5, 2009 showing few MISR retrievals, but at heights consistent with Puff model heights. For scale, the MISR plume is ~80 km. C) Sarychev Peak on June 14, 2009 showing lower, decreasing heights to the west of the volcano, and higher altitude material to the east of the volcano. For scale, the MISR plume has a maximum length of ~120 km. D) Sarychev Peak on June 16, 2009, showing lower altitude material on the north/northeast side of the plume, and higher altitude material on the south/southwest side of the plume. For scale, the MISR plume is ~180 km long.

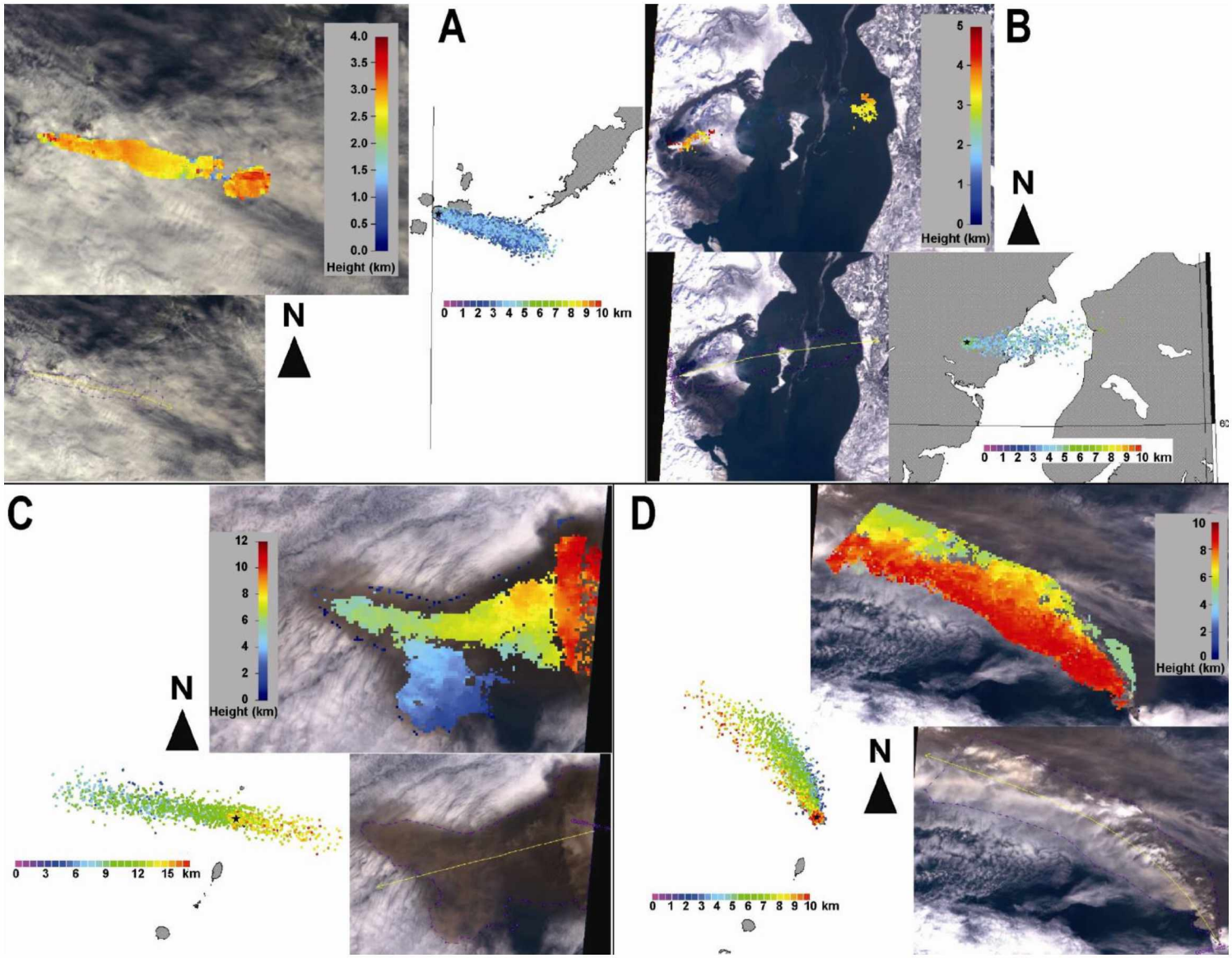
A
4.0
3.5
3.0
2.5
2.0
1.5
1.0
0.5
0.0
Height (km)
N
0 1 2 3 4 5 6 7 8 9 10 km
B
5
4
3
2
1
0
Height (km)
N
0 1 2 3 4 5 6 7 8 9 10 km
C
12
10
8
6
4
2
0
Height (km)
N
0 3 6 9 12 15 km
D
10
8
6
4
2
0
Height (km)
N
0 1 2 3 4 5 6 7 8 9 10 km

Figure 3.7: Two-dimensional height-distance results for Cleveland, Redoubt, and Sarychev Peak eruptions. A) Cleveland on July 22, 2009 showing relatively flat plume with only slight height oscillation, and inset showing altitude of weather cloud retrievals, B) Redoubt on April 5, 2009 showing slightly decreasing MISR heights, and temperature heights that are in poor agreement with MISR heights; C) Sarychev Peak on June 14, 2009 showing material that decreases in altitude with distance from the vent (as it moves further west); and D) Sarychev Peak on June 16, 2009, showing two levels of material – the lower altitude material on the north/northeast side of the plume, and the higher altitude material on the south/southwest side of the plume. MISR zero-wind heights are shown by green (lighter) squares, and MISR wind-corrected heights are shown by blue (darker) squares. Temperature heights are shown by teal (lightest) triangles.

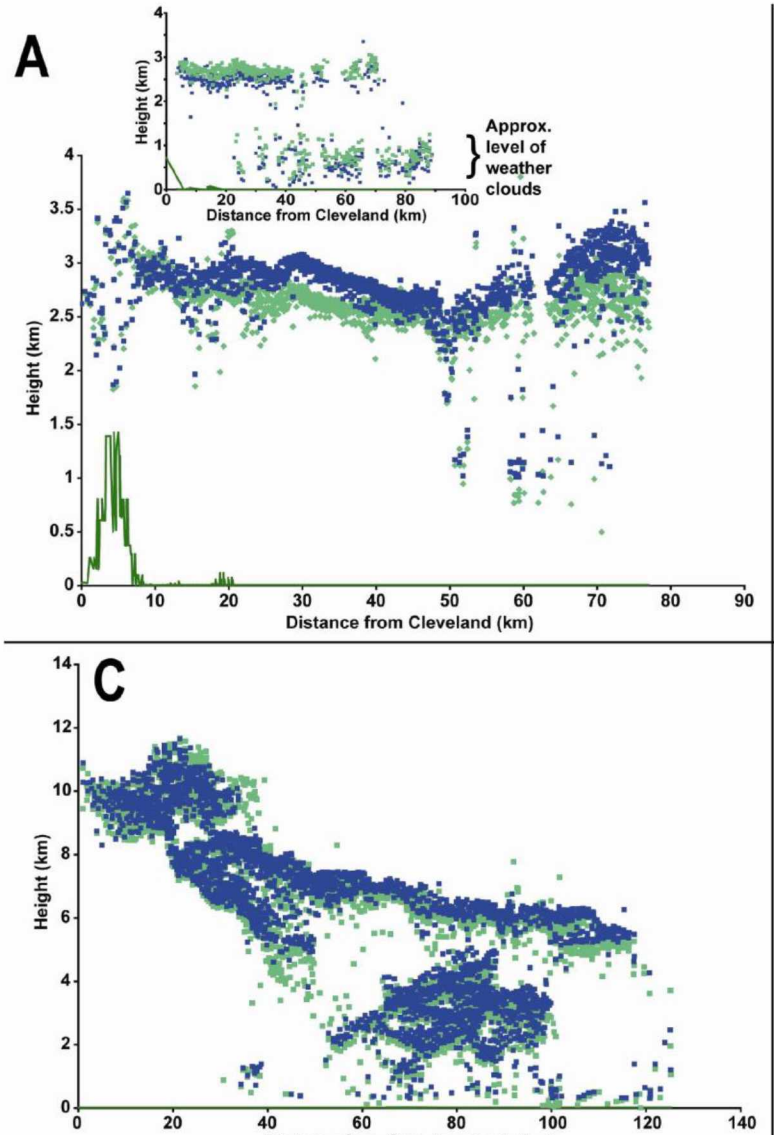
A
Height (km)
Distance from Cleveland (km)
Approx. level of weather clouds
Height (km)
Distance from Cleveland (km)
C
Height (km)
Distance from Sarychev Peak (km)

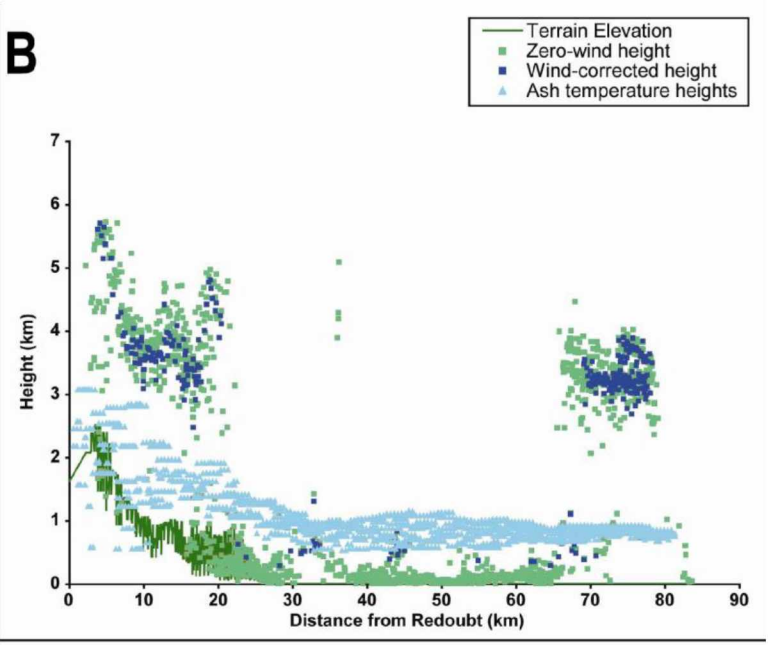
B
Terrain Elevation
Zero-wind height
Wind-corrected height
Ash temperature heights
Height (km)
Distance from Redoubt (km)

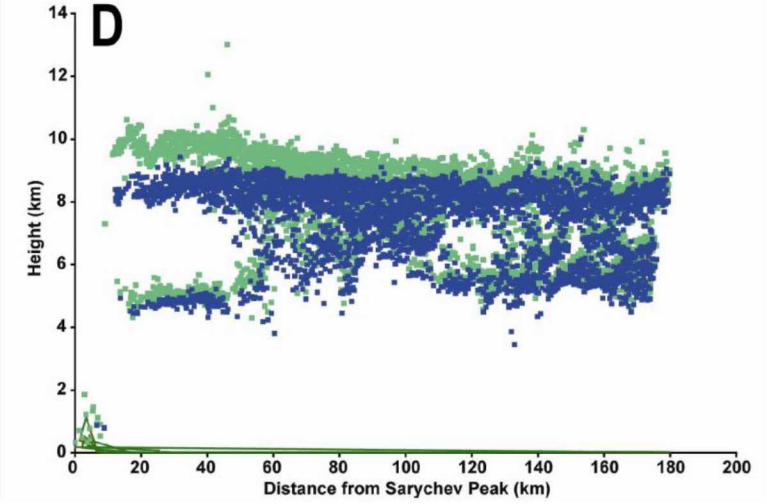
D
Height (km)
Distance from Sarychev Peak (km)

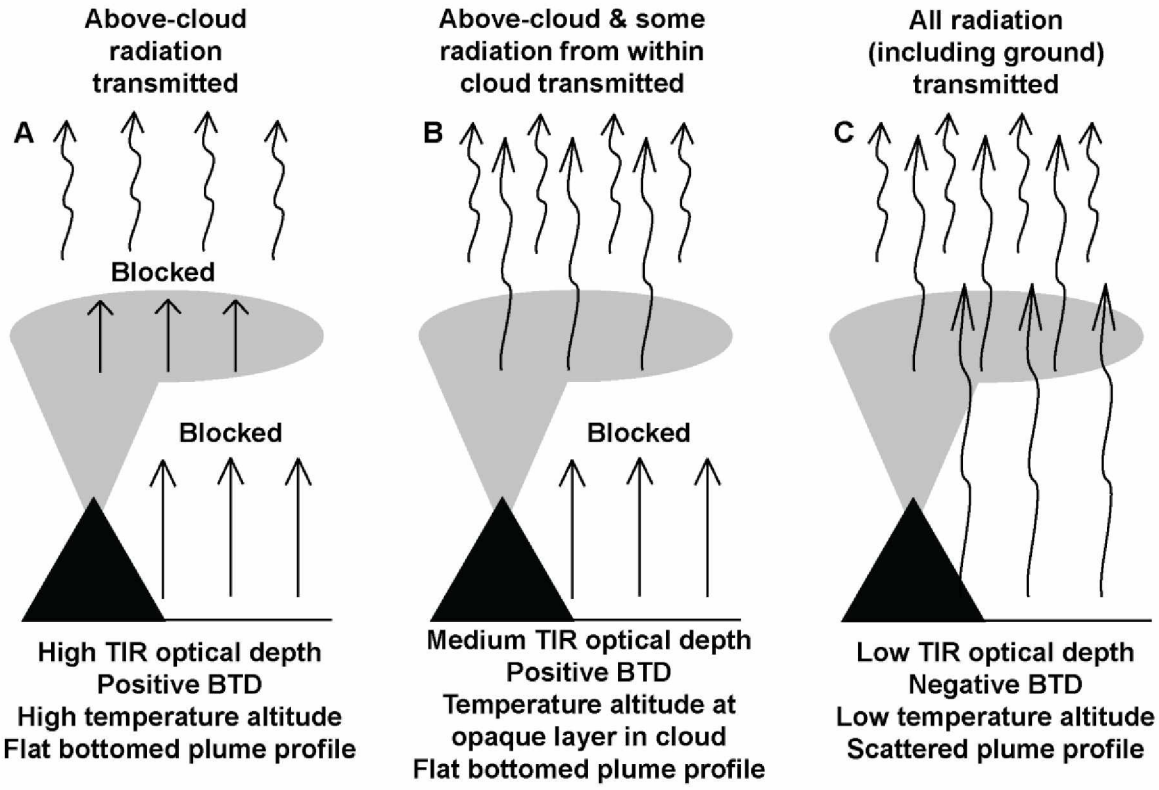

Figure 3.8: Schematic showing the effect of optical depth on thermal radiative signal transmitted from plume to infrared satellite sensor. A) High optical depth plume prevents radiative signal passing from within and below the plume, acting as opaque. B) Lower optical depth plume allows radiative signal from within the plume to reach the sensor, producing lower temperature heights than the fully opaque plume. C) Lowest optical depth plume allows radiation from ground to pass through the plume, being scattered, and reach the sensor, producing very low temperature altitudes relative to the fully opaque plume.

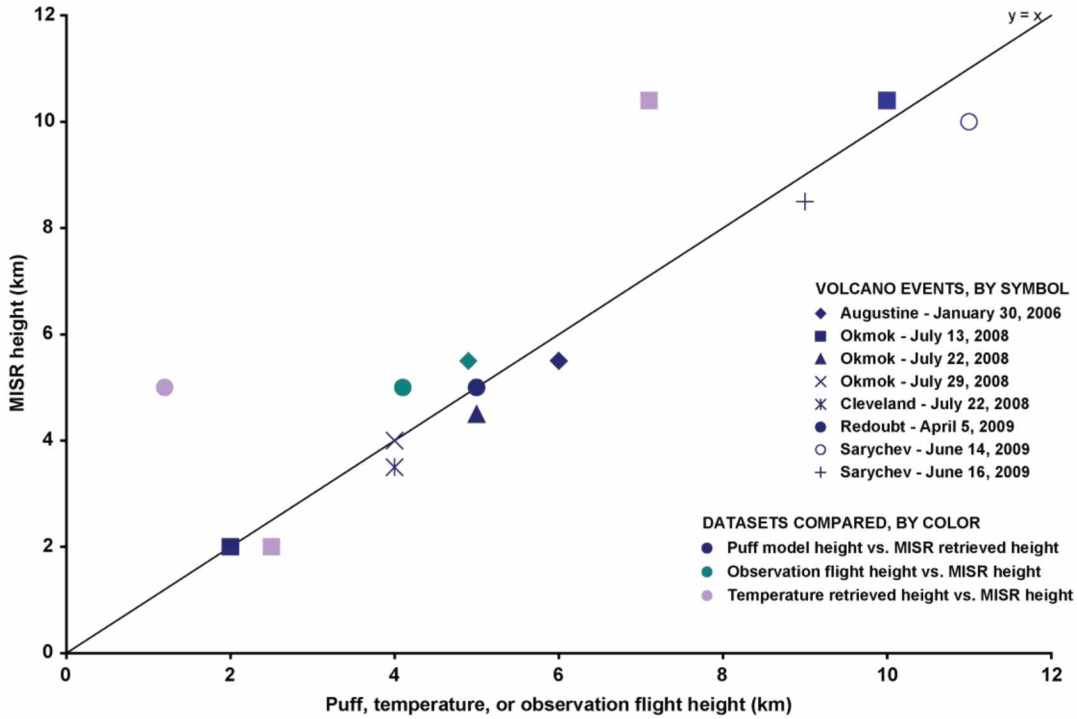

Figure 3.9: Plot of MISR retrieved heights vs. Puff, temperature, and observation flight heights. Volcanoes are denoted by symbols shown in legend, while type of height comparison is denoted by color. Note, the Okmok July 13 eruption has two retrievals: one for the higher altitude steam plume, and one for the lower altitude ash plume. Methods with good agreement with MISR heights fall close to the $y=x$ (or one-to-one) line, while methods that overestimate height in comparison to MISR fall below the line, and methods that underestimate height in comparison to MISR fall above the line. MISR/Puff and MISR/observation height comparisons are within ~1 km of the $y=x$ line, showing good agreement. MISR/temperature height comparisons plot above the line by as much as 4 km, suggesting underestimate of temperature heights. The exception is the point for the Okmok July 13 ash plume, for which temperature retrievals are affected by a surface temperature inversion.

Table 3.1: MISR specifications

Sensor	**MISR**
Number of cameras/sensors	9
Viewing angles	70.5°, 60.0°, 45.6°, 26.1° forward- and aft-looking, and nadir
Resolution	275 m in red bands of all nine cameras, and all bands of nadir camera; other bands 1100 m
Swath size	~400 km common field of view
Bands	4: B/G/R (446, 558, and 672 nm) and NIR (855 nm)[a]
Bands of interest	Heights retrieved using red cameras; 672 nm
Data acquired from	NASA Langley Research Center Atmospheric Sciences Data Center

[a] *NIR: near infrared; B/G/R: blue, green, red.*

Table adapted from Ekstrand et al. (in review)

Table 3.2: Data analyzed

Volcano	Month(s) of eruption	Year of eruption	MISR orbit	MISR blocks	Date of MISR pass	Time of MISR pass (UTC)	AVHRR/MODIS pass?[a] (UTC)	Airborne photos?[a]	Observation flight heights?[a]	Aerosol results?[a]
Augustine	January-March	2006	32555	42-43	30-Jan	21:31	-	Y	Y	N
Okmok	July-August	2008	45589	47-49	13-Jul	22:29	MODIS Terra 22:25	-	-	Y, steam and ash
			45720	48	22-Jul	22:23	-	-	-	N
			45822	47-48	29-Jul	22:29	-	-	-	N
Cleveland	July	2008	45720	48-49	22-Jul	22:23	-	-	-	N
Kasatochi	August	2008	45982	50-53	8-Aug	23:06-23:07	-	-	-	N
Redoubt	March-April	2009	49462	42-43	5-Apr	21:26	AVHRR 21:11	Y	Y	Y
Sarychev Peak	June	2009	50469	51-53	14-Jun	1:05	-	-	-	Y
			50498	51-52	16-Jun	0:53	-	-	-	Y

[a] *Since this data was not available for all eruptions, column title is posed as a question; Y/N: yes/no; for AVHRR/MODIS, pass is given if available*

Table 3.3: Aerosol results

Volcano	Orbit	Date	Location in plume	AOD range	AOD mean	AOD spherical fraction	Small	Medium	Large
Okmok	45589	July 13 2008	steam, edge near ash	0.21 - 0.38	0.29	0.40	0.40	0.24	0.36
			ash, edges	0.26 - 0.37	0.30	0.40	0.40	0.24	0.36
			ash, center	0.50 - 0.62	0.56	0.40	0.40	0.24	0.36
Redoubt	49462	April 5 2009	ash cloud over water across Cook Inlet	0.19 - 0.24	0.20	1.00	0.30	0.03	0.67
Sarychev Peak	50469	June 14 2009	near leading edge of cloud	0.50 - 0.57	0.54	0.40	0.41	0.31	0.28
			south edge of cloud	0.47 - 0.56	0.52	0.20	0.23	0.47	0.30
Sarychev Peak	50498	June 16 2009	base of plume near vent	0.82 - 0.95	0.88	0.40	0.39	0.18	0.43

Table 3.4: Height method comparison values used for Figure 3.9

Volcano	Year of eruption	Day, month[a]	Avg. max. MISR height (km)	Avg. max. Puff (km)	Avg. max temperature height (km)[b]	Avg. observation flight height (km)[b]
Augustine	2006	30-January	5.5	6	-	4.9
Okmok	2008	13-July ash	2	2	2.5	-
		13-July steam	10.4	10	7.1	-
		22-July	4.5	5	-	-
		29-July	4	4	-	-
Cleveland	2008	22-July	3.5	4	-	-
Redoubt	2009	5-April	5	5	1.2	4.1
Sarychev Peak	2009	14-June	10	11	-	-
		16-June	8.5	9	-	-

[a] *Also specifies portion of plume, if applicable*

[b] *Not available for all eruptions*

Chapter 4 Conclusions

4.1 Summary of findings

MISR data, as well as satellite temperature data, were analyzed for many eruptions to determine the accuracy of plume heights and resolve discrepancies between height determination methods. The studies detailed in Chapters 2 and 3 find the following:

- The basic satellite temperature method underestimates plume top height whenever optical depth is diminished (less than that of a blackbody) in an eruption cloud. Furthermore, without additional data, tropospheric and stratospheric clouds cannot be distinguished by the temperature method. Thus, this method has limited application for volcanic plumes.
- If optical depth is relatively high, the basic satellite temperature method may retrieve temperatures that correspond to some altitude within the cloud; however, this altitude is likely to be several kilometers below the plume top.
- If optical depth is relatively low, the basic satellite temperature method may retrieve the heights of land or water surfaces instead of plume heights. This is evidenced by significant scatter in height-distance profiles.
- Radar and MISR stereo heights provide accurate alternatives to the basic satellite temperature method.
- Radar is an excellent method to detect plume top heights, but has limited spatial application (effective only for volcanoes located near radar stations, such as those in the Cook Inlet region; also only effective for fairly large particle sizes of about 1-2 mm; Rose et al., 1995).
- MISR works extremely well for volcanic plumes in many circumstances:

  - MISR height retrievals work well for both steam and ash plumes.
  - MISR height retrievals work well for plumes of high visual optical depth (low transparency) in nearly any background condition (underlying clouds or water).
  - MISR height retrievals work well for plumes of low visual optical depth (high transparency) in conditions in which the background is composed of water (low reflectance background).
  - MISR height retrievals work well for plumes of any altitude.
  - MISR can easily detect cloud texture (height gradients or oscillations) via height retrievals, and these height patterns can sometimes provide insight into plume behavior.
  - MISR works in some cases to provide aerosol retrievals. When these are available, the results can be used to classify the general plume composition (ash- or water/sulfate-rich) by the method of Scollo et al. (2012).
- MISR has the following limitations, despite its excellent height retrieval capabilities:
  - Data is not real-time. Many files are required to process one MISR image in MINX (Nelson et al., 2009). In the case of AVO, this data must be separately downloaded (i.e., it is not part of the AVO data feed) in order to be analyzed. Due to the number of files required for one analysis, it is unlikely that MISR data could be practically incorporated into the regular AVO data feed.
  - MISR has poor temporal coverage. With a common field of view between cameras of 400 km, coverage is not frequent enough to use the data for real-time monitoring purposes. Every volcano is imaged only once every 2 days.
  - MISR height retrievals may be poor for plumes of low visual optical depth (high transparency) in conditions in which the background is composed of bright land

or weather clouds (high reflectance backgrounds). This is especially true at plume edges or for ash clouds that have drifted from the vent.

4.2 Future work

The previous studies have shown that the basic satellite temperature method has limited application for volcanic plumes in the NOPAC. AVO has relied on satellite temperature as one of its principal methods of plume height determination for many years (since the eruption of Redoubt in 1989; Dean et al., 1994). The development of new techniques, and a new understanding of how to treat the temperature method with an appropriate margin of error, when it is used, must be incorporated into monitoring practices at any volcano observatory that uses the basic satellite temperature method, including AVO.

If the basic satellite temperature method is used, it must be used with caution, with consideration of its height-distance profiles, which can indicate the accuracy of the temperature retrievals. As stated in Chapter 2, when BTD is negative, and retrievals produce a height-distance graph with minimal scatter, and a flat plume-bottom profile, then these retrievals likely correspond to an altitude within the cloud. When significant scatter appears in the plume, the temperature retrievals should be considered inaccurate. Furthermore, even supposedly "accurate" temperature retrievals should be treated as minimums. If MISR, radar, lidar, shadow, or any other method can be used in lieu of satellite temperature, then altitudes from these more accurate methods should be given preference. Additionally, it may be useful to continue to compare these other methods to temperature heights, if possible, to determine if there are any other caveats to the temperature method which have not been treated here. Lastly, when temperature method heights are used to

make forecasts of ash cloud motion, possible stratospheric altitudes must be taken into account, and dispersion should be modeled for a range of heights.

It would be extremely useful for AVO and other volcano observatories to incorporate the use of MISR data whenever possible, as its reliability is unparalleled for satellite temperature heights. Though MISR's temporal resolution is not frequent enough for it to be the first dataset relied upon during an eruption crisis, it may certainly useful in confirming heights determined by other methods. At AVO, if a MODIS Terra pass contains a plume of interest, the corresponding MISR data, if available, should be obtained and processed.

MINX is a user-friendly program that can easily be incorporated into existing software in remote sensing groups, and at AVO (IDL-based ENVI is already used at AVO and by many other remote sensing groups, and IDL is the required software for MINX). MINX allows processing of MISR data to be done easily and quickly. In addition to the graphical outputs given by MINX, aerosol outputs can easily be analyzed in ArcGIS (widely used by agencies that handle geospatial data, and also available at UAF-GI /AVO) or Excel. Heights can also be read directly from MINX graphical output with no additional work.

In addition, temperature methods should be further developed, taking into account the imperfect optical depth of clouds (e.g., weighing functions, etc). Basis for such work can be found in meteorology literature (Saunders and Kriebal, 1988; Zhang and Menzel, 2002; Huang et al., 2004; Joro and Saltikoff, 2004; Menzel et al., 2008), and some of these methods may be relatively easy to incorporate into algorithms in use at volcano observatories, including AVO. For this

future research, it would be most prudent to build upon the already existing body of meteorology cloud temperature height research available.

For BTD analysis, some changes are required as well. BTD is a method that works very well in some circumstances (e.g., dry clouds) and poorly in others (e.g., clouds with high water content). While this method can continue to be used with careful consideration of its limitations, an algorithm is provided by Pavolonis (2010) that utilizes beta functions, and provides a much more robust alternative. Future work should be conducted that explores the incorporation of this technique into automated detection of volcanic plumes. Furthermore, Mike Pavolonis (NOAA) has produced temperature algorithms that are more advanced than the basic temperature method (personal communication, Peter Webley), and when these are made publicly available, research should be undertaken that allows these temperature algorithms to be incorporated into automated processing as well.

The AVO remote sensing group at UAF-GI, or any other volcano remote sensing group that finds this work of interest to their operations, may want to consider two projects in particular for researchers or future students: (1) an investigation into the methods available in meteorology for robust temperature-height retrievals, compared to the processing algorithm (mentioned above) already developed by Mike Pavolonis, and (2) the creation of an algorithm for automated processing of satellite data using the favored method from the above study. For both studies, MISR data provides an accurate, easy to use method to determine if height results from these proposed studies are reliable.

References

Dean, K., Bowling, S.A., Shaw, G., Tanaka, H. 1994. Satellite analyses of movement and characteristics of the Redoubt Volcano plume, January 8, 1990. In Miller, T.P., Chouet, B.A., (Eds.), The 1989-1990 eruptions of Redoubt Volcano, Alaska. J. Volcanol. Geotherm. Res. 62, 339-352.

Dean, K.G., Dehn, J., Engle, K., Izbekov, P., Papp, K., Patrick, M., 2002. Operational satellite monitoring of volcanoes at the Alaska Volcano Observatory. Adv. Environ. Monit. Modell. 1, 70-97.

Dean, K.G., Eichelberger, J., Rothery, D., in press. Setting, history, and impact of the North Pacific region (Chapter 1). In: Dean, K.G., Dehn, J. (Eds.), Monitoring Volcanoes in the North Pacific: Observations from Space. Springer.

Diner, D.J., Beckert, J.C., Reilly, T.H., Bruegge, C.J., Conel, J.E., Kahn, R.A., Martonchik, J.V., Ackerman, T.P., Davies, R., Gerstl, S.A.W., Gordon, H.R., Muller, J.-P., Myneni, R.B., Sellers, P.J., Pinty, B., Verstraete, M.M., 1998. Multi-angle Imaging SpectroRadiometer (MISR) instrument description and experiment overview. IEEE Trans. Geosci. Rem. Sens. 36, 1072–1087.

Ekstrand, A.L., Dean, K.G., Webley, P., Dehn, J., 2009. Plume height analysis of two major Alaskan eruptions: Implications for operational use of satellite data. Abstr. V31A-1945 presented at 2009 Fall Mtg., AGU, San Francisco, Calif., 14-18 Dec.

Ekstrand, A.L., Webley, P., Dehn, J., Nelson, D.L., Garay, M.J., Dean, K.G., 2010. Plume height analysis of the 2009 Redoubt eruption: A comparison of MISR, AVHRR, and MODIS data. Abstr. NH43A-1492 presented at 2010 Fall Mtg., AGU, San Francisco, Calif., 13-17 Dec.

Ekstrand, A.L., Webley, P.W., Garay, M.J., Dehn, J., Prakash, A., Nelson, D.J., Dean, K., Steensen, T., in review. A multi-sensor plume height analysis of the 2009 Redoubt eruption. In: Webley, P., Waythomas, C.F. (Eds.), The 2009 Eruption of Redoubt Volcano, Alaska. J. Volcanol. Geotherm. Res.

Ekstrand, A.L., Webley, P.W., Nelson, D.J., Garay, M.J., Dehn, J., submitted. Application of MISR data to volcanic plumes in the North Pacific: Case studies for Augustine, Okmok, Cleveland, Redoubt, and Sarychev Peak volcanoes. J. Volcanol. Geotherm. Res.

Folch, A., Jorba, O., Viramonte, J., 2008. Volcanic ash forecast – Application to the May 2008 Chaiten eruption. Nat. Hazards Earth Syst. Sci. 94, 109-117.

Fromm, M.D., Kittaka, C., Vaughan, M., Eloranta, E.W., Ritter, C., Hoffman, A., Fricke, K.H., 2008. Plumes cover the northern hemisphere: Lidar views of summer 2008 volcanic and pryoconvective injections. Abstr. A52A-01 presented at 2008 Fall Mtg., AGU, San Francisco, Calif. 15-19 Dec.

Hoblitt, R.P., Schneider, D.J., 2009. Radar observations of the 2009 eruption of Redoubt Volcano, Alaska: Initial deployment of a transportable Doppler radar system for volcano monitoring. Abstr. V43A-2209 presented at 2009 Fall Mtg., AGU, San Francisco, Calif., 14-18 Dec.

Holasek, R.E., Self, S., 1995. GOES weather satellite observations and measurement of the May 18, 1980, Mount St. Helens eruption. J. Geophys. Res. 100, 8469-8487.

Holasek, R.E., Self, S., Woods, A.W., 1996. Satellite observations and interpretation of the 1991 Mount Pinatubo eruption plumes. J. Geophys. Res. 101, 27635-27655.

Huang, H.-L., Smith, W.L., Li, J., Antonelli, P., Wu, X., Knuteson, R.O., Huang, B., Osborne, B.J., 2004. Minimum local emissivity variance retrieval of cloud altitude and effective spectral emissivity - simulation and initial verification. J. App. Meteor. 43, 795-809.

Joro, S., Saltikoff, E., 2004. Determination of cloud top heights using weather radar and satellite data. Proceedings of ERAD, 237-241.

Kienle, J., Shaw, G.E., 1979. Plume dynamics, thermal energy, and long-distance transport of vulcanian eruption clouds from Augustine Volcano, Alaska. J. Volcanol. Geotherm. Res. 6, 139-164.

Marchand, R., Ackerman, T., Smyth, M., Rossow, W.B., 2010. A review of cloud top height and optical depth histograms from MISR, ISCCP, and MODIS. J. Geophys. Res. 115, D16206. doi:10.1029/2009JD013422.

Mastin, L.G., 2009. A user-friendly one-dimensional model for wet volcanic plumes. Geochem. Geophy. Geosy. 9. doi:10.1029/2006GC001455.

Menzel, W.P., Frey, R.A., Zhang, H., Wylie, D.P., Moeller, C.C., Holz, R.E., Maddux, B., Baum, B.A., Strabala, K.I., Gumley, L.E., 2008. MODIS global cloud-top pressure and amount estimation: Algorithm description and results. J. App. Meteor. Climat. 47, 1175-1198.

Miller, T.P., Casadevall, T.J., 2000. Volcanic ash hazards to aviation. In: Sigurdsson, H. (Ed.), Encyclopedia of Volcanoes. Academic Press, San Diego, 915-930.

Nelson, D.L., Averill, C., Boland, S., Morford, R., Menzies, A., Garay, M., Diner, D., Rheingans, B., Thompson, C., Hall, J., Scholes, M., Campbell, H., 2009. MISR INteractive eXplorer (MINX) v1.2 user's guide. JPL Tech. Rep. D-41552. http://www.openchannelsoftware.com/projects/MINX/

Pavolonis, M.J., 2010. Advanced in extracting cloud composition information from spaceborne infrared radiances – A robust alternative to brightness temperatures. Part I: Theory. J. Appl. Meteorol. Climatol. 49, 1992–2012.

Rose, W.I., Kostinski, A.B., Kelley, L., 1995. Real time C band radar observations of 1992 eruption clouds from Crater Peak, Mount Spurr Volcano, Alaska. USGS Bull. 2139, 19-28.

Saunders, R.W., Kriebel, K.T., 1988. An improved method for detecting clear sky and cloudy radiances from AVHRR data. Int. J. Rem. Sens. 9, 123-150.

Schneider, D., Hoblitt, R., in press. Doppler weather radar observations of the 2009 eruption of Redoubt Volcano, Alaska. In: Webley, P., Waythomas, C.F. (Eds.), The 2009 Eruption of Redoubt Volcano, Alaska. J. Volcanol. Geotherm. Res.

Scollo, S., Folch, A., Coltelli, M., Realmuto, V.J., 2010. Three-dimensional volcanic aerosol dispersal: A comparison between Multiangle Imaging Spectroradiometer (MISR) data and numerical simulations. J. Geophys. Res. 115, D24210. doi:10.1029/2009JD013162

Scollo, S., Kahn, R.A., Nelson, D.L., Coltelli, M., Diner, D.J., Garay, M.J., Realmuto, V.J., 2012. MISR observations of Etna volcanic plumes. J. Geophys. Res. 117, D06210, doi:10.10.29/2011JD016625.

Searcy, C., Dean, K., Stringer, W., 1998. PUFF: A high-resolution volcanic ash tracking model. J. Volcanol. Geotherm. Res. 80, 1-16.

Sparks, R.S.J., Bursik, M.I., Carey, S.N., Gilbert, J.S., Glaze, L.S., Sigurdsson, H., Woods, A.W., 1997. Volcanic Plumes. Wiley, Chichester, 574 pp.

Tupper, A., Wunderman, R., 2009. Reducing discrepancies in ground and satellite-observed eruption heights. J. Volcanol. Geotherm. Res. 186, 22-31.

Webley, P.W., Dehn, J., Lovick, J., Dean, K.G., Bailey, J.E., Valcic, L. 2009. Near-real-time volcanic ash cloud detection: Experiences from the Alaska Volcano Observatory. J. Volcanol. Geotherm. Res. 186, 79-90.

Werner, C., Kelly, P.J. Doukas, M., Lopez, T., Pfeffer, M., McGimsey, R.G., Neal, C.A., in press. Degassing associated with the 2009 eruption of Redoubt Volcano, Alaska. In: Webley, P., Waythomas, C.F. (Eds.), The 2009 Eruption of Redoubt Volcano, Alaska. J. Volcanol. Geotherm. Res.

Winker, D.M., Pelon, J., McCormick, M.P., 2002. The CALIPSO Mission: Spaceborne lidar for observation of aerosols and clouds. Proc. SPIE 4893, 1–11.

Winker, D.M., Hunt, W.H., Hostetler, C.A., 2004. Status and performance of the CALIOP Lidar. Proc. SPIE 5575, 8–15.

Winker, D.M., Vaughan, M.A., Omar, A., Hu, Y., Powell, K.A., Liu, Z.-A., Hunt, W.H., Young, S.A., 2009. Overview of the CALIPSO mission and CALIOP data processing algorithms. J. Atmos. Ocean. Techn. 26, 2310-2323.

Wood, J., Scott, C., Schneider, D., 2007. WSR-88D radar observations of volcanic ash. 4th Int. Workshop on Volcanic Ash, World Meterol. Org, Int. Civil Aviation Org., and Civil Aviation Authority New Zealand, Rotorua, New Zealand, 26-20 Mar., 9 pp.

Zhang, H., Menzel, W.P., 2002. Improvement in thin cirrus retrievals using an emissivity-adjusted CO_2 slicing algorithm. J. Geophys. Res. 107. doi 10.1029/2001JD001037.